2010

EXPERIMENTAL STUDY OF BLAST RESISTANT GLAZING SYSTEM RESPONSE TO EXPLOSIVE LOADING

William Chad Wedding
University of Kentucky, chad.wedding@uky.edu

ABSTRACT OF THESIS

EXPERIMENTAL STUDY OF BLAST RESISTANT GLAZING SYSTEM RESPONSE TO EXPLOSIVE LOADING

This thesis recounts the experimental study of the dynamic response of a blast resistant glazing system to explosive loading. A combination of triaxial force sensors, pressure gauges, and laser displacement gauges capture the response in detail over a wide range of scenarios. The scenarios include low level blast loading to characterize the reaction at points around the perimeter of the window, moderate level blast loading to examine the repeatability of the blast scenario, and high level blast loading to capture the response during failure as the tensile membrane forms. The scenarios are modeled via an analytical Single-Degree-of-Freedom model as well as finite element modeling in ANSYS Explicit Dynamics. In addition, this study investigates some of the differences between experimental data and the predictions made by modeling.

KEYWORDS: Blast Resistant Glazing System Response, Explosively Driven Shock Tube Testing, Single Degree of Freedom Model, Dynamic Reaction Measurements, Tensile Membrane

William Chad Wedding

December 14, 2010

EXPERIMENTAL STUDY OF BLAST RESISTANT GLAZING SYSTEM RESPONSE TO EXPLOSIVE LOADING

By

William Chad Wedding

Dr. Braden T. Lusk

Director of Thesis

Dr. Rick Honaker

Director of Graduate Studies

December 14, 2010

Date

RULES FOR THE USE OF THESES

Unpublished theses submitted for the Master's degree and deposited in the University of Kentucky Library are as a rule open for inspection, but are to be used only with due regard to the rights of the authors. Bibliographical references may be noted, but quotations or summaries of parts may be published only with the permission of the author, and with the usual scholarly acknowledgments.

Extensive copying or publication of the thesis in whole or in part also requires the consent of the Dean of the Graduate School of the University of Kentucky.

A library that borrows this thesis for use by its patrons is expected to secure the signature of each user.

Name Date

_____

_____

_____

_____

_____

_____

_____

_____

_____

THESIS

William Chad Wedding

The Graduate School

University of Kentucky

2010

EXPERIMENTAL STUDY OF BLAST RESISTANT GLAZING SYSTEM RESPONSE TO EXPLOSIVE LOADING

THESIS

A thesis submitted in partial fulfillment of the requirements for the degree of Masters of Science in the College of Engineering at the University of Kentucky

By

William Chad Wedding

Lexington, Kentucky

Director: Dr. Braden T. Lusk, Professor of Mining Engineering

Lexington, Kentucky

2010

DEDICATION

This thesis is dedicated to my wife, Kathy and to my family and friends. I've been fortunate to have the love and support that I need to pursue the opportunities available to me. I know that my wife will always be there for me when I need her. I am unable to express my gratitude properly.

I'd also like to give thanks for my Grandfather Gough, who taught me the value of a journey has nothing to do with the price of gas.

ACKNOWLEDGMENTS

This thesis was made possible by the support of many individuals to whom I owe gratitude. I would like to thank Dr. Braden Lusk, host of the Discovery series “The Detonators”, and my advisor. He provide the necessary guidance and criticism to direct me down this path in a timely fashion. I would like to thank the thesis committee: Dr. Joseph Sottile and Dr. Kozo Saito. Each contributed in their own way, adding to the quality of this finished product.

In addition to those above, I would like to recognize the support I received from my fellow graduate students in my research group, Josh Hoffman and now Dr. Kyle Perry. Finally, I’d like to acknowledge the support I received from my family and friends, primarily my wife Kathy.

TABLE OF CONTENTS

ACKNOWLEDGMENTS III

LIST OF TABLES VII

LIST OF FIGURES VIII

CHAPTER 1 INTRODUCTION 1

1.1 THESIS PROBLEM STATEMENT 1

CHAPTER 2 BACKGROUND INFORMATION 3

2.1 THE NATURE OF EXPLOSIVE LOADING 3

2.2 BLAST RESISTANT GLAZING COMPONENTS 5

2.3 EQUIVALENT DESIGN METHOD 9

2.4 SOFTWARE DESIGN TOOLS 11

2.5 BLAST RESISTANT GLAZING EVALUATION 12

CHAPTER 3 ANALYTICAL AND NUMERICAL METHODS 16

3.1 SINGLE DEGREE OF FREEDOM MODEL 17

3.1.1 Static Resistance Function 18

3.1.2 SDOF Model Parameters 19

3.1.3 SDOF Model Implementation 19

3.2 HAZL 21

3.3 FINITE ELEMENT ANALYSIS MODEL 22

3.3.1 Window Glass Modeling Parameters 24

3.3.2 Interlayer Modeling Parameters 25

3.3.3 Structural Silicone Glazing Modeling Parameters 27

3.3.4 Convergence Study 29

CHAPTER 4 INSTRUMENTATION AND EQUIPMENT DESIGN 31

4.1 PRESSURE TIME HISTORY MEASUREMENT 31

4.2 WINDOW DEFLECTION MEASUREMENT 33

4.3 WINDOW REACTION FORCE MEASUREMENT 34

4.4 SENSOR BRACKET DESIGN 36

4.5 Proxy Sensor 37
4.6 Buck Design 39
4.7 Supporting Electronics 40
CHAPTER 5 EXPERIMENTAL METHODOLOGY 42
5.1 Explosive Protocol 42
5.2 Perimeter Testing 43
5.3 Repeatability Testing 44
5.4 Test to Window Failure 45
CHAPTER 6 PERIMETER TESTING RESULTS AND ANALYSIS 46
6.1 Pressure Results 46
6.2 Deflection Results 48
6.3 Reaction Results 50
6.4 Modeling Results 54
6.4.1 SDOF Results 55
6.4.2 HazL Results 56
6.4.3 Finite Element Analysis Results 58
CHAPTER 7 REPEATABILITY TESTING RESULTS AND ANALYSIS 60
7.1 Pressure Results 60
7.2 Deflection Results 62
7.3 Reaction Results 63
7.4 Modeling Results 65
7.4.1 SDOF Results 66
7.4.2 Finite Element Analysis Results 67
CHAPTER 8 TEST TO FAILURE 69
8.1 Pressure Results 71
8.2 Deflection Results 75
8.3 Reaction Results 77
8.4 Modeling Results 84
8.4.1 SDOF Modeling Results 84

8.4.2 Equivalent Design Results 86
8.4.3 Finite Element Analysis Results 88
CHAPTER 9 CONCLUSIONS 93
REFERENCES 95
VITA 100

LIST OF TABLES

Table 2.1 Blast Resistance Level Specifications 5
Table 2.2 BRGS Hazard Rating per ASTM F 1642 (2004b) 14
Table 2.3 GSA Performance Conditions for Window System Response (2003). 15
Table 3.4 Laminated Glass SDOF Model Parameters 19
Table 3.5 Glass Modeling Parameters 25
Table 3.6 Interlayer Modeling Parmeters 26
Table 3.7 Silicone Modeling Parameters 29
Table 4.8 Flush Mount Pressure Sensor Attributes 31
Table 4.9 Laser Distance Gauge Attributes 33
Table 4.10 Triaxial Force Sensor Attributes 35
Table 6.11 Perimeter Testing Pressure Values 47
Table 6.12 Perimeter Testing Summary Deflection Values 49
Table 6.13 Perimeter Testing Summary Reaction Forces 51
Table 6.14 Perimeter SDOF Modeling Results 56
Table 7.15 Repeatability Testing Summary Pressure Values 61
Table 7.16 Repeatability Testing Summary Deflection Values 63
Table 7.17 Repeatability Testing Summary Reaction Forces 64
Table 7.18 Repeatability SDOF Modeling Results 66
Table 8.19 Test to Failure Summary Reaction Forces 77
Table 8.20 Test to Failure SDOF Modeling Results, 300g Charge 84
Table 8.21 Test to Failure SDOF Scenario Modeling Results, 300g Charge 85
Table 8.22 Test to Failure SDOF Modeling Results, 400g Charge 85
Table 8.23 Equivalent Threats 87
Table 8.24 Equivalent Threat Blast Parameters 87

LIST OF FIGURES

Figure 2.1 Blast Wave Pressure from Ngo et al. 2007 3
Figure 2.2 Oklahoma City Damage Potential Contour 4
Figure 2.3 Prince Rupert's Drops from Wikimedia Creative Commons (2006) 6
Figure 2.4 Nickel Sulfide Inclusion within glass (Bielecki et. al., 2008) 7
Figure 2.5 Spontaneous Glass Fracture due to NiS Inclusions over Time (Bordeaux and Kasper, 1997) 8
Figure 2.6 Static Equivalence Chart from ASTM F 2248-03 (2003) 10
Figure 2.7 Window Test Facilities from ASTM F 1642 - 04 (2004b) 13
Figure 3.8 Idealized Static Resistance Function 18
Figure 3.9 SDOF Spreadsheet 21
Figure 3.10 HazL User Interface 22
Figure 3.11 Window Glass Model 24
Figure 3.12 Structural Silicone Glazing from Vallabhan et al. 1997 28
Figure 3.13 Convergence Testing Results 30
Figure 4.14 Pressure Sensor Placement 32
Figure 4.15 Flush Mount Sensor within Trim 32
Figure 4.16 Laser Distance Gauge Placement 34
Figure 4.17 Sensor Bracket 36
Figure 4.18 Proxy Sensor 37
Figure 4.19 Proxy Sensor Z Axis Stiffness 38
Figure 4.20 Proxy Sensor X, Y Axis Stiffness 39
Figure 4.21 Completed Buck 40
Figure 5.22 Explosive Charge within Cannon 43
Figure 5.23 Attachment Point Labels 44
Figure 6.24 Representative Pressure Time History 46
Figure 6.25 Representative Deflection Time History 48
Figure 6.26 Representative Reaction Force Time History 50
Figure 6.27 Long Edge Peak Reaction Force (kPa) by Position 52
Figure 6.28 Short Edge Peak Reaction Force (kPa) by Position 53
Figure 6.29 Triangular Approximation of Pressure Time History 54

Figure 6.30 Static Resistance Function from HazL 55
Figure 6.31 HazL Output 57
Figure 6.32 Perimeter Modeling Deflection via FEA 58
Figure 6.33 Perimeter Modeling Safety Factor using Griffith's Criterion via FEA 59
Figure 7.34 Representative Pressure Time History 60
Figure 7.35 Representative Deflection Time History 62
Figure 7.36 Triangular Approximation of Pressure Time History 65
Figure 7.37 Repeatability Modeling Deflection via FEA 67
Figure 7.38 Repeatability Safety Factor using Griffith's Criterion via FEA 68
Figure 8.39 Before and After Failure Images of BRGS 69
Figure 8.40 Post Test to Failure Window Glazing with Torn Interlayer 70
Figure 8.41 Test to Failure Pressure Time History, 300g Charge 71
Figure 8.42 Test to Failure Triangular Approximation of Pressure Time History, 300g Charge 72
Figure 8.43 Test to Failure Pressure Time History, 400g Charge 73
Figure 8.44 Test to Failure Triangular Approximation of Pressure Time History, 400g Charge 74
Figure 8.45 Test to Failure Deflection Time History, 300g Charge 75
Figure 8.46 Test to Failure Deflection Time History, 400g Charge 76
Figure 8.47 Test to Failure Membrane Reaction, Z Axis, 400g Charge 78
Figure 8.48 Test to Failure Membrane Reaction, Z Axis, 400g Charge 79
Figure 8.49 Membrane Tensile Response across Span D to R 80
Figure 8.50 Tension within Membrane across Span D to R 81
Figure 8.51 Membrane Tensile Response across Span E to Q 82
Figure 8.52 Tension within Membrane across Span E to Q 83
Figure 8.53 Test to Failure Deflection via FEA, 300g Charge 89
Figure 8.54 Test to Failure Safety Factor using Griffith's Criterion via FEA, 300g Charge 90
Figure 8.55 Test to Failure Deflection via FEA, 400g Charge 91
Figure 8.56 Test to Failure Maximum Principal Stress via FEA, 400g Charge ... 92

Chapter 1 Introduction

A tragic consequence of modern life is the aftermath of accidental or malicious explosions in urban areas. Such events can potentially cause significant loss of life, injury, and damage to property. Much of the hazard to human life comes from glass fragments turned into projectiles when explosively loaded. Kiger notes that historically, glass fragments cause 80% or more of the injuries sustained during urban blast events (2009). As a result of the Oklahoma City bombing, 362 of 426 hospitalized persons had lacerations, abrasions, and contusions due to glass fragments (OKDCEM, 1995). Consequently, dramatic improvements to community resilience can be achieved by promoting the development of blast resistant glazing systems or BRGS.

The upswing in domestic and international terrorism recently has increased the demand for BRGS. New federal building projects require the use of BRGS and they are becoming more common in high profile commercial construction projects. Window manufacturers that can deliver a proven, cost effective BRGS have an obvious advantage in the marketplace.

1.1 Thesis Problem Statement

This thesis investigates the reaction forces transmitted to the members surrounding a BRGS undergoing a blast loading. Three phases of testing will be used to isolate separate premises concerning the nature of those forces. The results will then be compared with common analytical techniques and software packages available to the design community.

The first phase of testing characterizes the reaction forces at the individual attachment points securing the BRGS to the supports. This will allow one to determine the distribution of the reaction loading along all four edges of the perimeter. This will provide insight into the accuracy of the models investigated.

The second phase of testing examines the repeatability of the measurements for a given scenario. If the measurements prove to be repeatable, the hope is that the total peak reaction forces encountered during the blast can be determined by just a few sensors placed strategically around the perimeter.

The final phase of testing involves testing the window to failure. The peak reaction forces at four points about the frame will be determined. The tensile membrane that forms upon glass fracture will be measured.

The objective of the thesis is to record the reaction forces and displacement of a blast resistant glazing system undergoing a range of explosive loads and compare these results to modeling procedures common to the field.

Chapter 2 Background Information

2.1 The Nature of Explosive Loading

An explosion is marked by a very rapid release of energy. The source can be physical, nuclear, or chemical in nature. Physical explosions would include rupturing compressed gas cylinders or volcanic eruptions. With nuclear explosions, the energy is the result of the redistribution of protons and neutrons within the elements in play. Chemical explosions are usually the result of rapid oxidation of fuel elements (Ngo et al., 2007). Figure 2.1 typifies a blast pressure wave associated with an explosion.

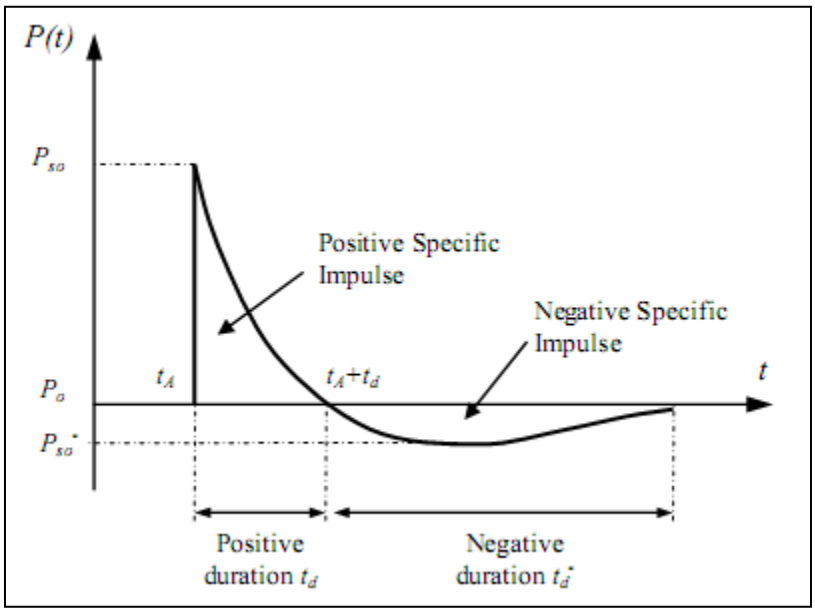

Figure 2.1 Blast Wave Pressure from Ngo et al. 2007

Figure 2.1 calls out the important characteristics of air blast waves. The quantity P_{so} represents the peak overpressure associated with the blast wave. It rapidly decays over the positive duration of the wave, t_d. A partial vacuum is formed as the decay continues in the negative phase of the blast. The area under the curve in each case, represents the specific impulse or energy in the pressure wave (TM5-1300, 1990).

Explosions have the potential to affect a very large footprint in an urban environment. Figure 2.2 shows a damage potential contour for the Oklahoma City bombing. The varying contours indicate the probability of glass fracture for common annealed glass windows. Injuries due to glass fragments were observed at a distance of 460 meters (1500 feet) from the Alfred P. Murrah Building (Swofford, 1996).

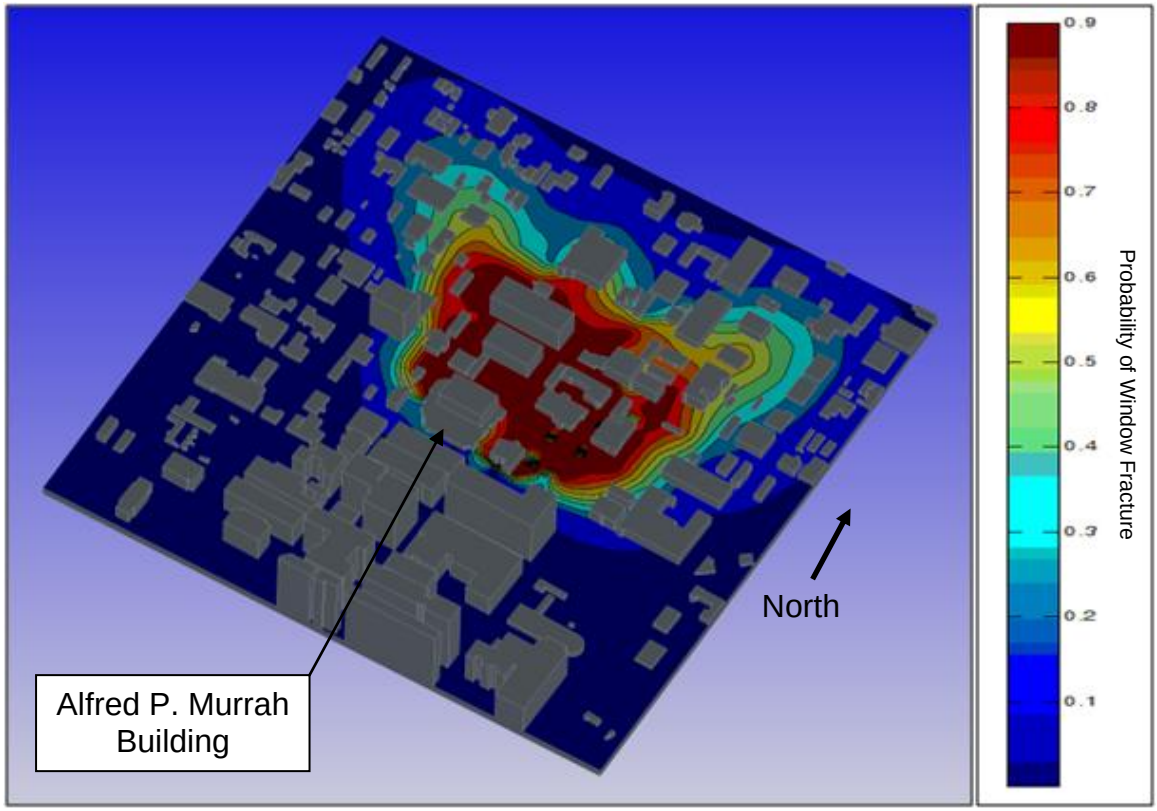

Figure 2.2 Oklahoma City Damage Potential Contour
(Lusk and Wedding, 2009)

The damage potential contour demonstrates the influence of shielding and channeling that occurs within urban environments. Blast waves interact with the environment, flowing around obstacles and even intensifying when focused by buildings (Smith and Rose, 2006). Points to the south of the Murrah building were shielded from the blast, while other areas north and west of the building demonstrate pressure concentrations.

Federal building projects would be covered by one of two government entities. The US General Services Administration or GSA sets the specifications for 8,600 federally owned or leased buildings. The Department of Defense maintains its own standards as detailed in the Unified Facilities Criteria 4-010-01 (2007). Commonly used specifications are listed in Table 2.1. The key parameters for these include the peak pressure and the positive phase impulse. Norville and others contend that the application of the GSA hazard level C would have been sufficient to virtually eliminate all glass related injuries in buildings other than the Murrah building during the Oklahoma City Bombing (Norville et. al., 1999).

Table 2.1 Blast Resistance Level Specifications

Common Blast Wave Specifications					
GSA	Level C	27.6	kPa	4.0	psi
		193	kPa·ms	28.0	psi·ms
	Level D	68.9	kPa	10.0	psi
		613.6	kPa·ms	89.0	psi·ms
DoD	Explosive Weight I	33.1	kPa	4.8	psi
		283.4	kPa·ms	41.1	psi·ms
	Explosive Weight II	40.0	kPa	5.8	psi
		204.8	kPa·ms	29.7	psi·ms

2.2 Blast Resistant Glazing Components

Annealed or float glass is common in glazing construction. It has been cooled gradually to allow residual stresses to relieve, allowing it to be processed easily. It has long been known to be unsuited for use in blast resistant glazing designs. Practitioners in the field prefer tempered glasses or polycarbonate (Meyers et. al., 1994). When broken, it forms sharp and pointed shards making it unsuited for use as in a BRGS without lamination (Leitch, 2005). It finds a place in insulated BRGS as an outside layer where the shards can be isolated from the interior occupants.

Heat-strengthened glass undergoes a heating and cooling process that locks in residual stresses to strengthen the glass. The process has been known since the seventeenth century through the study of a phenomenon called Prince Rupert's Drops. They are formed by dripping molten glass into cold water. The rapid cooling

yields a tear shaped drop that exhibits much higher strength than ordinary glass, capable of withstanding hammer blows to the spherical head. They disintegrate upon breaking the tail, which can be easily fractured. Robert Hooke was the first to offer an accurate description of the phenomena in 1665. It continued to intrigue researchers through the years and has been studied by such luminaries as Lord Kelvin and A. A. Griffith (Brodsley et. al., 1986). An example of Prince Rupert's Drops can be seen in Figure 2.3.

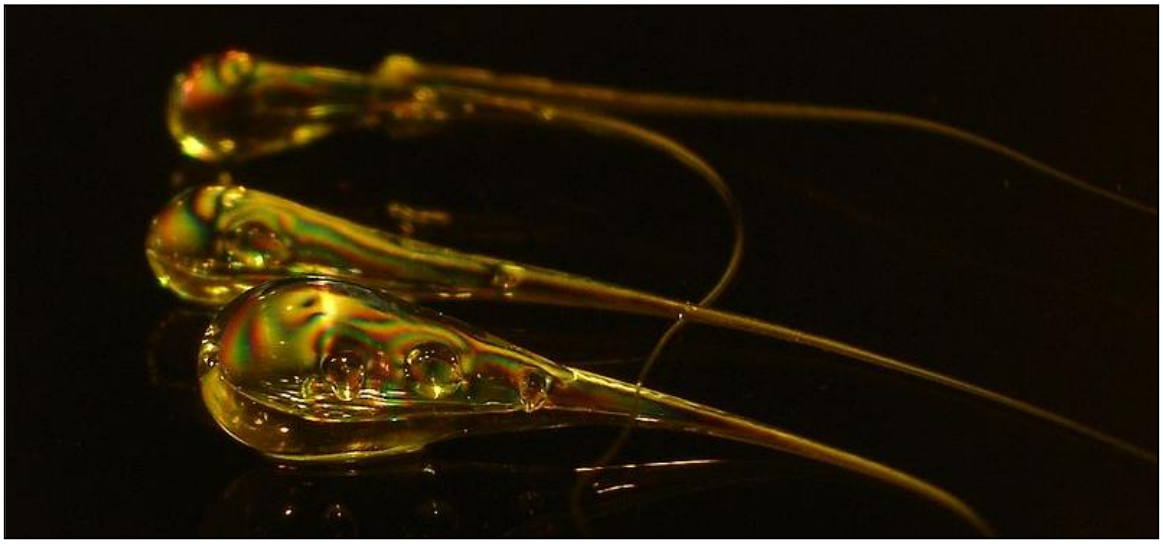

Figure 2.3 Prince Rupert's Drops from Wikimedia Creative Commons (2006)

Heat-strengthening glass locks in compressive surface stresses that increase the bending strength to a level unavailable with annealed glass. The surface stresses must be overcome before bending failure will occur as dictated by the principle of superposition (Ledbetter et al, 2006). The typical surface compression present in heat strengthened glass ranges from 40 to 80 MPa (Haldiman et.al., 2008). ASTM C 1048-04 dictates that the compressive surface stress fall in the range of 24 to 52 MPA in order to be deemed heat-strengthened (2004a). This greatly reduces the likelihood of breakage. Another advantage of heat strengthened glass is size of fragments usually produced. It tends to produce small, light fragments, usually

rectangular in shape, that are less likely to cause lacerations (Zijlstra and Burggraaf, 1968).

Toughened or fully tempered glass is processed in the same fashion as heat-strengthened glass. The glass is cooled more rapidly than heat-strengthened glass resulting in higher locked in residual stress. The typical surface compression present falls in the range of 80 to 170 MPa (Haldiman et.al., 2008). ASTM C 1048-04 dictates that fully tempered glass should contain no less than 69 MPa of residual compressive stress (ASTM 2004a). Toughened glass produces significantly smaller fragments that are relatively blunt compared to annealed glass as the size of fragments decreases with increasing levels of locked in residual stress (Allen et al., 1998).

The process to temper glass is not without its challenges. The heating process is an energy intensive process, requiring the glass material to be heated to 650 °C. The cooling process must be completed in a controlled fashion which increases the production costs. There is also the potential for spontaneous fracture due to small nickel sulfide inclusions. A representative nickel sulfide inclusion can be seen in Figure 2.4.

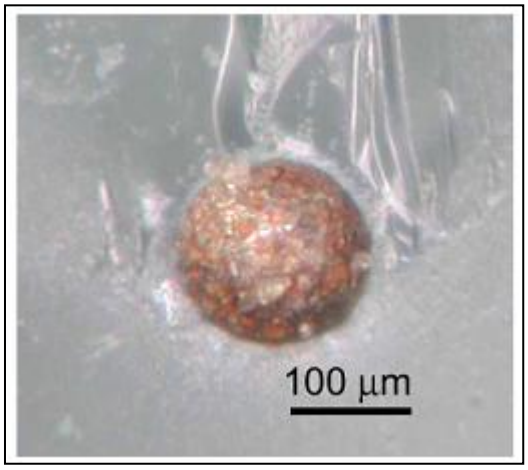

Figure 2.4 Nickel Sulfide Inclusion within glass (Bielecki et. al., 2008)

Nickel sulfide was identified as a problem for tempered glass in the early 1960s. The ICI House building in Melbourne, Australia, was one of the first to use fully tempered glass. The building was finished in September of 1958 and started to exhibit failures in 1960. Ballantyne traced the problem back to NiS inclusions (Jacob, 1997). The NiS defects are locked into the glass at a high temperature hexagonal crystalline structure. A phase transition to a low temperature rhombohedral state occurs at 379 °C. Over time, this phase transition occurs accompanied by a 2.8% volume increase in the inclusion (Barry and Ford, 2001). These defects can cause spontaneous fracture in tempered glass over periods from a few minutes to more than ten years after installation. Bordeaux and Kasper documented this phenomena on a single 40,000 square meter glazed building as seen in Figure 2.5 (1997).

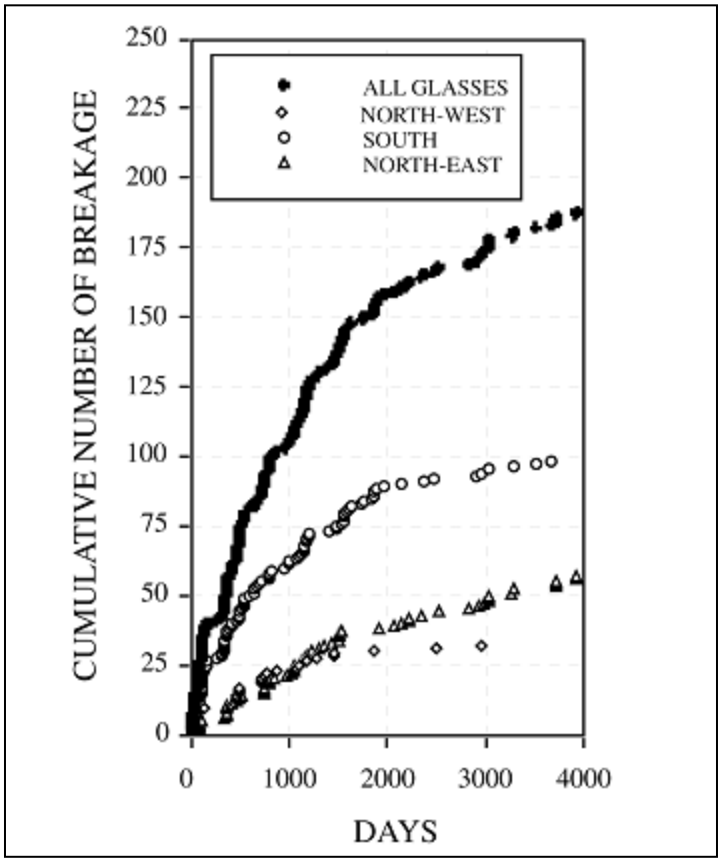

Figure 2.5 Spontaneous Glass Fracture due to NiS Inclusions over Time (Bordeaux and Kasper, 1997)

Lamination is the most successful modification to glass to increase its blast resilience. Glass is fundamentally brittle by nature, so adding a flexible interlayer improves its strength and impact resistance. Various types of glass or other materials such as polycarbonate can be combined to tailor the laminated unit to the needs of the project. The key benefit is the post failure behavior of the unit. Once the glass is broken the laminate keeps the fragments together reducing the likelihood of damage from flying shards. It also maintains a barrier against the environment further preventing the ingress of the pressure wave (Nichols and Sowers, 2009).

Laminating materials generally fall in one of two categories. The prevalent technology is a polyvinyl butryal film that has been in use since the 1930s. The film is bonded to the layers of glass through the application of a vacuum to remove trapped air, and heat and pressure to form the bond. Newer technologies include liquid systems that polymerize through the application of ultra-violet light. Regardless of the technology, the lamination bond must withstand a blast loading and resist weathering or discoloring over time (Vargas 2006).

Structural silicone glazing joins the glazing to the frame in a BRGS. The material fulfills two essential functions. It provides structural support to the window glazing, transferring loads applied to the framing. In the event of a blast, the silicone serves to retain the window fragments within the frame. It also serves to seal the opening against the environment (Hautekeer et al., 2001).

The framing system for BRGS is typically aluminum, though steel can be used if loads will be high or for long spans. The design for such components requires meeting the peak reaction forces the window glazing is capable of generating just prior to breakage (Hinman and Arnold, 2010) based upon calculated values lacking experimental validation.

2.3 Equivalent Design Method

One of the popular methods to simplify the design of blast resistant glazing systems is a method developed by Norville and Conrath (2001). The procedure involves converting an explosive loading to an equivalent static load of a relatively long duration. The explosive load is reduced to two parameters, the mass of an equivalent TNT charge and the standoff distance between charge and window. The procedure originally called for an equivalent duration of 60 seconds. It was later updated to be more consistent with the durations used for wind gusts, 3 second equivalent loading (ASTM 2003). Figure 2.6 provides the means to convert a blast loading to an equivalent design load. Once the design load has been determined, window design proceeds using methodologies common to the practice as detailed in ASTM E 1300-09a (2009).

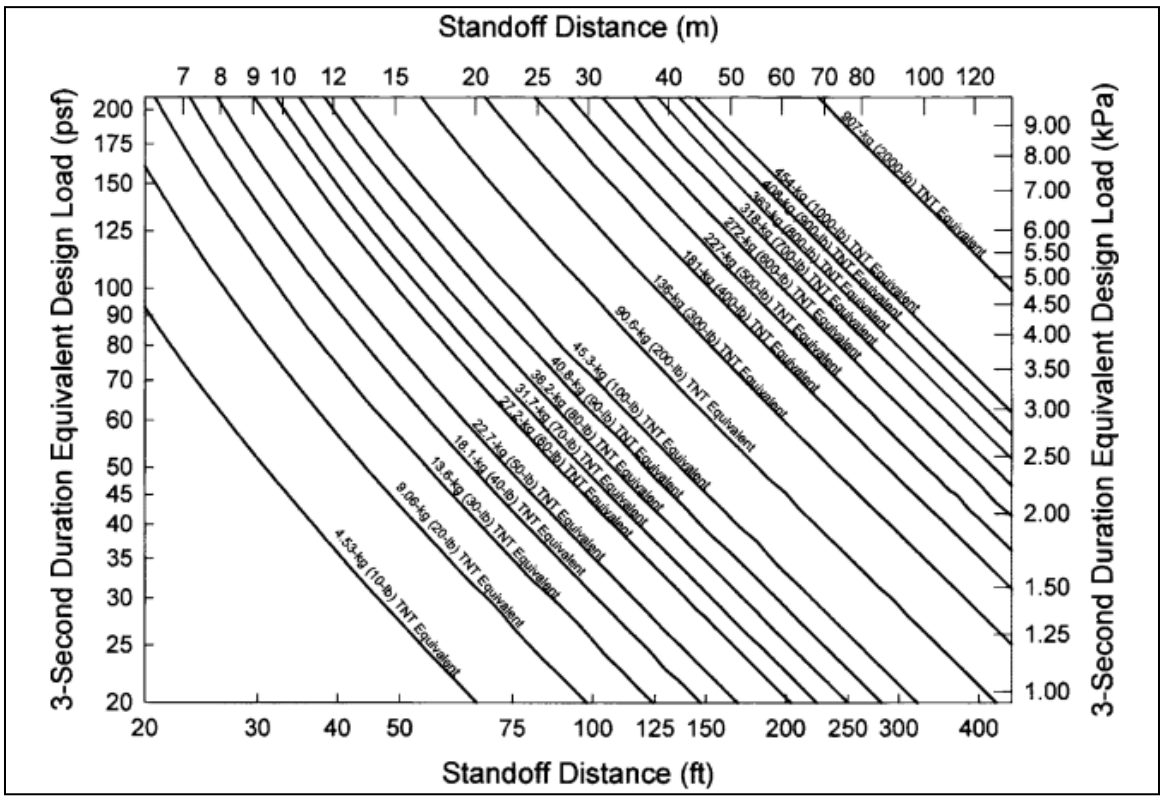

Figure 2.6 Static Equivalence Chart from ASTM F 2248-03 (2003)

Minor and Norville examine the procedures in ASTM E 1300-04 for the selection of glass thickness to resist lateral pressure (2006). The basis of the procedure

consists of 42 charts that define the strength of various configurations of annealed, heat strengthened, or fully tempered glass used in monolithic, laminated or insulating glass units as calculated to correspond to 20 years of service. After 20 years of service, weathered glass has a strength that has been reduced by 35%. Specific procedures detailed in sections 6.2 through 6.14 determine the factors necessary to adjust the strength of the glass from the chart to the specific application. However, the standards only call out specific sizes, limiting the choices of the engineer. This restricted selection of available sizes and the 20 year service life assumption lead to a very conservative design.

Blast resistant glazing systems designed in this manner should comply with the principle that the glass should fail before the surrounding elements in the event of a blast loading (Norville and Conrath, 2006). Alternatives exist that are capable of resisting peak pressures as high as 275 kPa. The unfortunate consequence is the additional cost to the supporting walls that in turn must support this loading (Ettouney et. al., 1996). A balanced design is preferred.

2.4 Software Design Tools

Stand-alone design tools to assist with the analysis of blast resistant glazing systems are available. HazL, short for Window Fragment Hazard Level Analysis, is a tool produced by the United States Army Corps of Engineers Protective Design Center. Another example is Wingard, or Window Glazing Analysis Response and Design, a product of the GSA. The packages are available to researchers and contractors with an established need. They typically perform a single degree of freedom analysis on the window system to predict the window response. This response is mapped to a database of finite element results to predict the peak principal stress. This, in conjunction with a limited set of experimental results, determines the probability of failure when compared to the normal distribution of glass strength expected in the window (Anonymous, 1998).

The second major category of software design tools includes finite element analysis. The study of blast loading and other high strain rate physics problems is

best handled by hydrodynamic codes. Numerous commercial packages are available to industry, such as ABAQUS, LS-DYNA, CTH, ALEGRA, ALE-3D, and AUTODYN. A recently undertaken benchmark compared several commercial codes for the use in nuclear reactor design (Lacy et al., 2007). Such facilities must be designed to resist a variety of malevolent attacks. The scenarios included classical solid dynamics and shock physics problems that have been well characterized to determine the software package suitability for the design tasks to overcome those attacks. In general, the commercial packages are in close agreement with one another are all suited for numerical simulation of these kinds of problems (Lacy et. al., 2008). The author had access to ANSYS Explicit Dynamics, which utilizes the AUTODYN solver, for the modeling exercise.

2.5 Blast Resistant Glazing Evaluation

The procedures for evaluating the performance of a blast resistant glazing system are set forth in ASTM F 1642-04. It provides a structured method to determine a hazard rating of a system undergoing a blast loading. The hazard rating is a qualitative scale that relates the performance of the window glass and the movement of fragments within the interior of the protected environment. This is in accordance with the historical precedent that a significant source of personal injury comes from failed window glazing.

Validation of BRGS, according to ASTM F 1642-04, requires appropriately configured testing facilities. A repeatable means of generating the airblast loading is required which can be either compressed air or explosively driven shock tubes or an open-air arena. The window is mounted to a frame in a manner consistent with the installation in the field. A witness panel is placed at a distance of 3 meters from the window under test. The witness panel consists of a 2.5 cm thick layer of aluminum faced extruded Styrofoam insulation. The witness panel serves to record the presence of fragments that impinge upon its surface. Instrumentation to record the blast wave pressure time loading is required to assure the desired loading is achieved. A cross-sectional representation of the testing facilities can be seen in Figure 2.7.

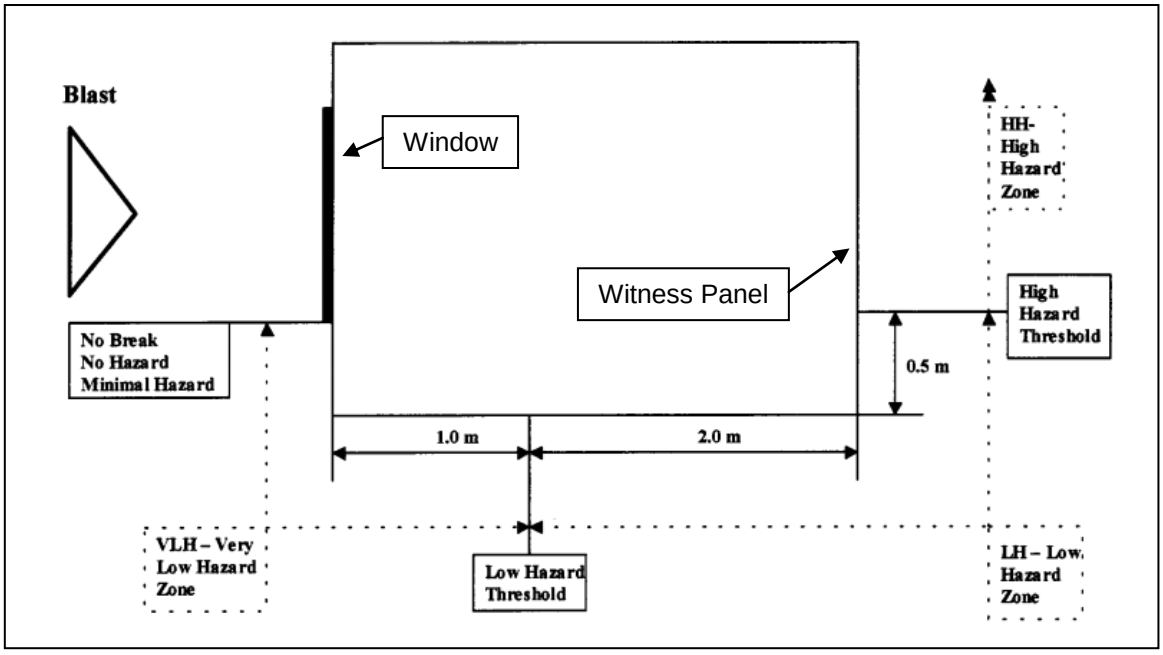

Figure 2.7 Window Test Facilities from ASTM F 1642 - 04 (2004b)

When glass breakage is encountered during testing, the witness area is examined closely for the presence of fragments. Glass dusting and slivers are discounted, leaving only those fragments with a united dimension of one inch or greater. The united dimension of a fragment is determined by adding the width, length, and thickness of the fragment. The number and placement of the window fragments, and the condition of the interlayer determine the window's hazard rating (ASTM 2004b). A summary of the hazard ratings is seen in Table 2.2.

Table 2.2 BRGS Hazard Rating per ASTM F 1642 (2004b)

Window Hazard Rating System from ASTM F 1642 (2004)			
Hazard Rating	***Description***	***Fragments***	
		1m to 3m	***Witness Panel***
No Break	Glazing is not allowed to break and there is no visible damage to the framing system.	None	None
No Hazard	Glazing fractures but is fully retained in the facility test frame or glazing system frame and the inner glass light is unbroken.	None	None
Minimal Hazard	Glazing fractures and the total length of tears in the glazing plus the total length of pullout from the edge of the frame is less than 20 per cent of the glazing sight perimeter.	Fragments less than 10 in. united Dimension	Three or less perforations from glazing slivers and no fragment indents
Very Low Hazard	Glazing fractures and is located within one (1) meter of the original location.	Fragments less than 10 in. united Dimension	Three or less perforations from glazing slivers and no fragment indents
Low Hazard	Glazing fractures.	Glazing fragments generally fall between 1 meter and 3 meters	< 10 perforations 50 cm below the bottom of the specimen and none of the perforations penetrate through the full thickness of the witness panel
High Hazard	Glazing fractures.	One (1) meter and three (3) meters	> 10 perforations in the area of the witness panel and one or more fragments penetrate fully through the witness panel

In general, the hazard rating increases as the number of fragments increase with distance from the window. The distance from the window before the test strongly correlates with the velocity imparted to the fragment during the blast loading. It is obvious that the interlayer plays a strong role in reducing the hazard rating of a BRGS. If it can retain all the window fragments without tearing, it is much less likely to eject material into the room and cause harm to occupants.

There are other specifications used in the industry to evaluate the performance of blast resistant glazing systems. The United States General Services Administration has published its own specification for use on projects under their control and responsibility (GSA, 2003). The testing regime is very similar to the procedures laid down by ASTM F 1642. The performance criteria are derived from an Interagency Security Committee document entitled the ISC Security Design Criteria (GSA, 2003). It provides guidance to ensure that security is a priority during the planning,

design, and construction of federal office buildings and during renovation projects. The guidance for the performance of BRGS is summarized in Table 2.3. In general, it follows the ASTM hazard rating scheme. The distinction lies in the number and location of fragments in the witness panel.

Table 2.3 GSA Performance Conditions for Window System Response (2003)

Performance Condition	Protection Level	Hazard Level	Description of Window Glazing Response
1	Safe	None	Glazing does not break. No visible damage to glazing or frame.
2	Very High	None	Glazing cracks but is retained by the frame. Dusting or very small fragments near sill or on floor acceptable.
3a	High	Very Low	Glazing cracks. Fragments enter space and land on floor no further than 3.3 ft. from the window.
3b	High	Low	Glazing cracks. Fragments enter space and land on floor no further than 10 ft. from the window.
4	Medium	Medium	Glazing cracks. Fragments enter space and land on floor and impact a vertical witness panel at a distance of no more than 10 ft. from the window at a height no greater than 2 ft. above the floor.
5	Low	High	Glazing cracks and window system fails catastrophically. Fragments enter space impacting a vertical witness panel at a distance of no more than 10 ft. from the window at a height greater than 2 ft. above the floor.

Chapter 3 Analytical and Numerical Methods

The general equations most suited to analyzing the window glass while undergoing a blast loading are the von Karman equations (1910). Equations 3.1 and 3.2 are coupled, non-linear, partial differential equations of the fourth order that describe the deflection of thin plates undergoing large deflection.

$$\frac{\partial^4 \Phi}{\partial x^4} + 2\frac{\partial^4 \Phi}{\partial x^2 \partial y^2} + \frac{\partial^4 \Phi}{\partial y^4} = Eh\left[\left(\frac{\partial^2 w}{\partial x \partial y}\right)^2 - \frac{\partial^2 w}{\partial x^2}\frac{\partial^2 w}{\partial y^2}\right] \quad \text{Eq 3.1}$$

$$\frac{\partial^4 w}{\partial x^4} + 2\frac{\partial^4 w}{\partial x^2 \partial y^2} + \frac{\partial^4 w}{\partial y^4} = \frac{1}{D}\left(p + \frac{\partial^2 \Phi}{\partial y^2}\frac{\partial^2 w}{\partial x^2} + \frac{\partial^2 \Phi}{\partial x^2}\frac{\partial^2 w}{\partial y^2} - 2\frac{\partial^2 \Phi}{\partial x \partial y}\frac{\partial^2 w}{\partial x \partial y}\right) \quad \text{Eq 3.2}$$

Where:

$w(x,y)$ is the deflection of the plate

Φ is the stress function

E is Young's Modulus

h is the plate thickness

p is the applied pressure

D is the flexural rigidity or $\frac{Eh^3}{12(1-\nu^2)}$

ν is Poisson's Ratio

Few theoretical studies have been conducted on laminated glass plates which add another layer of complexity to solving the above equations. Vallabhan extended this methodology for laminated plates using variational principles and verified it against experimental results from the Glass Research and Testing Laboratory at Texas Tech University (1993). The techniques used to solve the system of

equations are beyond the scope of this thesis. Numerical analysis, for this reason, is the preferred method investigating these problems.

3.1 Single Degree of Freedom Model

For structures undergoing blast loadings, the system is often represented with a simplified dynamic model called the single degree of freedom model, or SDOF, to predict the gross behavior of the structure. The SDOF method offers an efficient method to perform this analysis. Extension to the method can even offer insight into the overall damage level of a structure represented (Li and Meng, 2002). The key to this simplified dynamic model is making appropriate choices regarding how best to represent the system being analyzed. The process examines components and the loading scenario and abstracts those elements as a combination of springs and masses.

A blast resistant window can be reduced to a single mass and spring combination. The distributed mass of the window glass is replaced by a single equivalent point mass, at the center of the glass. The motion of the window can then be described in terms of the motion of this single coordinate operating at the midspan of the window. Ultimately the motion of the window can be described with Equation 3.3 and the application of the well known D'Alembert's Principle of dynamic equilibrium.

$$F(t) - ky - M\ddot{y} = 0 \qquad \text{Eq 3.3}$$

The term $F(t)$ refers to the externally applied loading. The spring force provided by the stiffness of the structure is represented by the term ky and the final term, $M\ddot{y}$ is the inertia of the system. Both the load term and the mass term must be modified to accurately describe the system as part of the SDOF modeling. In addition, the spring rate cannot be sufficiently described by a single constant spring rate. The preferred method is to replace the constant spring rate with a Static Resistance Function.

3.1.1 Static Resistance Function

Not all systems can be accurately represented in a SDOF model with a constant spring rate. Systems often exhibit non linear behavior such as the transition from elastic to plastic deformation. It is also true for composite structures that are designed to fail in a controlled fashion such as laminated glass windows. In these cases, the spring rate is replaced with a static resistance function.

The static resistance function is an approximate relation between the applied loading and the deflection it produces under static conditions. The slope of the curve at a point represents the spring rate at the moment. A representative static resistance function for an ideal laminated window made up of two panes of glass with an interlayer is shown in Figure 3.8 (Salim, 2010).

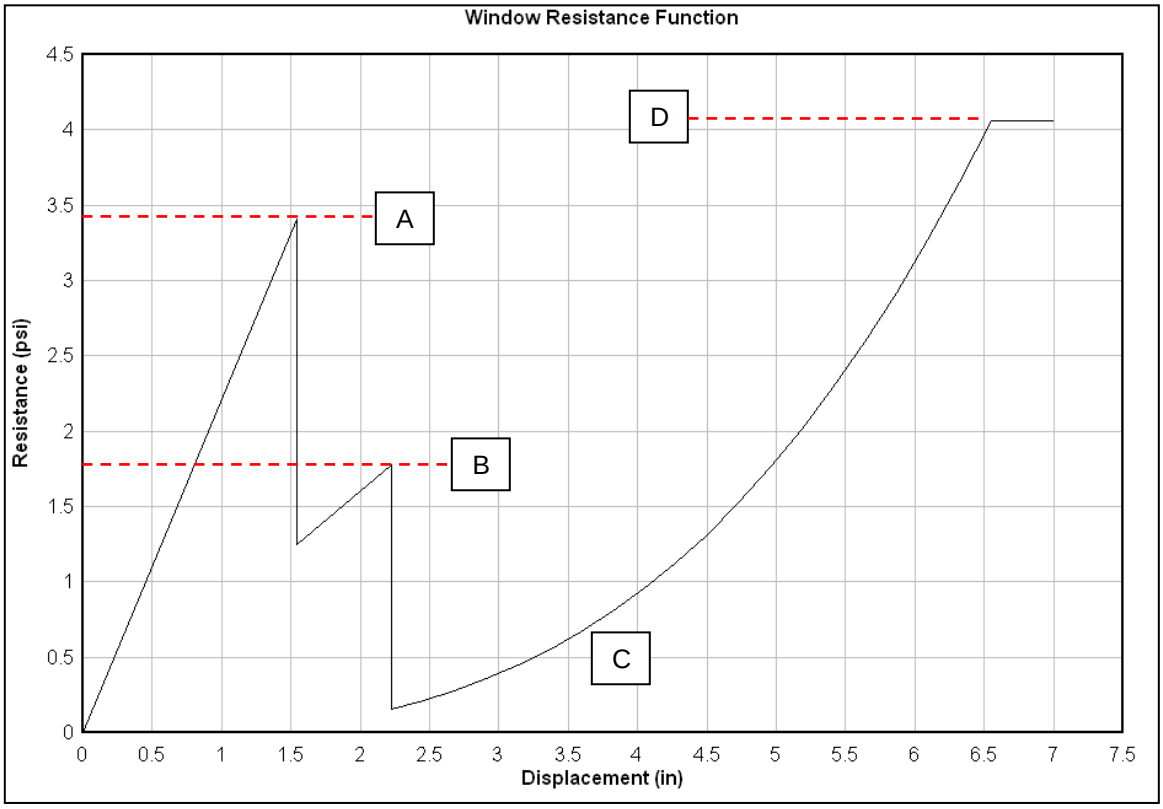

Figure 3.8 Idealized Static Resistance Function

Initially, the relationship is linear. This represents the laminated layers working together elastically. Once the elastic limit is reached, point A, the outer pane fails due to the formation of tensile cracks in the brittle glass. The resistance function then falls until the system is supported by just the inner glass. This single pane is capable of supporting the load up to its elastic limit, point B. Upon failure, the system then is supported by just the interlayer. This forms a tensile membrane much like an expanding balloon that continues to support the load along a non-linear load path. This continues until either it reaches its ultimate strength and bursts, denoted by point D, or the membrane is pierced by glass shards or other debris.

3.1.2 SDOF Model Parameters

A laminated glass window is immediately recognizable as a slab supported on all sides. The glazing, the material that bonds the glass to the window frame, is many times less stiff that either the glass or the framing material. It is reasonable to assume the window is simply supported at the edges. The procedures for converting such a simply supported slab into an equivalent SDOF model is straightforward (Biggs 1964). Table 3.4 indicates the necessary conversion factors for the laminated glass SDOF model.

Table 3.4 Laminated Glass SDOF Model Parameters

SDOF Model Parameters	
Applicable Strain Range	Elastic
Ratio of Sides, a/b	0.7
Load Factor, K_L	0.51
Mass Factor, K_M	0.37
Dynamic Reaction, Short Edge	0.05F + 0.13R
Dynamic Reaction, Long Edge	0.08F + 0.24R

3.1.3 SDOF Model Implementation

The SDOF model of the laminated glass window is implemented in Excel through the use of a numerical integration technique called the constant velocity method.

Through successive iterations the expected displacement for a given iteration is extrapolated from the previous iteration's position and acceleration. The derivation of the extrapolating function is as follows.

$$y^{(s+1)} = y^{(s)} + \dot{y}_{av}\Delta t \qquad \text{Eq 3.4}$$

The position of an object will change by the average velocity over the time interval, as in Equation 3.4. The average velocity can be approximated by Equation 3.5.

$$\dot{y}_{av} = \frac{y^{(s)} - y^{(s-1)}}{\Delta t} + \ddot{y}^{(s)}\Delta t \qquad \text{Eq 3.5}$$

The average velocity is equal to the change in position over the time interval plus the acceleration that occurs during that time interval. Combining the two formulae yields the following recurrence formula, as in Equation 3.6.

$$y^{(s+1)} = 2y^{s} - y^{(s-1)} + \ddot{y}^{(s)}(\Delta t)^2 \qquad \text{Eq 3.6}$$

The recurrence formula is not difficult to implement in Excel. The time interval can be made very small relative to the natural time period of the system and the changes in the loading function to minimize errors in the extrapolation. The inputs to the spreadsheet include the SDOF model parameters as seen in Table 3.1, the weight and area of the window, the load time function, and the static resistance function. The load time and static resistance function are both input as linear piecewise approximations to simplify calculations. Outputs include the expected window deflection at midspan and the reaction forces experienced by the supporting members. The spreadsheet is shown in Figure 3.9.

SDOF Model for 2 Way Slab Models
Chad Wedding

SDOF Model Parameters		
Calculation Time	0.015	s
Weight	59.8026	lbf
Delta time	1.5E-05	
Area	2649.06	in^2
Load Factor, K_L	0.51	
Mass Factor, K_M	0.37	

SDOF Model Output			
Max Deflection		1.1406	in
At Time		0.0066	s
Peak Reaction Force		7235.3	lbf
At Time		0.0061	s
Long Edge	Peak Reaction Force	2342.5	lbf
	Peak Loading	35.5	lbf / in
Short Edge	Peak Reaction Force	1275.5	lbf
	Peak Loading	26.6	lbf / in

Load Time Function	
Time (s)	Pressure (psi)
0	4.93
0.0066	0
0.0097	-0.88
0.0127	0

Static Resistance Function		
Deflection (in)	Pressure (psi)	Region
0	0	1
0.26	0.17	1
0.43	0.341	1
0.56	0.511	1
0.76	0.85	1
0.84	1.02	1
0.91	1.19	1
1.04	1.53	1
1.15	1.88	1
1.29	2.39	1
1.38	2.72	1
1.47	3.07	1
1.54	3.41	1
1.55	0.05	2
1.77	0.08	2
2	0.115	2
2.9	0.355	2
3.59	0.665	2
4.27	1.125	2
4.96	1.76	2
5.64	2.59	2
6.32	3.65	2
7	4.97	2
		3
		3

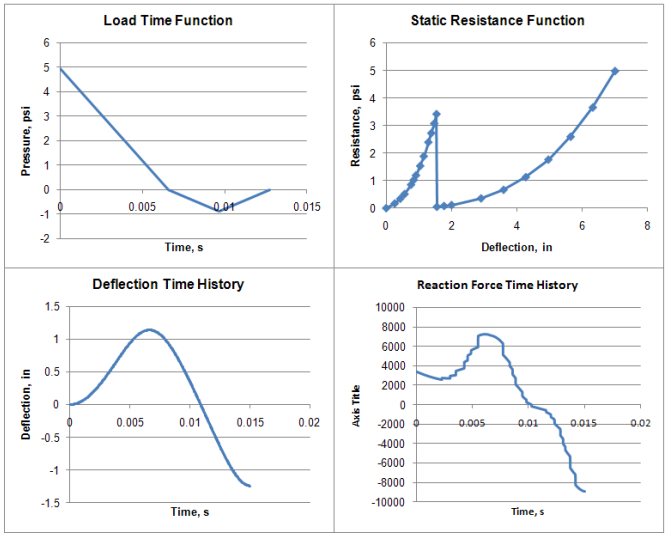

Input Parameters				SDOF System Dynamics				Reaction (lbf)		
Time (s)	Force (psi)	Force (lbf)	Region	k	R	ÿ	y	Long Edge	Short Edge	Total
0	4.93	13060	1	0.65385	0	116191.6	0	1044.8	652.99	3395.6
2E-05	4.918789	13030	1	0.65385	0.0226	115927	1E-05	1042.4	651.51	3387.9
3E-05	4.907577	13000	1	0.65385	0.0905	115661.6	5E-05	1040.1	650.04	3380.2
5E-05	4.896366	12971	1	0.65385	0.2034	115395.4	0.0001	1037.7	648.57	3372.6
6E-05	4.885155	12941	1	0.65385	0.3612	115128.4	0.0002	1035.4	647.1	3364.9
8E-05	4.873943	12911	1	0.65385	0.564	114860.7	0.0003	1033	645.64	3357.4

Figure 3.9 SDOF Spreadsheet

3.2 HazL

HazL, short for Window Fragment Hazard Level Analysis, is a tool produced by the United States Army Corps of Engineers Protective Design Center (HazL, 1998). It performs a SDOF analysis to calculate the glazing response to a blast event using the same techniques detailed above. With the response calculated, it then applies a debris transport model to predict the trajectory of the fragments formed. Such information is crucial for assessing the performance of a blast resistant window system. The intended users are engineers or architects with varying levels of experience with blast resistant design. With an experienced user, it is appropriate for the final design of blast resistant window systems, but experimental validation is still preferred.

HazL is applicable over a wide range of window systems, covering nearly every system commonly encountered in the market. It can accommodate monolithic glass or plastic windows, laminated windows, insulated glass units and anti-shatter film retrofits of existing windows. Unfortunately, the program is somewhat dated and doesn't include the full range of popular laminating materials such as Uvekol. Users input the geometry, glazing type, and material for the window along with the parameters for the blast event. The system uses this information to then calculate the response. The user interface can be seen in Figure 3.10.

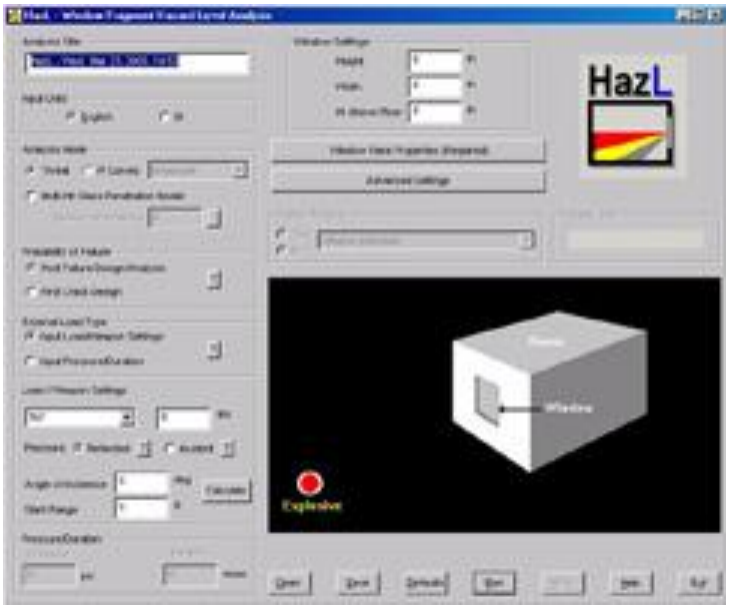

Figure 3.10 HazL User Interface

The window under test will be modeled in HazL. The expected response can then be compared to experimental data. The Static Resistance Function generated from HazL will also be used as the input for the SDOF spreadsheet developed independently.

3.3 Finite Element Analysis Model

The blast resistant window undergoing a blast loading was modeled in ANSYS Explicit Dynamics. The software package is well known in the field of blast related modeling for its ability to handle high strain rates and large deformations. The hope

was to obtain some additional insight into some of the more subtle aspects of the window's response, including the distribution of stress and strain throughout the part.

The window to be modeled and experimentally tested is a laminated unit consisting of two panes of 3 mm heat strengthened glass. The two layers are bonded together with a liquid called Uvekol from Cytec Industries. A shallow layer, 1.5 mm in thickness, is pumped between glass layers and cured in a UV oven. The resulting solid polymer layer bonds the glass together, increasing its strength, and locks the fragments safely in place in the event the window fractures. Structural silicone glazing secures the laminated glass to the extruded aluminum frame. The material properties for the various components are covered in greater detail in the following sections.

The geometry for the window to be modeled can easily be recreated within the Design Modeler module of ANSYS 12. The glass and interlayer are obviously represented by rectangular cuboids. The silicone glazing material is be represented by an approximate shape, a U shaped box surrounding the perimeter. Modeling the shape of the silicone as dispensed would be a needlessly tedious task and add little to the value of the model. The final geometry can be seen in Figure 3.11.

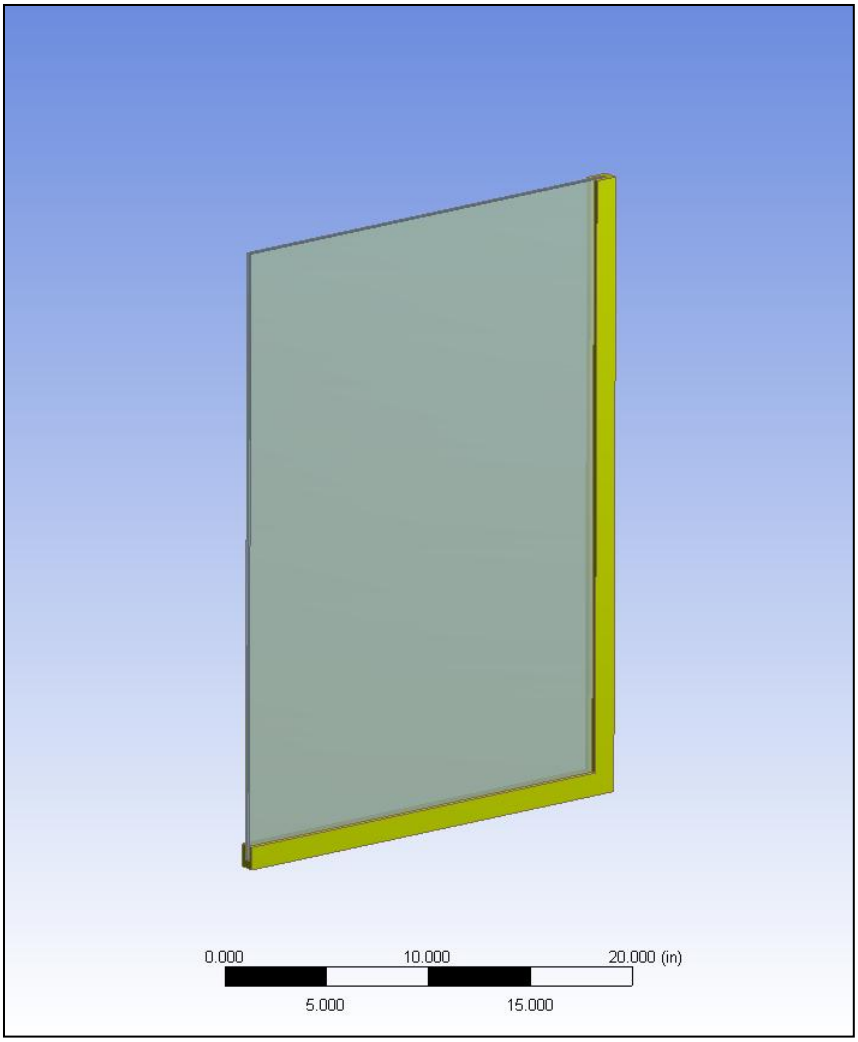

Figure 3.11 Window Glass Model

3.3.1 Window Glass Modeling Parameters

Glass is a well studied material. The prevailing model for the material is isotropic linearly elastic. The necessary parameters for the model include density, Young's Modulus, and Poisson's Ratio. Within the literature are a narrow band of values, of which median values were chosen in order to be conservative.

The failure mode for glass follows Griffith's work on brittle materials. The theory, with much of the experimentation completed on glass from an English test tube manufacturer, predicts failure to occur due to tension concentrating at small imperfections naturally occurring in the material. These small cracks then grow

leading to failure in the manner consistent with brittle materials (Griffith, 1921). As an aside, this is the very defect that heat strengthening and tempering hope to overcome. These techniques rapidly cool heated glass in a controlled fashion. In this way, residual compressive surface stresses are induced that act in quasi-uniform biaxial compression. This residual stress must be overcome before tensile cracks can form. It follows then that heat strengthened laminated glass has a mean failure strength 2.5 times higher than monolithic annealed glass (Norville et al., 1993). As with the elastic parameters, the literature includes a range of values for the maximum tensile stress and maximum principle strain. The values used for modeling the material properties of the glass is summarized in Table 3.5.

Table 3.5 Glass Modeling Parameters

Glass Modeling Parameters		
Density	2,500	kg/m^3
Young's Modulus	70	Gpa
Poisson's Ratio	0.23	
Maximum Tensile Stress	168.0	MPa
Maximum Principle Strain	0.0024	

The glass sheets are modeled using 8-noded solid elements, as opposed to shell or surface elements. The Map Faced Meshing technique is applied to break the glass plane into a regular array of rectangular elements. A Body Sizing Mesh technique manages the size of the elements generated, which contributes significantly to the computation time required to solve the finite element analysis.

3.3.2 Interlayer Modeling Parameters

The interlayer of the laminated glass is composed of Uvekol A. The material's intended application is noise suppression in a laminated window. The layer serves to decouple the inner and outer panes of glass reducing the sound transmission efficiency, effectively dampening the external noise (Vargas, 2006). Unfortunately, this material is underrepresented in the literature.

With little information available on the material properties of Uvekol A, the interlayer material was replaced with polyvinyl butyral, PVB. PVB film has been used in the

glass trade since the late 1930s. Its performance in laminated glass applications is well known so material data is readily available.

The interlayer material properties are most significant after the glass has cracked. When the glass cracks, the interlayer is expected to behave in a plastic fashion in order to absorb as much of the energy from the blast event as possible. The interlayer also serves to retain the window fragments, lest they become hazardous projectiles (Leitch, 2005). The intent of this model is to only reproduce the window performance up to the point of initial crack formation. The exchange of materials plays a small role in this case. Some researchers go as far as removing the laminate when performing similar modeling exercises (Weggel and Zapata, 2008).

Larcher et al. espouse an elastic-plastic material law for PVB in this application (2009). This includes Young's Modulus, density, Poisson's ratio, yield stress, and tangent modulus. There is no specific failure theory associated with the PVB because the model does not extend past the initial crack formation. A large strain value of 2 was selected for the failure criteria. The values used in this model are in Table 3.6.

Table 3.6 Interlayer Modeling Parmeters

PVB Modeling Parameters		
Density	1,100	kg/m^3
Young's Modulus	220	MPa
Poisson's Ratio	0.495	
Yield Stress	28	MPa
Tangent Modulus	1.0	Pa
Maximum Principle Strain	2.0	

The interlayer is modeled as a thin shell. The elements are 4-noded quadrilateral elements. The same techniques as used with the glass elements were applied here to generate a regular array with elements of the preferred size.

3.3.3 Structural Silicone Glazing Modeling Parameters

The modeling of the structural silicone glazing, SSG, proved the most challenging portion of the modeling exercise. At the onset of the effort, it was decided not to include the aluminum frame that supports the glass. There is a limited number of element and nodes available in a problem formulation in the student version of ANSYS Explicit Dynamics. Keeping the number of parts modeled to a minimum would circumvent this obstacle. The aluminum, in a sense, was fixed as a rigid part. This is not entirely a safe assumption, as the stiffness of aluminum is equal to that of glass at 70 GPa.

Researchers versed in the practice have addressed this need in their own manner. One common technique described in the literature is to abstract the system entirely as a system of springs (Vallabhan et al., 1997). The SSG is resolved as three springs acting opposed to the deflection of the window glass. This is best seen in Figure 3.12. The displacement of the window edges is opposed by springs K_w and K_h while the rotation of the window is opposed by spring K_m.

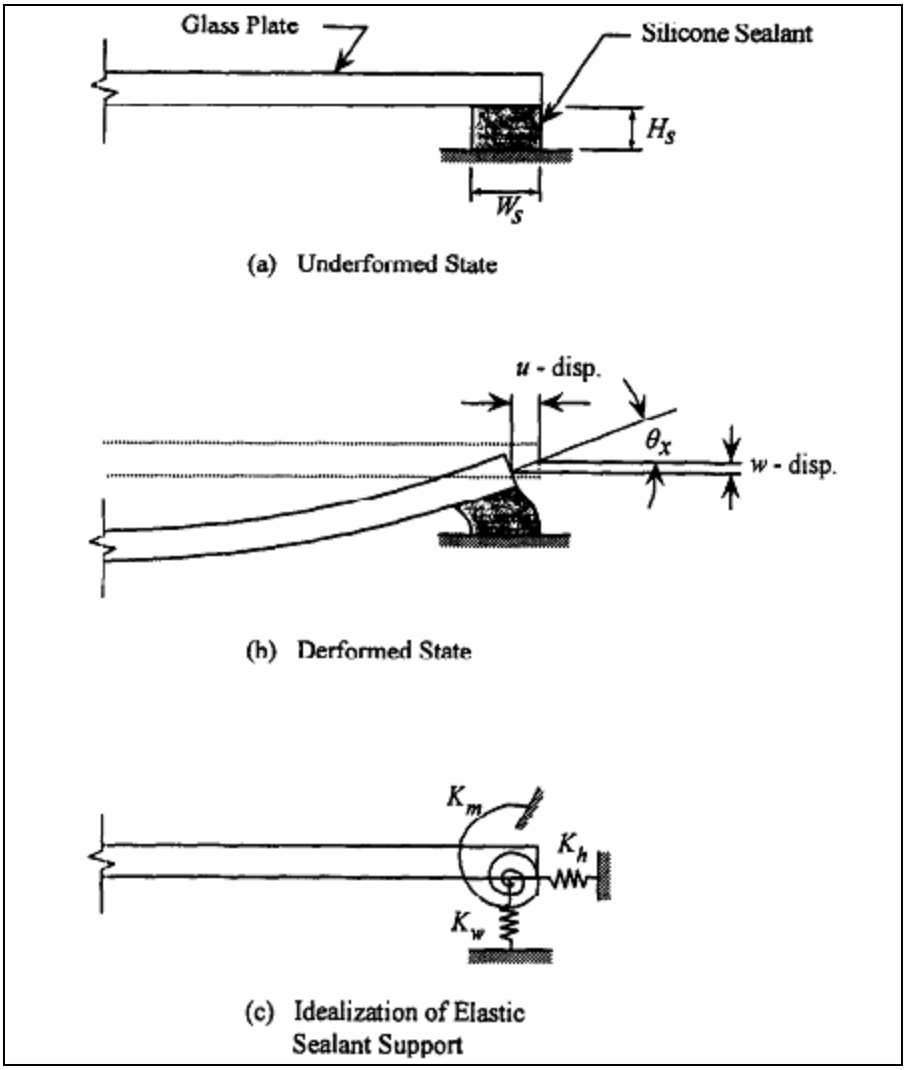

Figure 3.12 Structural Silicone Glazing from Vallabhan et al. 1997

A similar approach was undertaken for this project. The implicit behavior of the SSG and the aluminum frame was modeled as opposed to the explicit material and failure models. Spring elements like those above are unavailable in ANSYS Explicit Dynamics. The course of action required assuming material properties for the silicone material close to those found in the literature and then making fine adjustments to bring the model into close agreement with the experimental data.

It would be preferable to make detailed material studies at the rate of loading as experienced during a blast, but such an undertaking is beyond the scope of this thesis. The resulting material properties used to mimic the implicit behavior of this joint are as follows in Table 3.7.

Table 3.7 Silicone Modeling Parameters

Silicone Modeling Parameters		
Density	1,100	kg/m^3
Young's Modulus	10.4	MPa
Poisson's Ratio	0.495	
Yield Stress	28	MPa
Tangent Modulus	1.0	Pa
Maximum Principle Strain	2.0	

3.3.4 Convergence Study

A convergence study was conducted to determine the influence of glass element size on the results. The window as modeled was subjected to an idealized blast wave while varying the element size. The blast wave had a peak pressure of 29.0 kPa and an impulse of 144.8 kPa·ms. Peak deflection at the center of the window was used to measure the convergence. An element size of 2.54 cm was found to be sufficient for the modeling with a change of only 0.2% when decreasing the element size from 3.05 cm to 2.54 cm. The results are summarized in Figure 3.13.

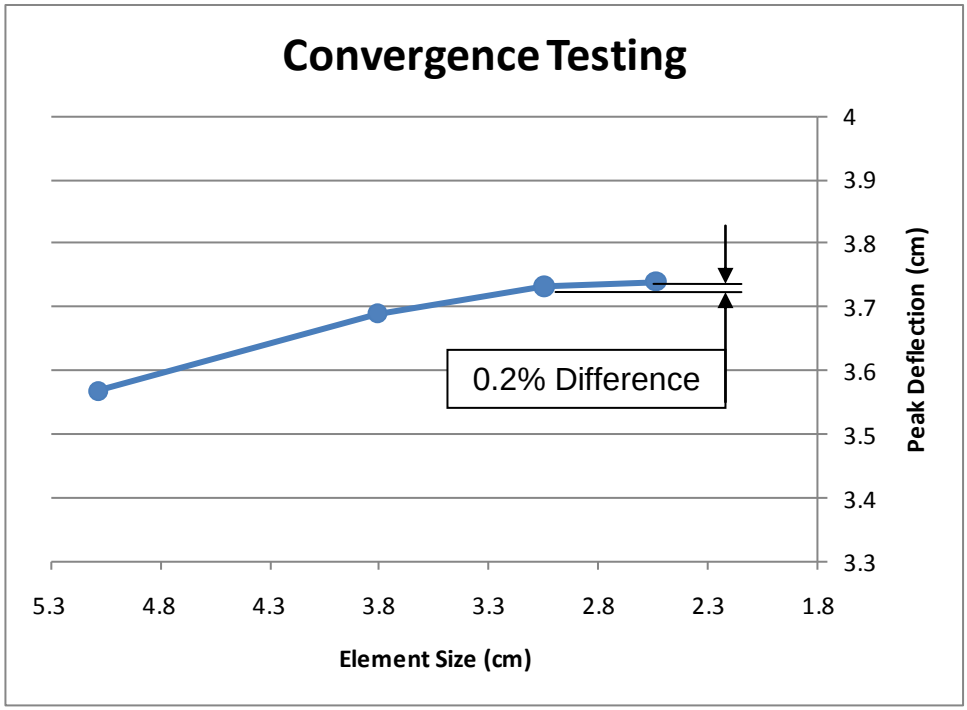

Figure 3.13 Convergence Testing Results

Chapter 4 Instrumentation and Equipment Design

The characterization of a blast resistant window undergoing a blast loading requires overcoming a number of instrumentation challenges. Blast loadings are highly dynamic events usually lasting a few milliseconds, but during that time an enormous amount of energy is released. This plays havoc with systems and presents a unique and challenging opportunity for the investigator.

4.1 Pressure Time History Measurement

The pressure time history of the blast event is characterized via the use of dynamic pressure sensors from PCB Piezotronics, model 102B18. The sensors used during the testing were specifically designed with this purpose in mind with very high frequency, nearly non-resonant response. The sensing element is a small quartz piezoelectric element which is paired with the appropriate embedded signal amplifier. Some of the more important characteristics are listed in Table 4.8 for reference.

Table 4.8 Flush Mount Pressure Sensor Attributes

Pressure Sensor Attributes		
Measurement Range	± 344	kPa
Sensitivity (± 15%)	14.7	mV / kPa
Resolution	6.89	Pa
Resonant Frequency	≥ 500	kHz
Rise Time (Reflected)	≤ 1.0	µ sec
Output	± 5	V
Discharge Time Constant	≥ 1.0	sec

The intended application is to flush mount the device within, or in close proximity to, the specimen under test. It is readily apparent that the sensors must be placed on either side of the window during testing. With two sensor channels available for pressure measurements, two points to either side of the vertical span were chosen. These are located at the midpoint of the window frame. This can be seen in Figure 4.14.

Figure 4.14 Pressure Sensor Placement

Nylon nuts are threaded onto the sensor and then press fitted into holes drilled in the trim surrounding the window. The sensors are placed flush to the surface of the wood which is in turn aligned to the plane of the window glass, as seen in Figure 4.15.

Figure 4.15 Flush Mount Sensor within Trim

4.2 Window Deflection Measurement

Window deflection characterization is accomplished through the use of a laser distance gauge. The gauge, built by Acuity Laser Measurement, offers the ability to record non-contact measurements that have the necessary speed and accuracy for blast loadings. The sensor functions by bouncing a visible laser beam off of the specimen under test. The reflected laser light from the target is captured by a CMOS sensor spaced a known distance from the laser source. The internal microprocessor then calculates the distance based upon the flight time of the laser light and the geometry.

Table 4.9 Laser Distance Gauge Attributes

Acuity Laser Gauge Attributes		
Measurement Range	± 63.5	cm
Measurement Distance	142	cm
Resolution	1	mm
Sample Rate	9.4	kHz
Laser Power	20	mW
Output	0-10	V

For the purposes of measuring the deflection in the window, the sensor is placed upon a tripod at a height of interest. The tripod is set at the preferred measurement distance from the window and aimed at a center of the window. White duct tape provides a good surface to reflect the laser light to the sensor head. In order to protect the laser distance gauge from flying debris in the event of a window failure, the tripod is placed to one side of the window. Familiar trigonometric identities are used to adjust the sensor output to reflect the window's movement. The placement of the sensor can be seen in Figure 4.16.

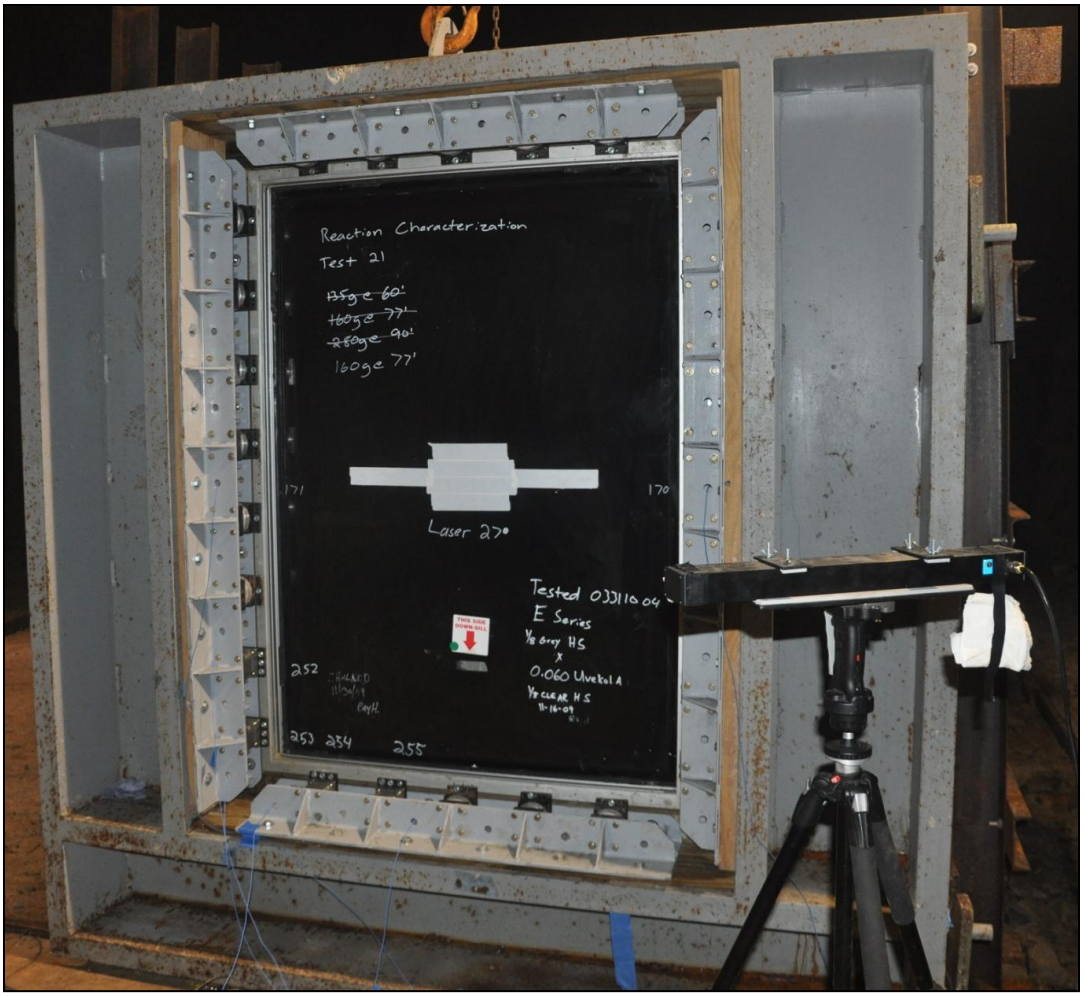

Figure 4.16 Laser Distance Gauge Placement

4.3 Window Reaction Force Measurement

The major challenge and the focus of the effort concerned measuring the reaction forces at the perimeter of a window during a blast loading. The research group had significant experience with the other measurement types and the challenges therein are well known. Reaction force measurements were a new undertaking.

PCB Piezotronics are one of the acknowledged leaders in the realm of dynamic force measurements. They were selected to provide an appropriate solution for measuring the expected reaction forces that would be compatible with the equipment already owned. The model 261A03 triaxial force link was selected for

the application. As a force link, it includes a calibrated reaction structure eliminating the need to establish the correct preloading during installation and allows forces to be measured directly. The Z axis measures applied tension, compression, and impact forces while the remaining two axes report the shear force to which the reaction structure is subjected. It includes sufficient measurement range for this and future applications. An extremely high upper frequency limit allows it to capture the event as it rapidly unfolds. A summary of the relevant attributes are available in Table 4.10.

Table 4.10 Triaxial Force Sensor Attributes

Triaxial Force Sensor Attributes		
Measurement Range (z axis)	± 44.5	kN
Measurement Range (x, y axis)	± 17.8	kN
Sensitivity (± 20%) (z axis)	0.056	mV / N
Sensitivity (± 20%) (x, y axis)	0.281	mV / N
Resolution (z axis)	0.222	N - rms
Resolution (x, y axis)	0.044	N - rms
Upper Frequency Limit	10	kHz
Stiffness (z axis)	7	kN / μm
Stiffness (x,y axis)	2.6	kN / μm
Output (z axis)	± 2.5	V
Output (x, y axis)	± 5	V

Per the window manufacturer's instructions, blast resistant windows are secured to the supporting members at 20 cm intervals around the entire perimeter of the window. For the size of window used in the course of this investigation, there are 26 points that need to be securely fastened to support members. Due to the high cost of each triaxial force sensor, it was infeasible to place a sensor at every attachment point. This placed a few design constraints on the experimental apparatus that would need to be met for testing.

- Attachment points consistent with the bolt pattern on the triaxial force sensor need to be defined.
- It should be easy to move sensors between the different attachment points with the window installed.

- Proxy sensors should be built to place in the unoccupied attachment points.
- Proxy sensors should minimally affect the sensor readings.
- Test apparatus should be consistent with the buck system in place at the shock tube testing facility.

4.4 Sensor Bracket Design

The sensor bracket provides the necessary attachment points around the perimeter of the window. The final bracket design can be seen in Figure 4.17. It represents one of the brackets used at the top and bottom of the window. The triaxial force sensor is shown populating one of the five available locations spaced on eight inch intervals. The bracket used along the vertical sides is nearly identical in design except capable of accepting eight sensors locations.

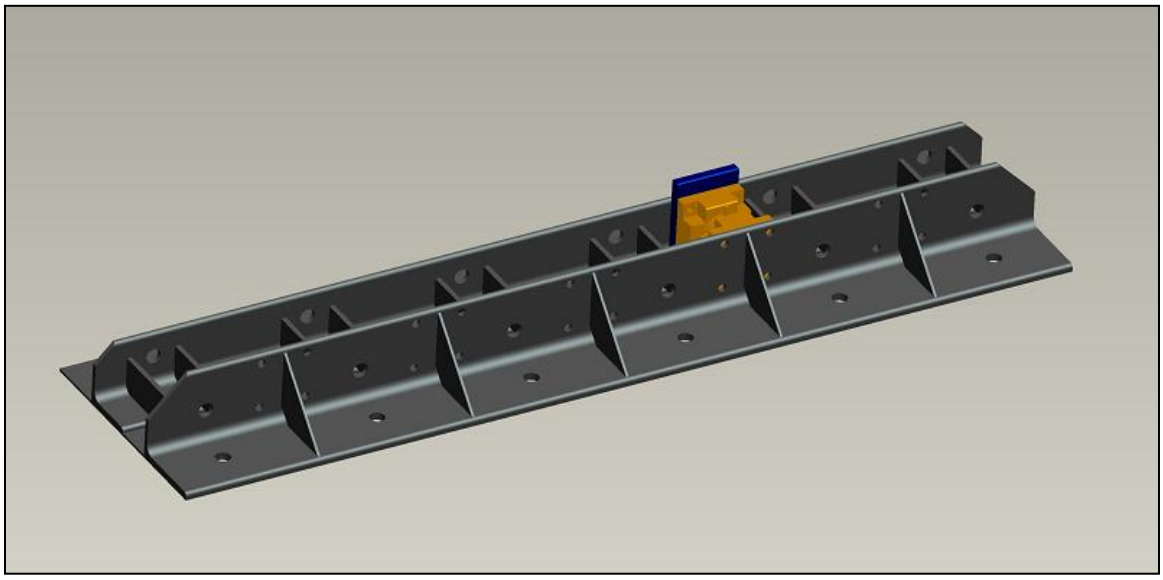

Figure 4.17 Sensor Bracket

4.5 Proxy Sensor

The proxy sensor was designed in ANSYS Workbench. The bolt pattern from the triaxial force sensor was duplicated to ensure compatibility when moving them around the perimeter of the window. The static stiffness was established through finite element analysis and design iterations were tested until the static stiffness matched the characteristics of the sensors it would imitate. The resulting geometry is shown in Figure 4.18. The final design consisted of three parts bolted together with a defined preload of 4.45 kN. The upper and lower halves are steel parts, while the inner ring is an aluminum part which provides the desired stiffness.

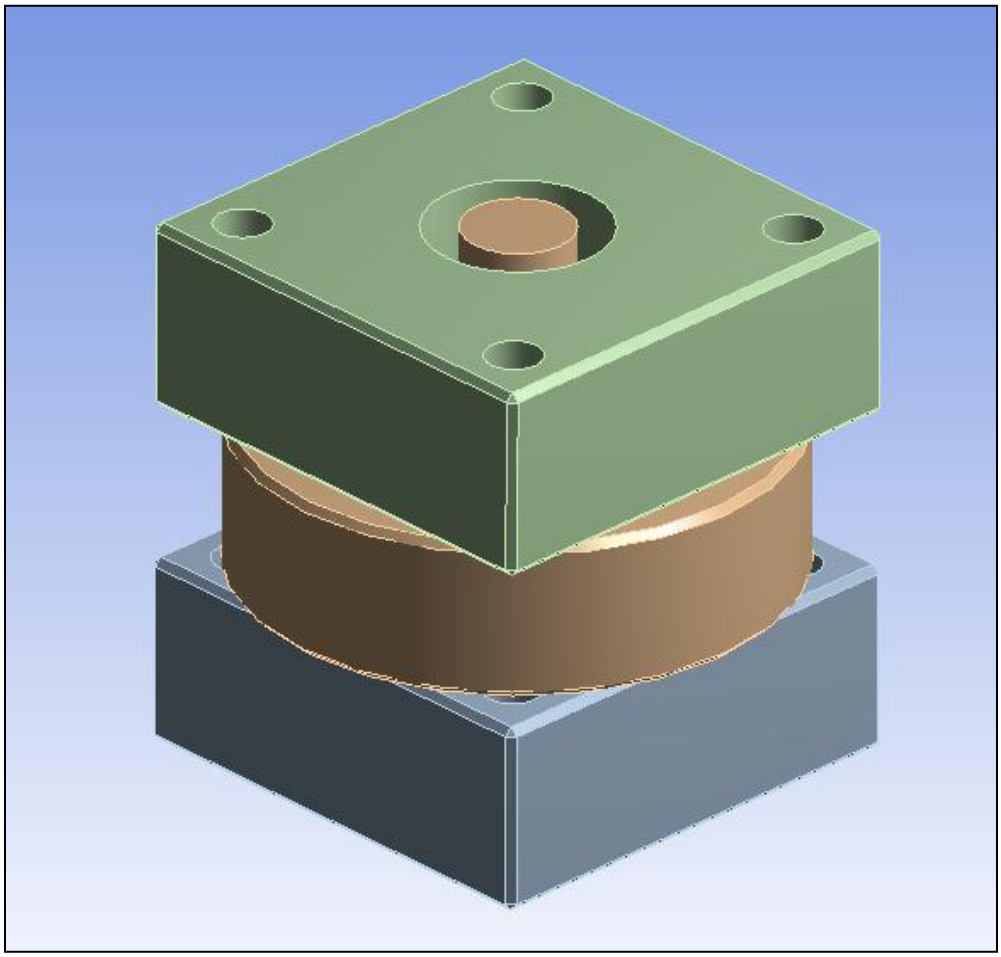

Figure 4.18 Proxy Sensor

The desired stiffness along the z axis was 7 kN per µm. This was tested by applying a 17.8 kN load which should result in 2.55 µm of deflection. As seen in Figure 4.19, this target is met very uniformly across the top of the part.

The X and Y axis was verified in a similar fashion. The desired stiffness was 2.6 kN per µm. The deflection was slightly higher than desired, but still within a ten percent margin, as seen in Figure 4.20.

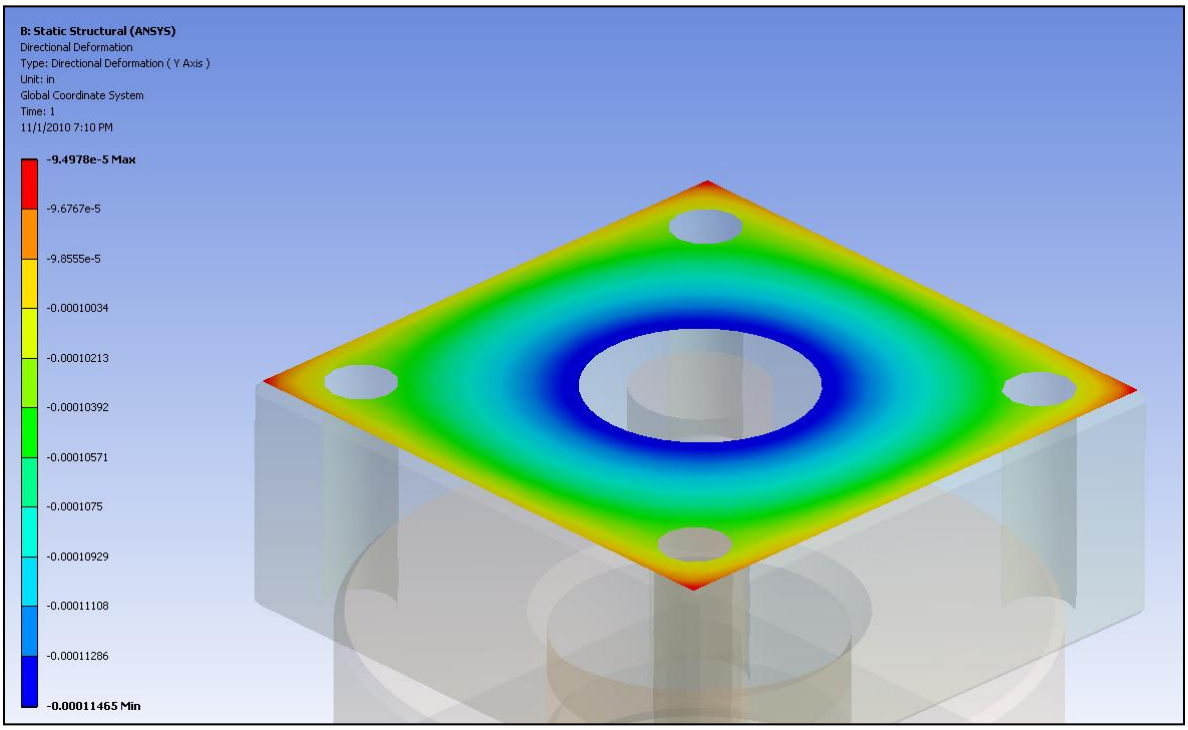

Figure 4.19 Proxy Sensor Z Axis Stiffness

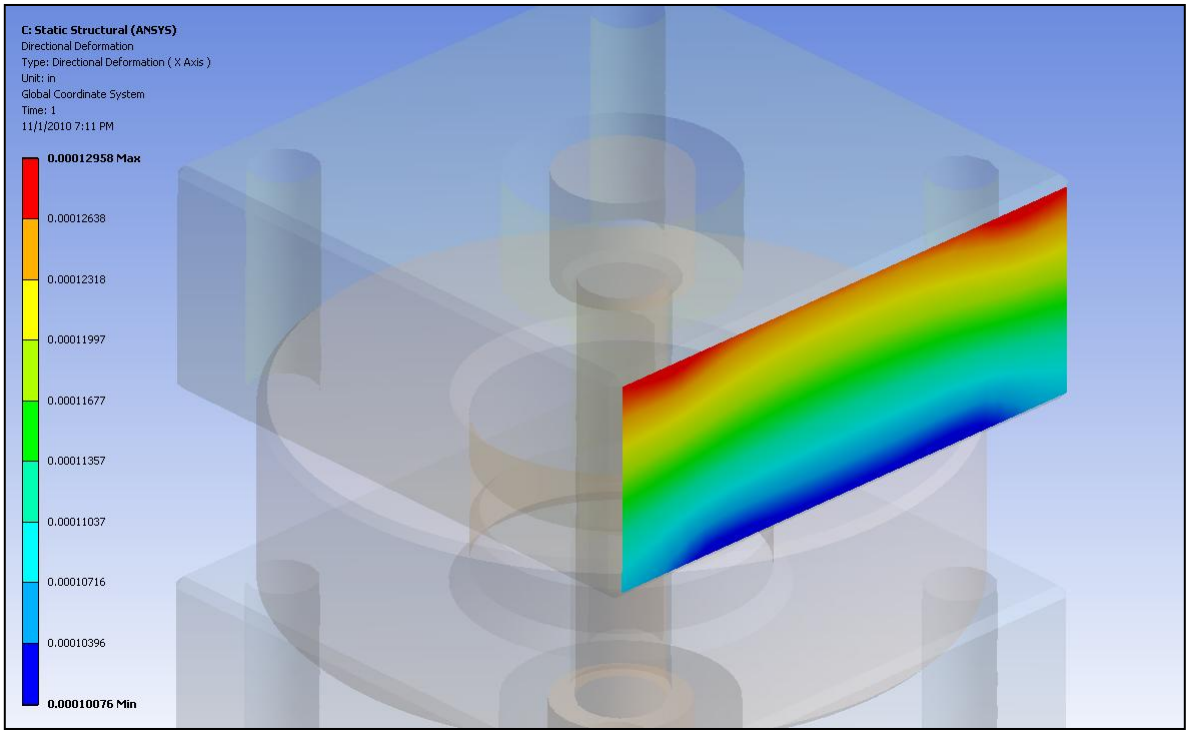

Figure 4.20 Proxy Sensor X, Y Axis Stiffness

4.6 Buck Design

The buck is an interchangeable frame that facilitates setting the shock tube up for different test conditions. The buck hangs from the end of the shock tube on pins at the corner of the buck. These mate to saddles located at the end of the shock tube. In this manner, bucks can be easily exchanged for one another to accommodate different tests. The buck for this testing only required an adjustment to the interior dimensions.

The completed buck, awaiting testing, is shown in Figure 4.21. The sensor brackets are readily seen bolted to the buck. The sensors and proxy sensors are in place and fastened to the window.

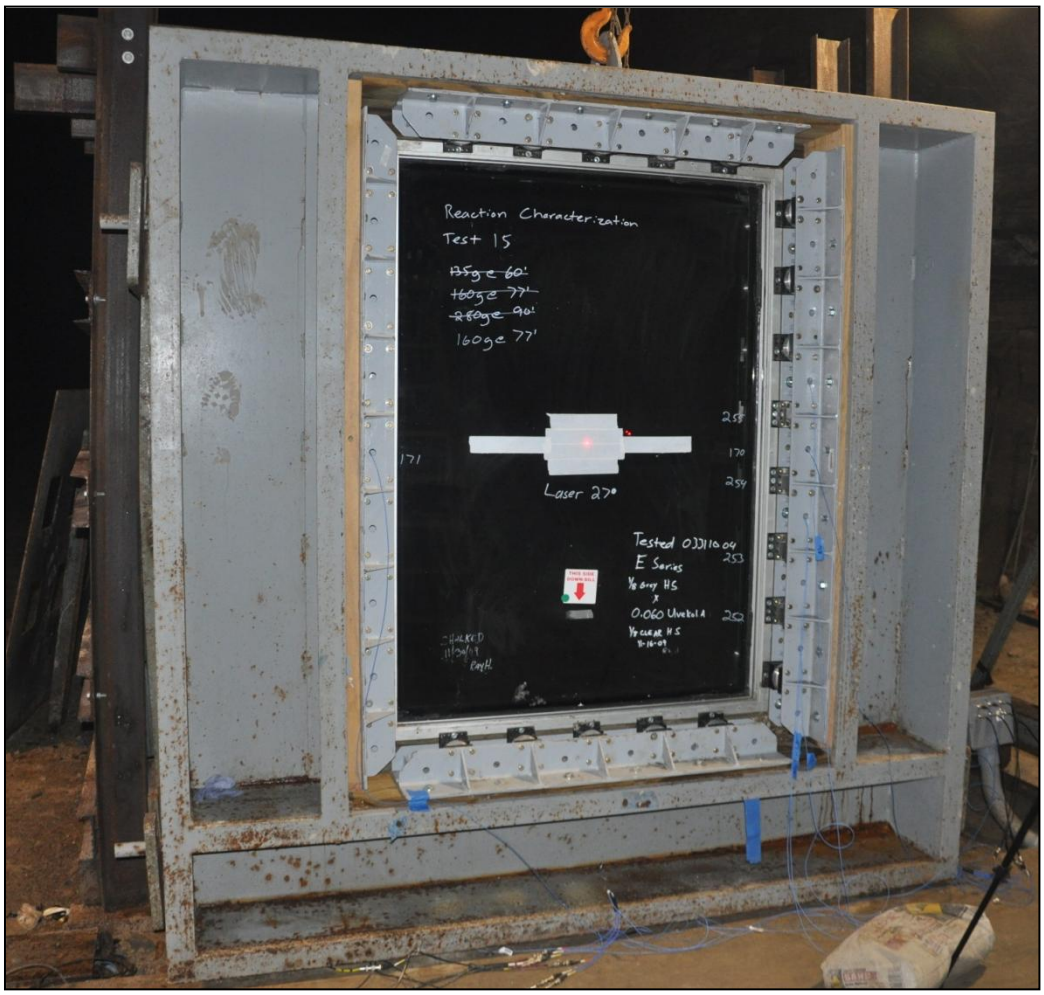

Figure 4.21 Completed Buck

4.7 Supporting Electronics

The various sensors and signals were coordinated with a pair of digital acquisition devices from MREL Group of Companies Limited. The Datatrap II is a standalone ruggedized data recorder capable of measuring eight channels of input, at rates of up to 10 MHz. Two data recorders were used during the course of this testing, with the pair interconnected for synchronous triggering and acquisition. This provided 16 channels for use during the testing.

A model 481A signal conditioner from PCB Piezotronics served as the interface between the sensors and the Datatraps. It provides the necessary voltage and current to power the pressure and force sensors. It warns for any input faults and protects against overloads before sending the signal to the Datatrap.

Chapter 5 Experimental Methodology

The stated goal of this research project is to characterize the behavior of a blast resistant window undergoing a blast loading. This activity was broken into three distinct phases. Reaction forces measurements were taken around the entire perimeter during successive shots. Second, the force sensors were placed at either side of the midspan along the long edges, where the reaction was expected to have the highest magnitude. Repeated testing was performed to judge the repeatability of the measurements. Finally, the charge size was increased to the point of failure to measure the window behavior after it fractures.

5.1 Explosive Protocol

Care was taken to ensure that the explosives used during the course of the investigation were handled in a safe manner. All applicable federal regulations were observed. Finally, all explosive product was used under the supervision of a licensed blaster.

The explosive product used in the testing was desensitized RDX. Charges are weighed on a electron gram balance to the nearest tenth of a gram. They are then placed in a nitrile glove and formed into a spherical charge into which the electric detonator is placed. The charge is then hung in the cannon that sits within the shock tube. The cannon, a 0.6 m diameter pipe with a substantial wall thickness, serves to direct the blast along the length of the shock tube thereby sparing the walls of the shock tube from the most intense region of the blast. This is seen in Figure 5.22.

Figure 5.22 Explosive Charge within Cannon

5.2 Perimeter Testing

The attachment points were assigned labels starting in the bottom left corner, proceeding in clockwise fashion, with the letters A to Z as seen in Figure 5.23. Beginning with sensors placed in positions A through D, three tests were completed with a charge weight of 160 grams at a standoff distance of 23.5 m. After completing each trio of blasts, the sensors were exchanged with proxy sensors at points not yet tested. In this manner, the entire perimeter was tested over the course of 21 tests. These are referred to in the following manner:

- Setup A – positions A, B, C, and D populated
- Setup B – positions E, F, G, and H populated
- Setup C – positions I, J, K, and L populated
- Setup D – positions M, N, O, and P populated
- Setup E – positions Q, R, S, and T populated
- Setup F – positions U, V, W, and X populated
- Setup G – positions Y, Z, A, and B populated

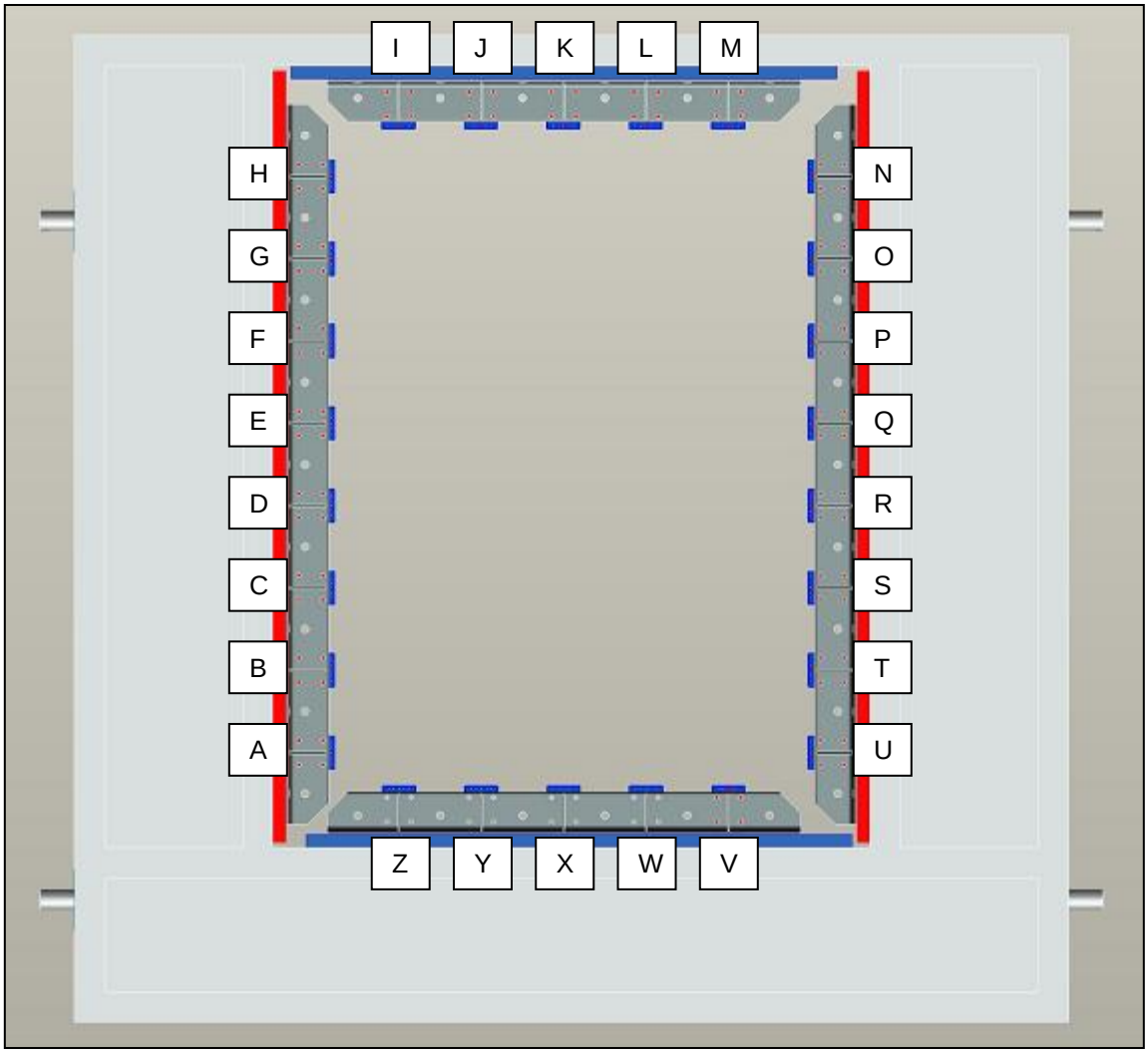

Figure 5.23 Attachment Point Labels

5.3 Repeatability Testing

For the repeatability testing, force sensors were placed in setup H, with sensors at locations D, E, Q, and R. These were chosen because of the expectation that the highest reaction forces would be encountered at these locations. The cannon was advanced to a standoff distance of 21 m and the charge weight was increased to 230 grams. The window was then tested 9 times at this new, more severe blast loading.

5.4 Test to Window Failure

The sensors were left in setup H and the cannon remained at a distance of 21 m. The charge weight was increased until the window fractured. The hope was to initiate fracturing without the subsequent failure of the tensile membrane that forms when the interlayer stretches under loading.

Two shots were required to cause breakage. The charge weight was first increased to 300 grams from 230 grams. This was then increased to 400 grams for the final shot.

Chapter 6 Perimeter Testing Results and Analysis

6.1 Pressure Results

As mentioned previously, the charge size for the perimeter testing was 160 grams of desensitized RDX at a standoff distance of 23.5 m. Figure 6.24 shows a representative pressure time history for the blast from test record 20. Test record 20 was very close to the average pressure and impulse for the suite of 21 tests. The two channels used to characterize the blast wave are shown, along with the impulse or the integral of pressure over time. There is a small bias with impulse measured by channel 1 being 2% higher on average.

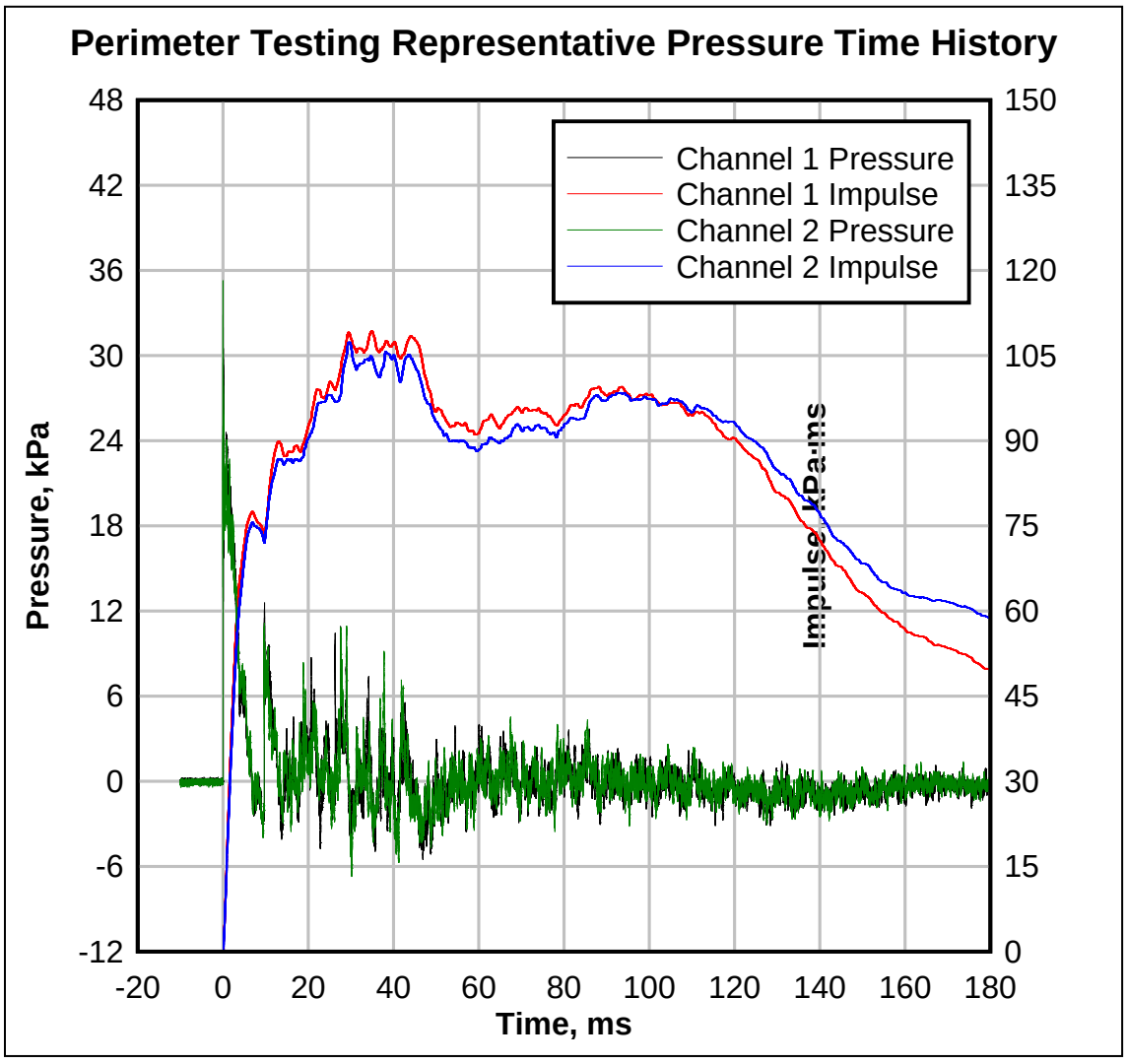

Figure 6.24 Representative Pressure Time History

The results for the entire suite of 21 tests is summarized in Table 6.11. Summary statistics are also included, which includes the average, standard deviation and a measure of process capability. The process capability index, C_{pk}, is a measure of the repeatability of a process (NIST 2003). It is calculated via Equation 6.7, for a one sided process such as this. A 10 percent tolerance is assigned to the values to enable the calculation.

$$C_{pk} = \frac{(\hat{\mu} - Lower\ Limit)}{3\hat{\sigma}} \qquad \text{Eq 6.7}$$

Table 6.11 Perimeter Testing Pressure Values

Blast Event		Positive Phase						Negative Phase					
Target Type	Record	1	2	Peak Pressure (kPa)	1	2	Impulse (kPa·ms)	1	2	Peak Pressure (kPa)	1	2	Impulse (kPa·ms)
Window	2	31.8	40.5	36.1	111.6	108.2	109.9	-6.2	-6.2	-6.2	-20.2	-21.9	-21.0
Window	4	34.2	38.7	36.4	115.5	113.5	114.5	-5.9	-6.0	-5.9	-19.4	-21.3	-20.4
Window	5	28.8	31.7	30.3	110.7	113.0	111.9	-6.4	-5.3	-5.9	-18.4	-21.2	-19.8
Window	6	32.3	29.9	31.1	115.1	111.0	113.1	-6.7	-6.3	-6.5	-19.6	-18.2	-18.9
Window	7	31.1	36.9	34.0	112.4	111.1	111.8	-5.5	-6.8	-6.1	-16.0	-18.1	-17.0
Window	8	30.6	29.7	30.1	113.4	110.6	112.0	-5.9	-6.3	-6.1	-16.9	-18.2	-17.6
Window	9	33.7	30.0	31.8	118.0	114.9	116.4	-6.6	-6.5	-6.5	-19.6	-19.3	-19.4
Window	10	31.5	39.1	35.3	112.7	111.9	112.3	-6.0	-6.2	-6.1	-17.3	-18.1	-17.7
Window	11	34.2	40.0	37.1	113.5	111.7	112.6	-5.5	-5.7	-5.6	-17.9	-18.5	-18.2
Window	12	36.2	31.8	34.0	114.6	112.4	113.5	-6.3	-6.9	-6.6	-18.3	-20.3	-19.3
Window	13	32.3	40.3	36.3	115.4	116.6	116.0	-5.4	-5.8	-5.6	-16.5	-16.4	-16.4
Window	14	31.2	40.2	35.7	118.5	114.5	116.5	-5.7	-6.4	-6.0	-17.3	-17.9	-17.6
Window	15	32.8	42.9	37.9	115.6	113.3	114.5	-6.3	-5.8	-6.0	-18.2	-19.0	-18.6
Window	16	31.9	40.9	36.4	112.9	109.7	111.3	-5.2	-5.7	-5.4	-16.1	-17.2	-16.6
Window	17	31.1	36.0	33.6	109.9	107.7	108.8	-5.1	-5.9	-5.5	-16.5	-17.9	-17.2
Window	18	33.1	41.7	37.4	117.2	113.4	115.3	-5.8	-6.2	-6.0	-18.4	-20.1	-19.3
Window	19	30.3	33.0	31.7	112.7	110.1	111.4	-6.1	-6.9	-6.5	-17.8	-19.5	-18.7
Window	20	31.9	35.3	33.6	109.3	107.4	108.3	-5.5	-6.7	-6.1	-18.3	-19.3	-18.8
Window	21	31.0	34.3	32.7	108.0	105.5	106.8	-6.9	-7.9	-7.4	-20.2	-20.7	-20.4
Window	22	30.7	29.2	29.9	109.2	107.6	108.4	-5.3	-6.5	-5.9	-18.7	-21.0	-19.8
Window	23	30.9	34.8	32.9	110.8	108.2	109.5	-5.1	-5.8	-5.5	-17.3	-18.4	-17.9
Average				34.0			112.1			-6.1			-18.6
Standard Deviation				2.5			2.8			0.5			1.3
Target				34.0			112.1			-6.1			-18.6
Lower Limit				30.6			100.9			-5.5			-16.7
Process Capability, C_{pk}				0.45			1.33			-0.43			-0.48

As one can observe, the average peak positive pressure was found to be 34.0 kPa. The impulse achieved was 112.1 kPa·ms. The negative phase of the blast had a peak pressure of -6.1 kPa and an accompanying impulse of -18.6 kPa·ms. It is further evident that the positive impulse is the most repeatable process. Due to the

high value for the capability index, it is virtually assured that the impulse will be within the 10% tolerance assigned to the 112.1 kPa·ms value. For the other values, there is at least an 80.3% chance of recording a measure within 10% of the mean value.

6.2 Deflection Results

Figure 6.25 shows the deflection measured at the midspan of the window from test record 20.

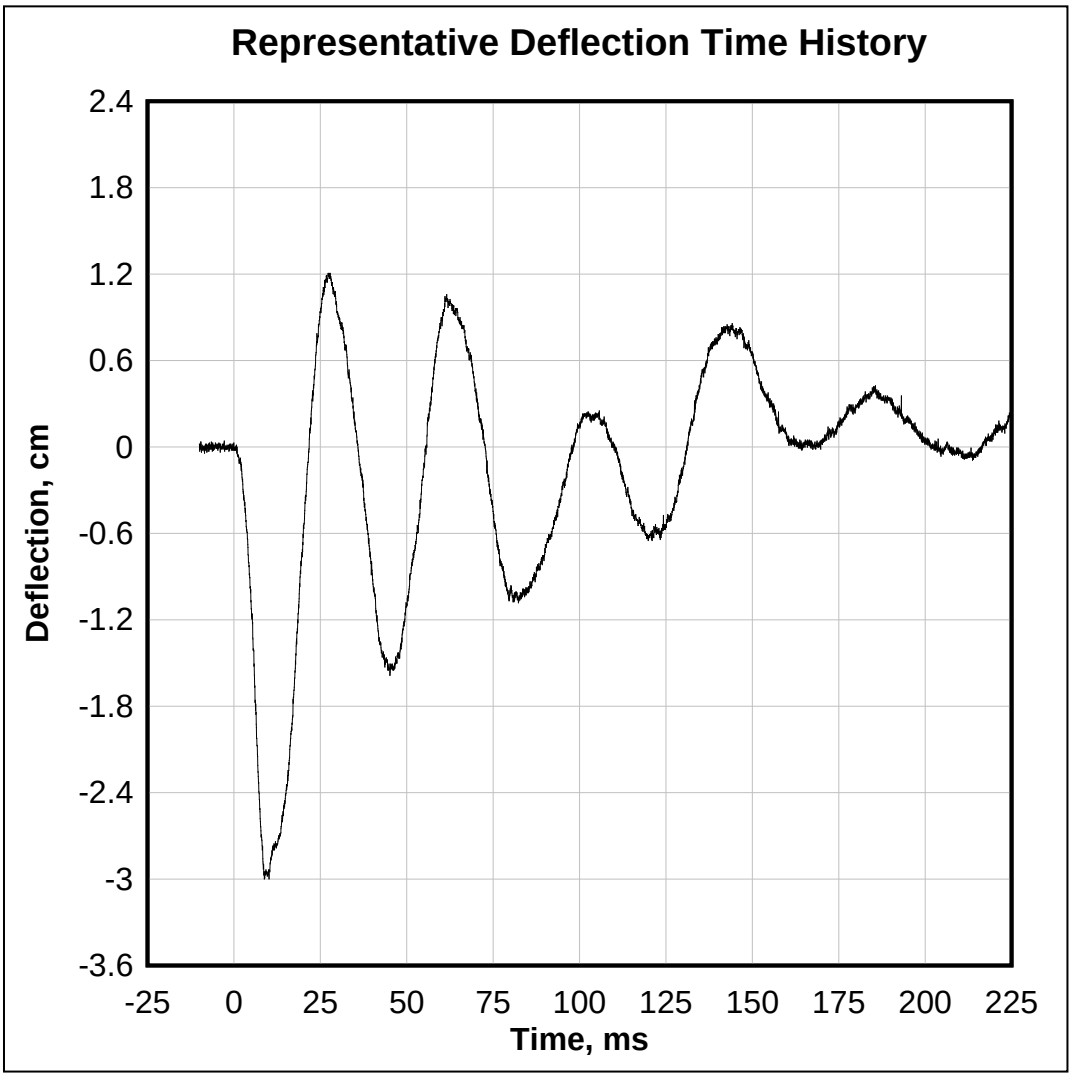

Figure 6.25 Representative Deflection Time History

The results for the suite of 21 tests are summarized in Table 6.12. The average peak deflection was found to be -3.11 cm, which is away from the origin of the blast. The peak deflection occurred 9.27 milliseconds after the arrival of the blast shock front. As with the impulse, the deflection and time were extremely repeatable over the 21 tests. The glass behaved perfectly elastic during this test with no discernible lasting effects.

Table 6.12 Perimeter Testing Summary Deflection Values

Blast Event		Displacement	
Target Type	Record	Mid Span (cm)	Time (ms)
Window	2	-3.155	9.350
Window	4	-3.178	9.150
Window	5	-3.096	9.600
Window	6	-3.160	9.200
Window	7	-3.084	9.350
Window	8	-3.058	9.450
Window	9	-3.175	9.250
Window	10	-3.084	9.250
Window	11	-3.071	9.300
Window	12	-3.152	9.300
Window	13	-3.101	9.750
Window	14	-3.119	9.250
Window	15	-3.205	9.450
Window	16	-3.155	9.450
Window	17	-3.091	9.200
Window	18	-3.160	9.700
Window	19	-3.023	8.850
Window	20	-2.997	8.800
Window	21	-3.109	9.200
Window	22	-3.056	9.000
Window	23	-3.101	8.900
	Average	-3.11	9.27
	Standard Deviation	0.05	0.25
	Target	-3.11	9.27
	Lower Limit	-2.80	8.35
	Process Capability, C_{pk}	-1.92	1.23

6.3 Reaction Results

Figure 6.26 shows the reaction force measured at the center of the bottom edge of the window, attachment point X, from test record 20. It is characterized by a sharp rise to the peak reaction achieved, followed by oscillations as the window vibrates.

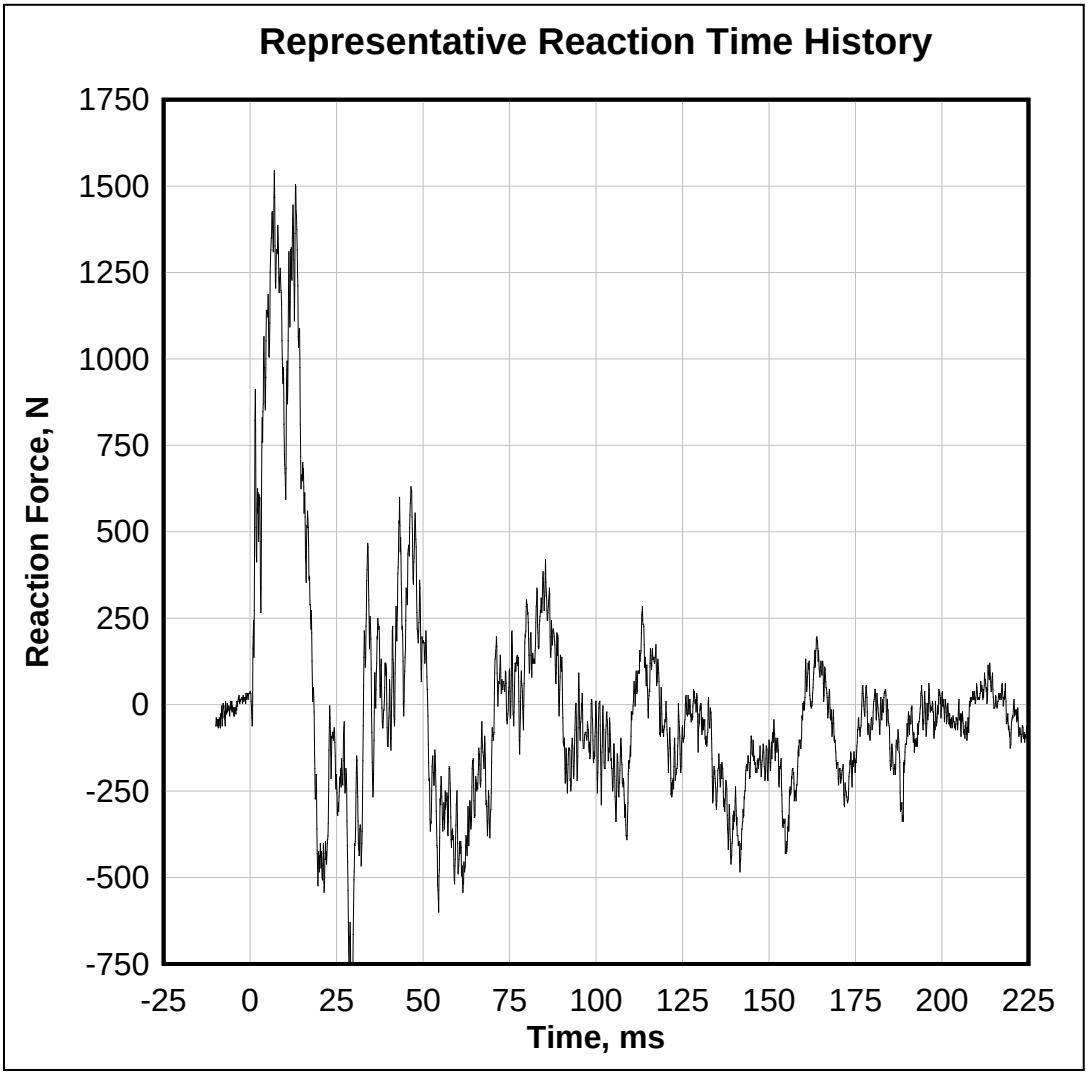

Figure 6.26 Representative Reaction Force Time History

The results for the suite of 21 tests are summarized in Table 6.13. It includes the total reaction force for the blast event, when summed over the entire perimeter, as well as the loading on a per edge basis. Those positions along the perimeter associated with the long edges of the window are highlighted.

Table 6.13 Perimeter Testing Summary Reaction Forces

Blast Event	Z Axis						
Position Along Perimeter	Record	Force (kN)	Record	Force (kN)	Record	Force (kN)	Ave Force (kN)
A	2	1.58	4	1.51	5	1.45	1.51
B	2	1.35	4	1.38	5	1.23	1.32
C	2	1.46	4	1.47	5	1.40	1.45
D	2	1.92	4	1.93	5	1.82	1.89
E	6	1.55	7	1.60	8	1.55	1.57
F	6	1.73	7	1.72	8	1.74	1.73
G	6	1.51	7	1.46	8	1.47	1.48
H	6	0.75	7	0.71	8	0.72	0.73
I	9	1.68	10	**0.32**	11	1.50	1.59
J	9	1.31	10	1.37	11	1.29	1.32
K	9	1.21	10	1.19	11	1.14	1.18
L	9	1.17	10	1.13	11	1.08	1.12
M	12	1.68	13	1.51	14	1.62	1.60
N	12	0.91	13	1.05	14	0.97	0.98
O	12	1.47	13	1.35	14	1.44	1.42
P	12	1.26	13	1.16	14	1.15	1.19
Q	15	1.31	16	1.52	17	1.54	1.45
R	15	1.52	16	1.60	17	1.56	1.56
S	15	1.29	16	1.29	17	1.26	1.28
T	15	1.37	16	1.41	17	1.34	1.38
U	18	0.99	19	0.99	20	0.93	0.97
V	18	0.98	19	1.21	20	1.15	1.11
W	18	1.24	19	1.26	20	1.18	1.23
X	18	1.50	19	1.59	20	1.54	1.54
Y	21	1.45	22	1.47	23	1.48	1.47
Z	21	0.93	22	1.01	23	0.93	0.96
					Total Peak Reaction Force (kN)		35.0
				Long Edge	Ave Reaction (kN)		10.9
					Loading (N /cm)		65.6
				Short Edge	Ave Reaction (kN)		6.6
					Loading (N/cm)		53.8

The total peak reaction force was found to be 35.0 kN which occurs approximately 10-12 milliseconds after the arrival of the blast. The average reaction force

encountered by an edge was different depending on whether it was a long edge or short edge as expected. The long edge experienced an average loading 21% higher than the short edge.

Over the course of the 21 tests, there was one anomalous reading. Test record 10 at position I had a remarkably low reading. The value, 0.32 kN, was identified as an outlier for the purposes of the analysis per the recommended outlier detection schema in the NIST Statistics Handbook. For small sample sizes, the recommended technique utilizes a modified Z-score as calculated in Equation 6.8. The modified Z-score was found to be 4.37, greater than the limit of 3.5 for outlier detection. The average value of this location, discounting the outlier was 357.8 lbf. The adjacent position J used during that test was a higher than recorded for the other two tests, but not abnormally so. The anomaly occurred during trial 2 of 3 trials at that location. The reason for this anomaly evades description.

$$M_i = \frac{0.6745(x_i - \tilde{x})}{median(|Y_i - \tilde{Y}|)} \qquad \text{Eq 6.8}$$

The distribution of forces around the perimeter is difficult to see from the above table. Figures 6.27 and 6.28 indentify the peak reaction force arranged as located around the window perimeter.

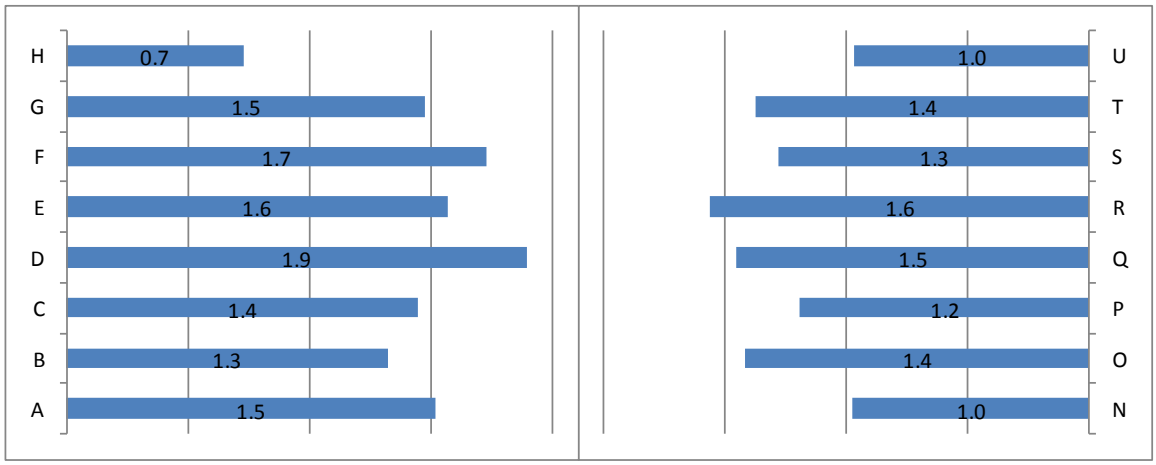

Figure 6.27 Long Edge Peak Reaction Force (kPa) by Position

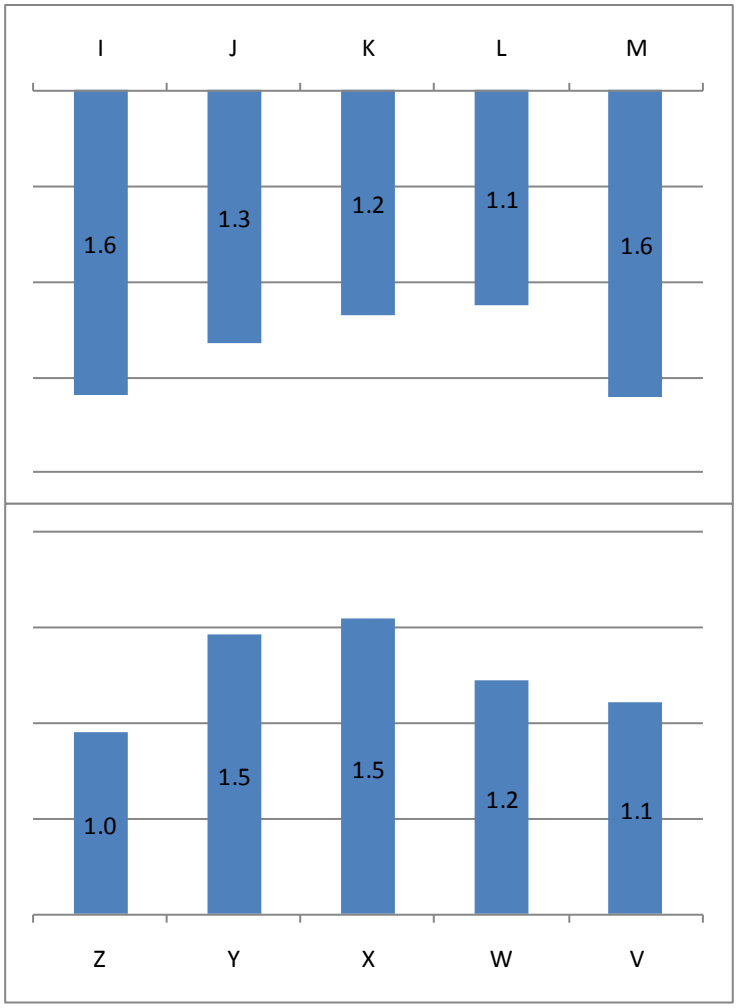

Figure 6.28 Short Edge Peak Reaction Force (kPa) by Position

The distribution of forces around the perimeter is irregular. The long edges tend to have the highest forces concentrated in the center of the span. The short edges have obvious trends that are directly opposed to one another. The bottom edge has the forces concentrated in the center, much like the two long edges, but the top edge has the forces concentrated towards the corners. If one then looks at the reactions experience in the top two corners, the long edges experienced lower forces as compared to the short edges. At the bottom, the left corner exhibited this phenomenon with the long edge supporting the greater share of the reaction, while the right side was more balanced. The likeliest explanation, though speculative, attributes this to a small misalignment among the four brackets. Such a misalignment would require different levels of flexure in the aluminum frame as the

loading transfers through the force sensor. While not optimum for experimentation, this is certainly a possibility with field installation of window units.

6.4 Modeling Results

The pressure developed during the perimeter testing is converted to an idealized triangular function for use in the modeling exercises. This involves preserving the peak pressures and setting the duration such that the impulses are equal, as seen in Figure 6.29.

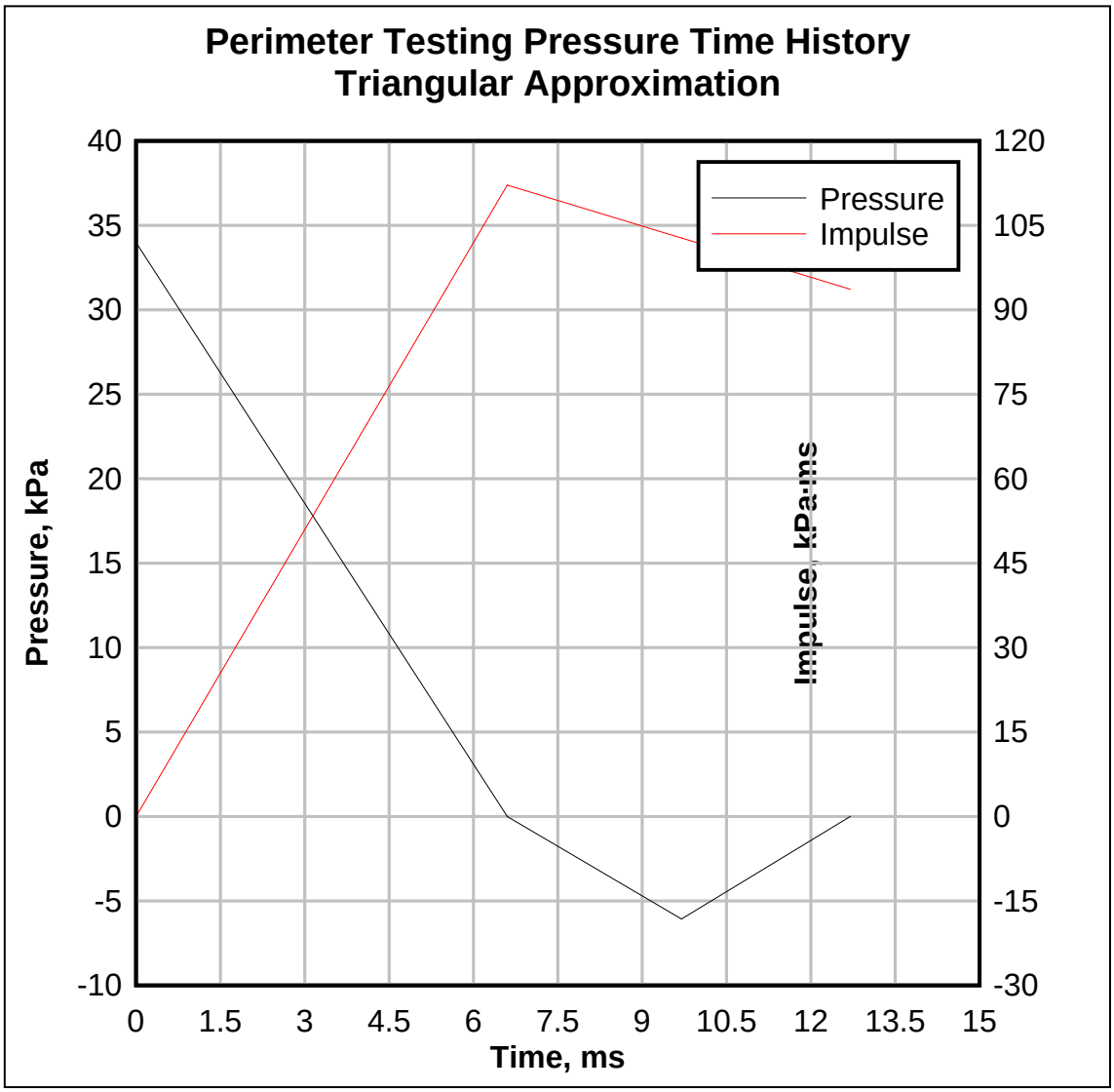

Figure 6.29 Triangular Approximation of Pressure Time History

6.4.1 SDOF Results

Along with the load time function calculated previously, the SDOF model requires a Static Resistance Function for the window under test. There was no access to the necessary test equipment to measure the Static Resistance Function so the output from HazL was used. That output was sampled to produce the piecewise linear approximation used in the Excel spreadsheet. The resulting function is shown in Figure 6.30.

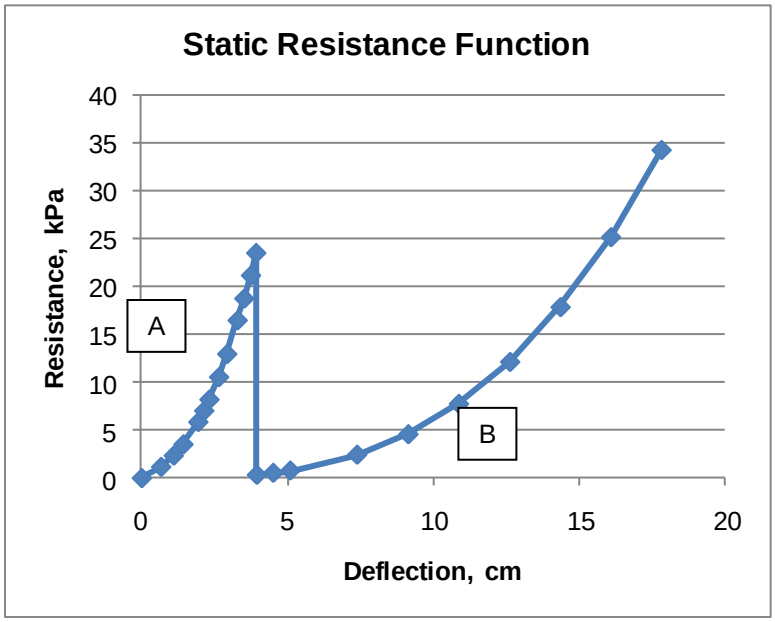

Figure 6.30 Static Resistance Function from HazL

The Static Resistance Function includes two regions. The first region, marked with an A, represents the glass flexing under load. The non-linearity is the result of the geometry. The window glass supported on all four edges and so its behavior is best described by plate theory as opposed to beam theory.

The output from the SDOF model is summarized in Table 6.14.

Table 6.14 Perimeter SDOF Modeling Results

SDOF Model Output				***Experimental***
Max Deflection		2.90	cm	3.10
At Time		6.62	ms	9.27
Final Resistance Function Region		1		---
Peak Reaction Force		32.18	kN	35.03
At Time		6.11	ms	10-12
Long Edge	Peak Reaction Force	10.42	kN	10.95
	Peak Loading	62.2	N / cm	65.3
Short Edge	Peak Reaction Force	5.67	kN	6.57
	Peak Loading	33.8	N / cm	39.2

There is exceptionally close agreement between the SDOF model and the experimental data. The measured peak deflection was within 7.0% of the predicted value. The peak reaction force was within 8.8% of the true value, similarly with the loading values. The only values that were off by a significant margin were the predicted times as compared to the measured times. They were off by 40%, or more. Biggs attributes this to a phase shift that occurs as a result of the modeling process and is expected (1964).

The SDOF modeling effort does a remarkably good job at predicting the overall system response but offers limited insight to the distribution of forces around the perimeter. Overall, it does an excellent job of predicting the gross behavior of the system.

6.4.2 HazL Results

HazL fails to accurately predict the response of the system. According to the output, the window glass fractures at this low level of loading. This is highly unexpected considering the other modeling efforts indicate the BRGS would not fail. The SDOF spreadsheet modeled the event superbly, using the same Static Resistance Function that HazL generated. The results are summarized in Figure 6.31.

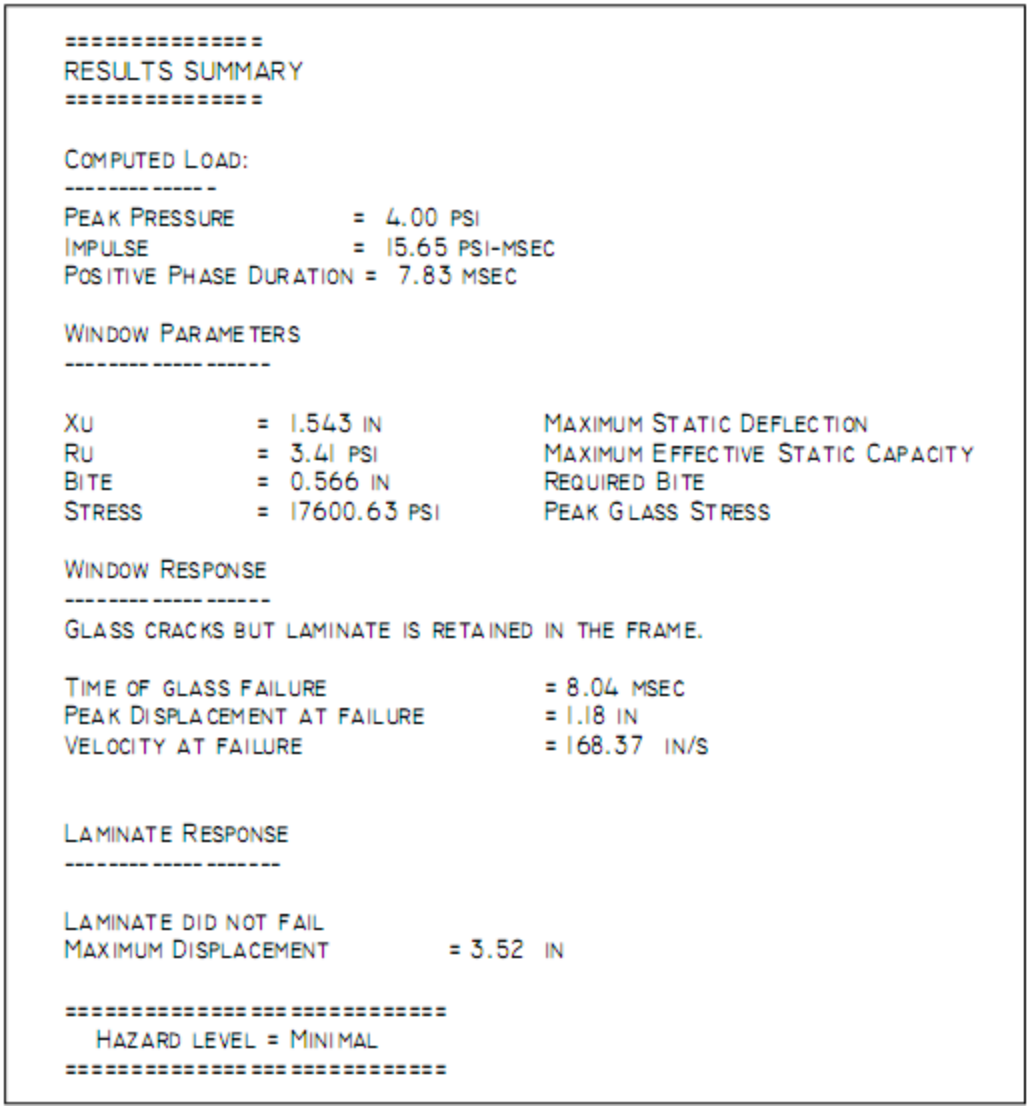

```
==============
RESULTS SUMMARY
==============

COMPUTED LOAD:
--------------
PEAK PRESSURE          =  4.00 PSI
IMPULSE                =  15.65 PSI-MSEC
POSITIVE PHASE DURATION =  7.83 MSEC

WINDOW PARAMETERS
-----------------

XU              =  1.543 IN          MAXIMUM STATIC DEFLECTION
RU              =  3.41 PSI          MAXIMUM EFFECTIVE STATIC CAPACITY
BITE            =  0.566 IN          REQUIRED BITE
STRESS          =  17600.63 PSI      PEAK GLASS STRESS

WINDOW RESPONSE
---------------
GLASS CRACKS BUT LAMINATE IS RETAINED IN THE FRAME.

TIME OF GLASS FAILURE                = 8.04 MSEC
PEAK DISPLACEMENT AT FAILURE         = 1.18 IN
VELOCITY AT FAILURE                  = 168.37  IN/S


LAMINATE RESPONSE
-----------------

LAMINATE DID NOT FAIL
MAXIMUM DISPLACEMENT          = 3.52  IN

============================
  HAZARD LEVEL = MINIMAL
============================
```

Figure 6.31 HazL Output

There are clear differences observed between the SDOF spreadsheet calculations and the HazL output. The program clearly does not rely solely on the SDOF method. It may consider the stress developed in the glass to determine failure as opposed to using the Static Resistance Function to indicate window pane fracture. For this low load scenario, the design information produced is highly suspect with its predicted 94.7% chance of failure. The window endured more than 30 tests at this loading or higher before finally fracturing.

6.4.3 Finite Element Analysis Results

The contour plot in Figure 6.32 shows the deflection experienced by the window, as modeled in ANSYS Explicit Dynamics.

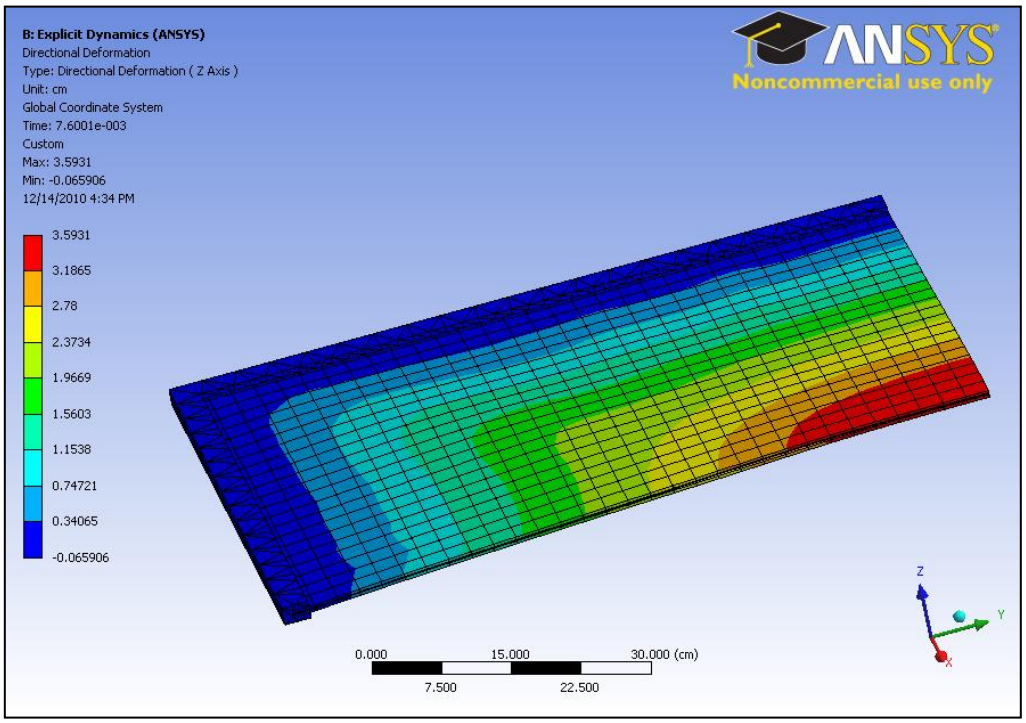

Figure 6.32 Perimeter Modeling Deflection via FEA

With an expected deflection of 3.59 cm, the model clearly over predicted the response of the window. It is within 16% of the experimental value. The problem lies in the abstraction of the structural silicone glazing. The adjustments made to the model favor matching the response over the range of blast loadings tested. At this particular loading, it experienced its largest error.

Figure 6.33 details the factor of safety for the window glass with the tensile failure mode predicted by Griffith's Criterion. It predicts a healthy margin with a minimum safety factor of 1.69.

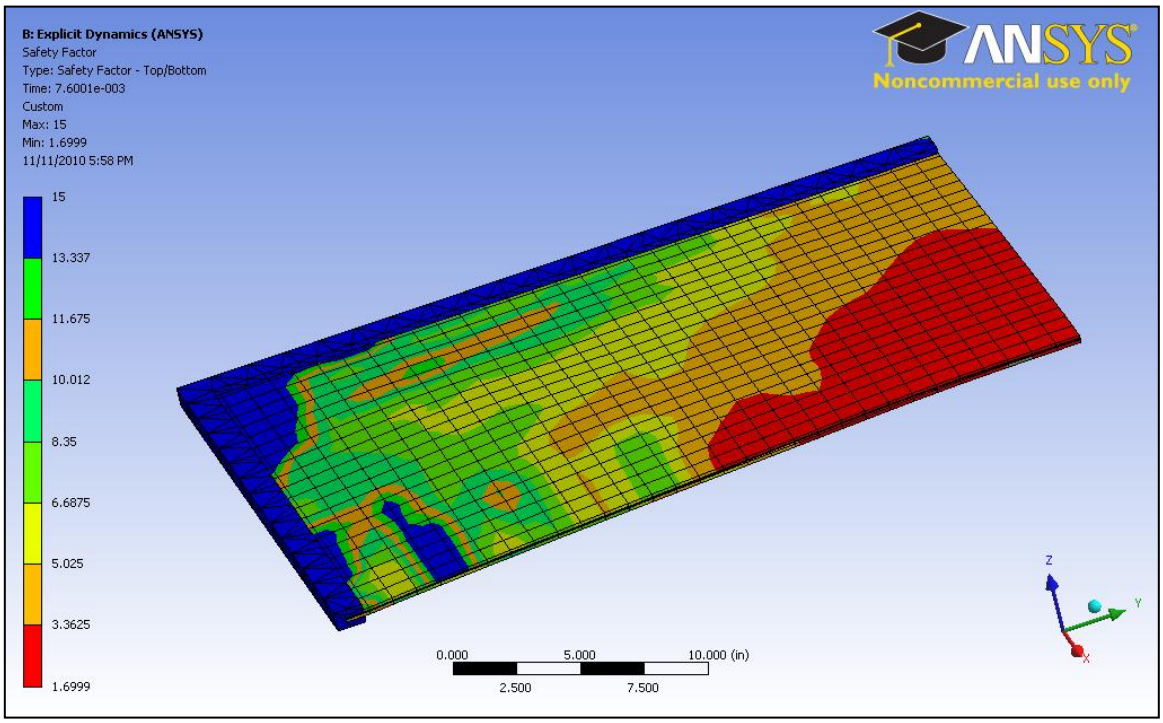

Figure 6.33 Perimeter Modeling Safety Factor using Griffith's Criterion via FEA

Extracting the reaction forces from the model proved problematic. The values, as calculated did not match reality due to the hourglass energies present. The model would require either a substantially larger number of elements in the abstracted structural silicone glazing or a more inclusive model with the aluminum framing included. With the limitations presented by the academic license in use, this was an insurmountable problem.

Chapter 7 Repeatability Testing Results and Analysis

7.1 Pressure Results

The charge size for the Repeatability testing was 230 grams of desensitized RDX at a standoff distance of 21.0 m. Figure 7.34 shows a representative pressure time history for the blast from test record 30. Test record 30 was very close to the average pressure and impulse for the suite of 9 tests. The two channels used to characterize the blast wave are shown, along with the impulse or the integral of pressure over time.

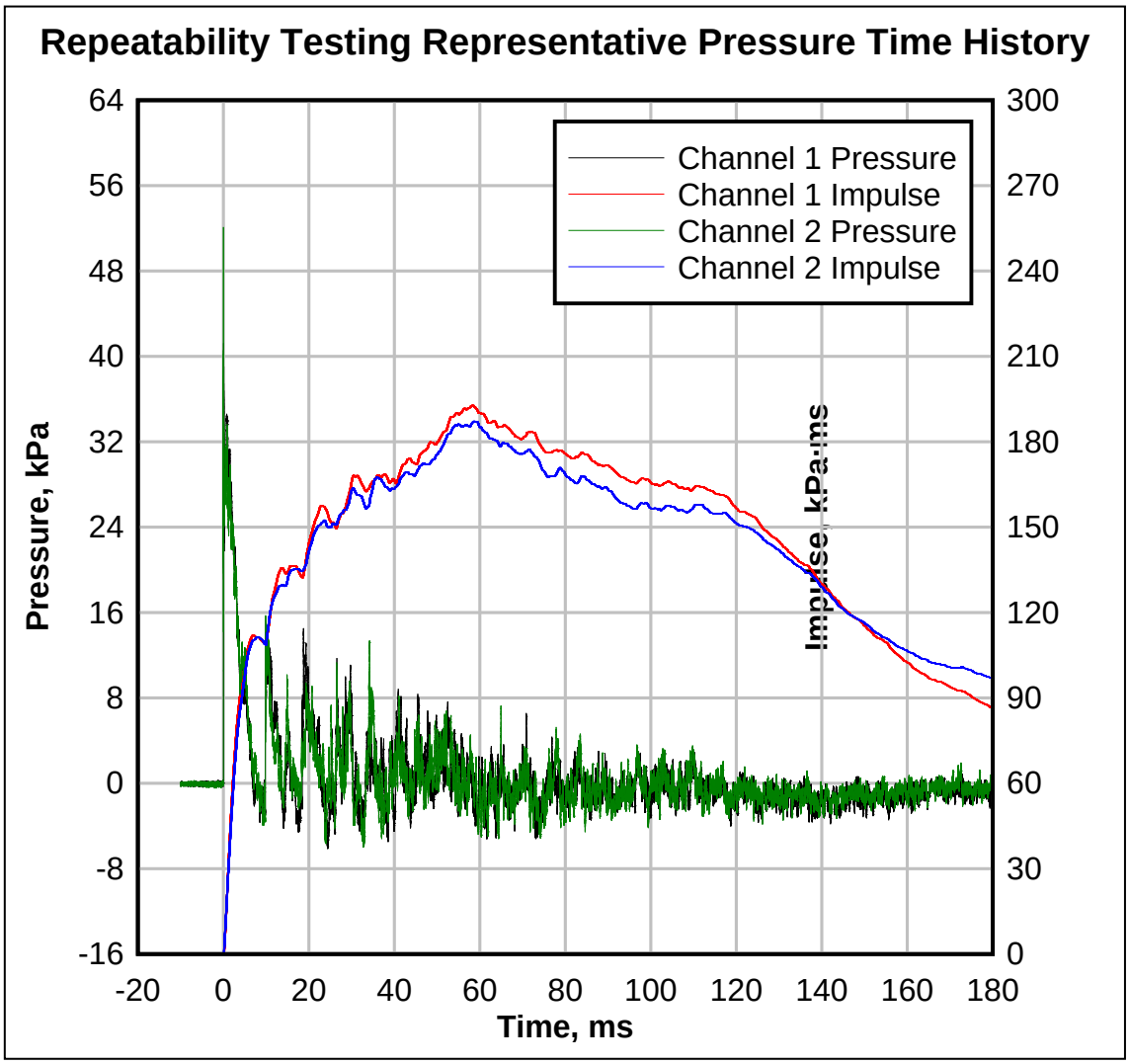

Figure 7.34 Representative Pressure Time History

The results for the entire suite of 9 tests is summarized in Table 7.15. The average peak positive pressure was found to be 44.6 kPa. The impulse achieved was 191.6 kPa·ms. The negative phase of the blast had a peak pressure of -7.1 kPa and an accompanying impulse of -29.6 kPa·ms. It is further evident that the positive impulse is the most repeatable process. It is virtually assured that the impulse will be within the 10% tolerance assigned to the 191.6 kPa·ms value. For the other values, there is at least an 74.6% chance of recording a measure within 10% of the mean value.

Table 7.15 Repeatability Testing Summary Pressure Values

Blast Event		Positive Phase						Negative Phase					
Target Type	Record	1	2	Peak Pressure (psi)	1	2	Impulse (psi·ms)	1	2	Peak Pressure (psi)	1	2	Impulse (psi·ms)
Window	27	42.3	57.2	49.8	202.4	190.7	196.5	-6.6	-8.1	-7.3	-27.4	-29.8	-28.6
Window	28	41.7	40.4	41.0	202.2	191.3	196.8	-6.4	-9.3	-7.9	-29.7	-29.1	-29.4
Window	29	43.0	39.1	41.1	188.6	179.6	184.1	-6.6	-8.1	-7.3	-28.2	-32.4	-30.3
Window	30	41.2	52.1	46.6	192.8	187.2	190.0	-6.1	-6.0	-6.0	-30.1	-32.2	-31.1
Window	31	40.5	44.6	42.5	194.7	183.8	189.3	-7.2	-7.2	-7.2	-28.2	-38.0	-33.1
Window	32	45.3	57.0	51.1	196.4	187.3	191.8	-6.6	-7.0	-6.8	-30.0	-31.4	-30.7
Window	33	40.0	46.2	43.1	194.5	185.7	190.1	-7.3	-6.0	-6.7	-27.6	-29.6	-28.6
Window	34	41.1	40.5	40.8	200.1	196.9	198.5	-6.8	-6.7	-6.7	-30.0	-29.5	-29.8
Window	35	42.3	47.6	45.0	201.5	172.3	186.9	-7.0	-8.6	-7.8	-24.1	-26.1	-25.1
Average				44.6			191.6			-7.1			-29.6
Standard Deviation				3.9			4.8			0.6			2.2
Target				44.6			191.6			-7.1			-29.6
Lower Limit				40.1			172.4			-6.4			-26.7
Process Capability, C_{pk}				0.38			1.32			-0.41			-0.45

7.2 Deflection Results

Figure 7.35 shows the deflection measured at the midspan of the window from test record 30.

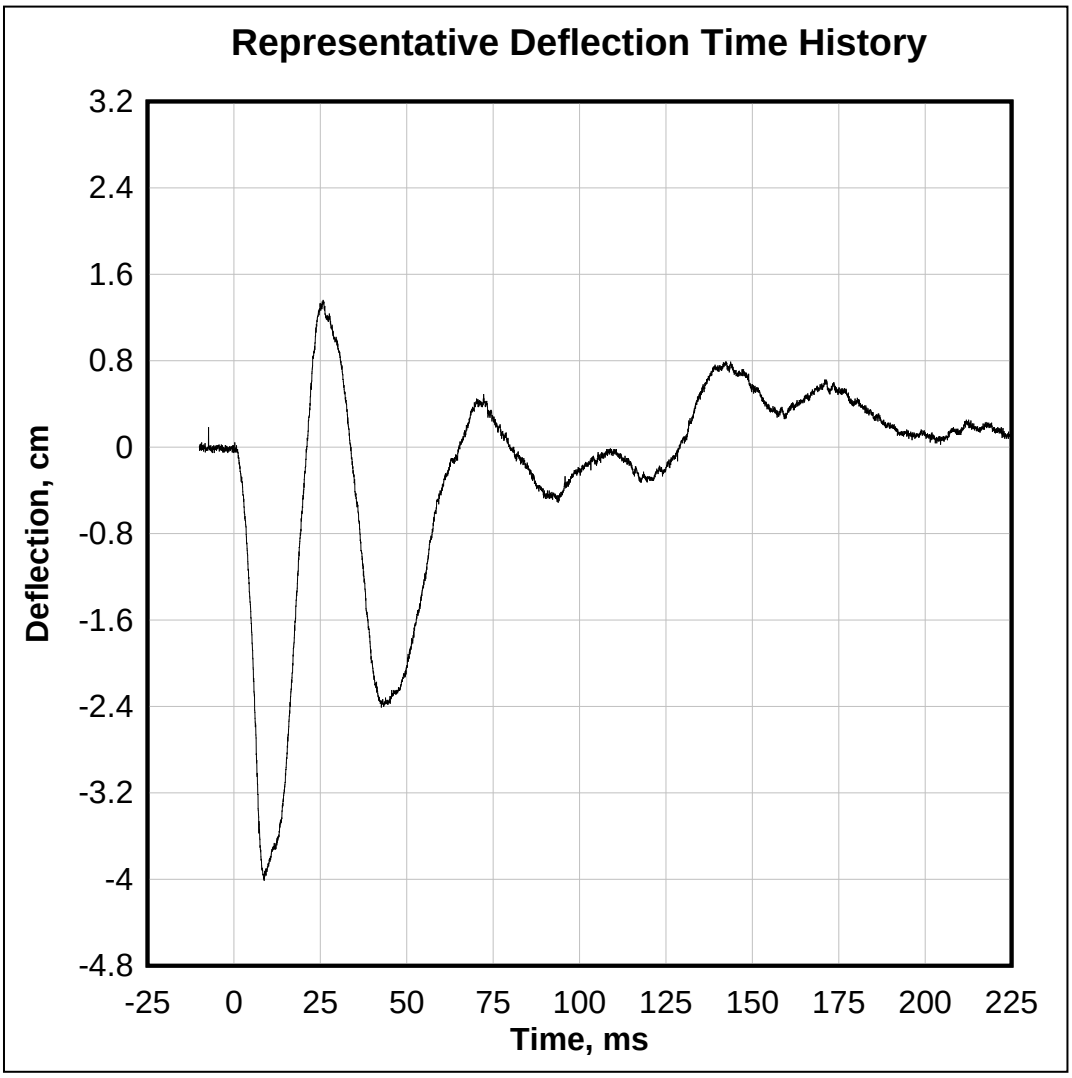

Figure 7.35 Representative Deflection Time History

The results for the suite of 9 tests are summarized in Table 7.16.

Table 7.16 Repeatability Testing Summary Deflection Values

Blast Event		Displacement	
Target Type	Record	Mid Span (in)	Time (ms)
Window	27	-4.02	8.65
Window	28	-3.96	8.75
Window	29	-3.92	8.75
Window	30	-4.01	8.75
Window	31	-3.99	8.85
Window	32	-4.02	8.70
Window	33	-3.98	8.70
Window	34	-4.10	8.65
Window	35	-3.99	8.60
	Average	-4.00	8.71
	Standard Deviation	0.05	0.07
	Target	-4.00	8.71
	Lower Limit	-3.60	7.84
	Process Capability, C_{pk}	-2.76	3.92

The average peak deflection was -4.00 cm. The peak deflection occurred 8.71 milliseconds after the arrival of the blast shock front. As with the impulse, the deflection and time were extremely repeatable over the 9 tests. The standard deviation over the nine tests was 0.05 cm. The process capabilities indicate that the chance of the deflection and time being within 10% of the mean value to be virtually assured.

7.3 Reaction Results

The results for the suite of 9 tests are summarized in Table 7.17. It includes the reaction force encountered at each of the positions available for Test Setup H, as well as the process capability estimates for the forces measured.

Table 7.17 Repeatability Testing Summary Reaction Forces

Blast Event	Force (lbf)			
Test Record	Position D	Position E	Position Q	Position R
27	1.96	2.79	3.35	1.81
28	2.14	2.90	3.44	1.93
29	1.95	2.76	3.29	1.73
30	2.06	2.86	3.48	1.85
31	1.96	2.79	3.38	1.79
32	1.96	2.81	3.41	1.77
33	2.02	2.83	3.52	1.85
34	2.00	2.90	3.62	1.90
35	1.92	2.88	3.64	1.85
Average	2.00	2.84	3.46	1.83
Standard Deviation	0.07	0.05	0.12	0.06
Lower Limit	1.80	2.55	3.11	1.65
Process Capability, C_{pk}	0.96	1.85	0.98	0.96

The measurements in this configuration proved to be very repeatable over successive blast events. The value for process capability was nearly 1 for all four measurement locations. This implies that 99.6% of measurements at these locations will be with 10% of the reported average. When a 5% tolerance is placed upon the process, 85% of the values will fall within that tolerance and 23.6% of measurements will be within 1% of the average value.

If one assumes that the distribution of forces around the window perimeter did not change significantly with the change in loading, one can make a prediction concerning the total reaction force that the window supports will experience. Scaling the values yields a prediction of 54.8 kN for the total reaction.

7.4 Modeling Results

The triangular approximation intended to represent the blast loading measured during the repeatability testing is shown in Figure 7.36. The response was not modeled with HazL for this testing because it was not expected to yield any additional information.

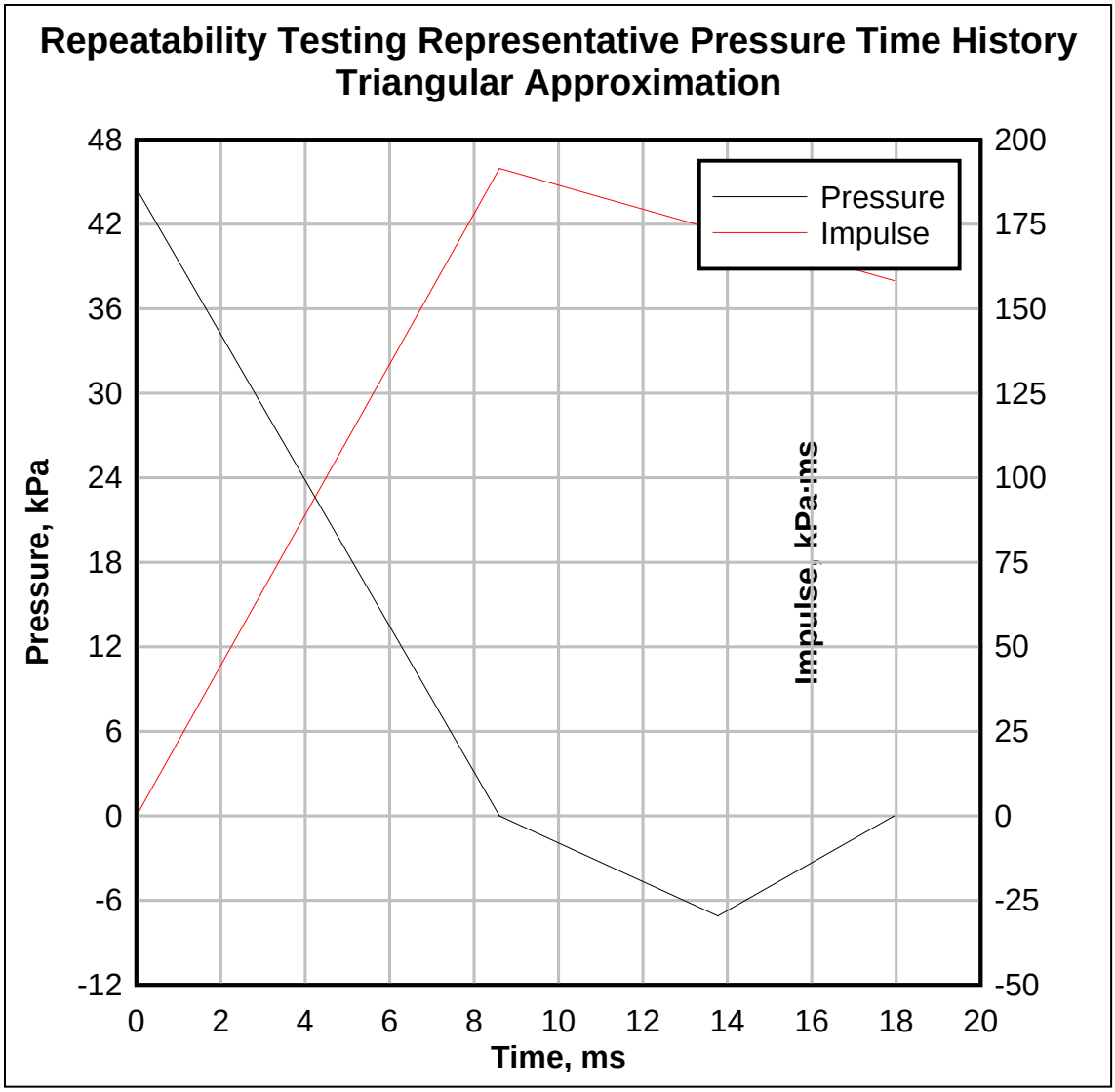

Figure 7.36 Triangular Approximation of Pressure Time History

7.4.1 SDOF Results

The output from the SDOF model is summarized in Table 7.18.

Table 7.18 Repeatability SDOF Modeling Results

SDOF Model Output				*Experimental*
Max Deflection		3.73	cm	3.99
At Time		6.62	ms	9.27
Final Resistance Function Region		1		---
Peak Reaction Force		67.56	kN	54.8*
At Time		6.11	ms	10-12
Long Edge	Peak Reaction Force	21.82	kN	---
	Peak Loading	130.2	N / cm	---
Short Edge	Peak Reaction Force	11.96	kN	---
	Peak Loading	71.3	N / cm	---

As before, the SDOF model did an admirable job predicting the response of the window glass to the blast loading. It is within 7% of the experimental results. The two predicted peak reaction forces are not in close agreement, but rather differ by more than 20%. Considering how well the model is predicting the response, and its accuracy in predicting the peak reaction force for the perimeter testing, it is likely that scaling up the results from any four force sensors is inadequate for making predictions about the total loading. The distribution of forces around the perimeter must also be a function of the loading. This is supported by theoretical analysis of laminated glass deflection using Karman's equations. Asik discusses the nonlinear distribution of stress fields in laminated glass as load scenarios change (2003). It follows that the distribution of reaction forces also vary with loading in a nonlinear fashion.

7.4.2 Finite Element Analysis Results

The contour plot in Figure 7.37 shows the deflection experienced by the window, as modeled in ANSYS Explicit Dynamics.

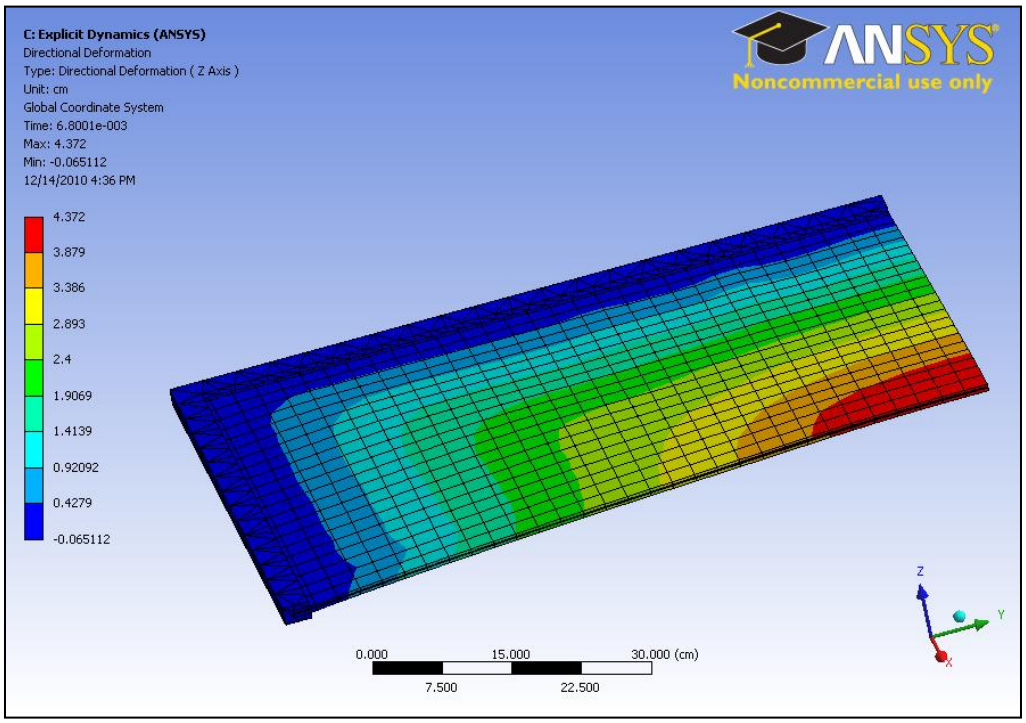

Figure 7.37 Repeatability Modeling Deflection via FEA

With an expected deflection of 4.37 cm, the model once again over predicted the response of the window. The prediction is improving, with the percent difference closing to within 9.6% of the experimental value.

Figure 7.38 details the factor of safety for the window glass with the tensile failure mode predicted by Griffith's Criterion. It predicts a minimum safety factor of 1.17.

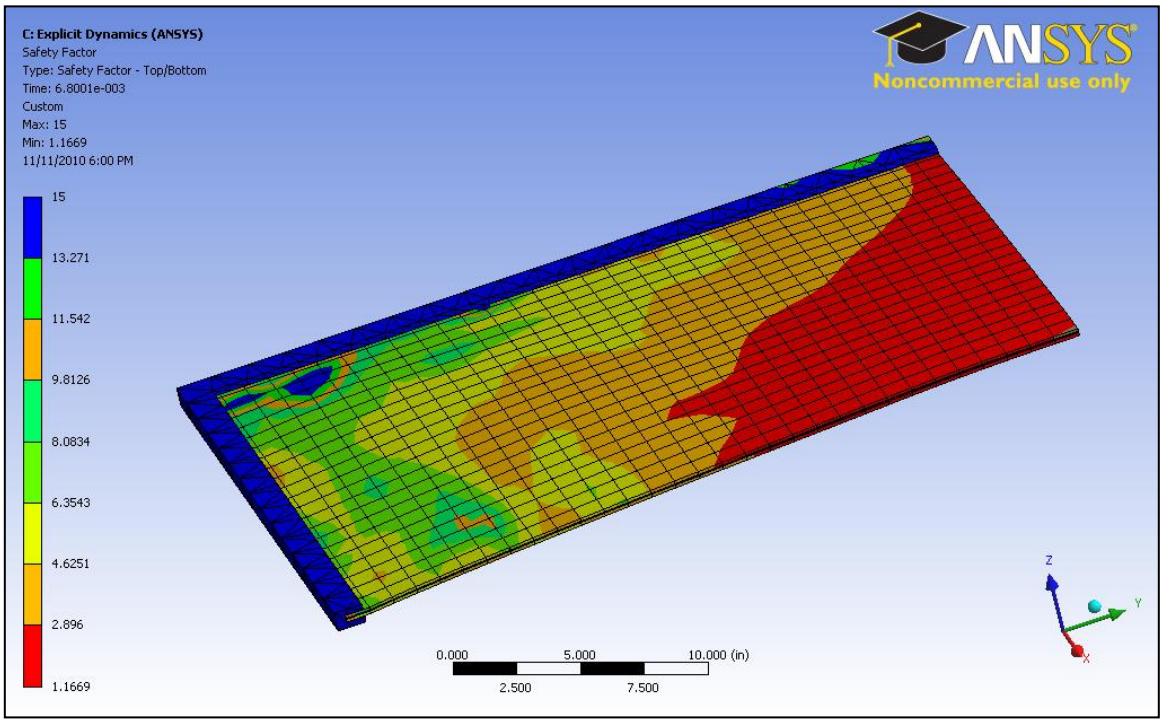

Figure 7.38 Repeatability Safety Factor using Griffith's Criterion via FEA

Chapter 8 Test to Failure

The first attempt to induce failure used a 300 gram charge at a distance of 21.0 m. When this failed to break the window, the charge size was increased to 400 grams which succeeded in fracturing the glass.

The images in Figure 8.39 were taken immediately prior to and after the 400 gram charge that fractured the window. The heat strengthened glass fractures, leaving small fragments adhering to the interlayer. The phenomenon, called crazing, is the result of releasing the tension locked in place during the tempering process. This forms fragments that tend to be smaller in size compared to plain annealed glass which pose less threat to occupants. This is offset somewhat by the higher velocities imparted to these particles due to the magnitude of the blast loading required to overcome extra resilience possessed by the glass (Smith 2001).

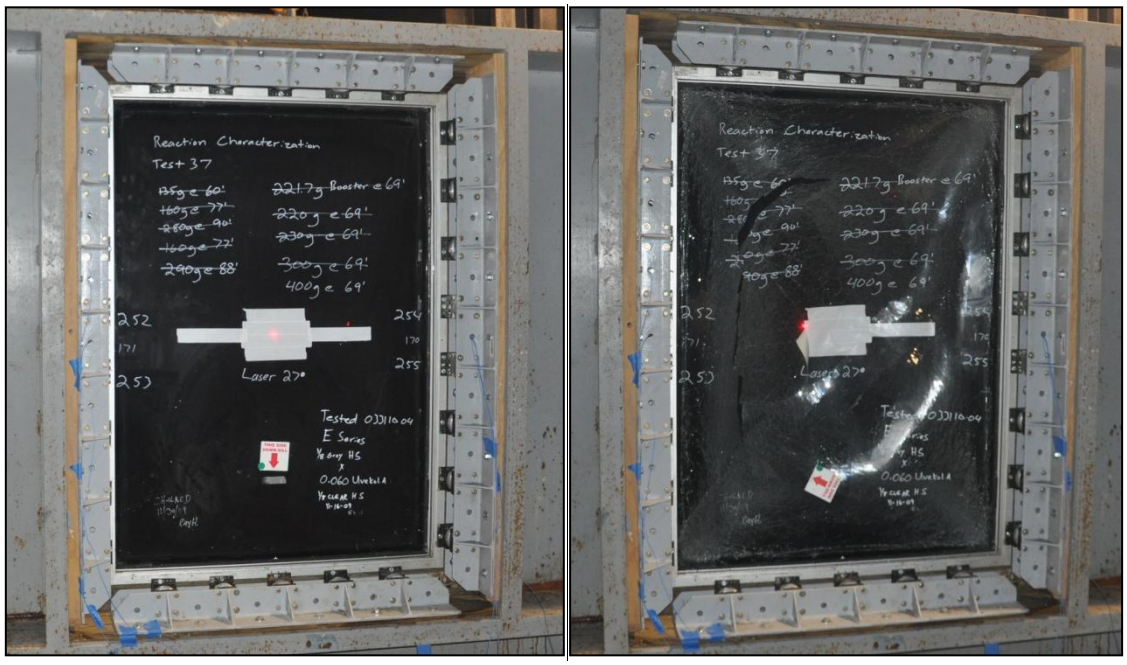

Figure 8.39 Before and After Failure Images of BRGS

A detailed view of the fractured glass can be seen in Figure 8.40.

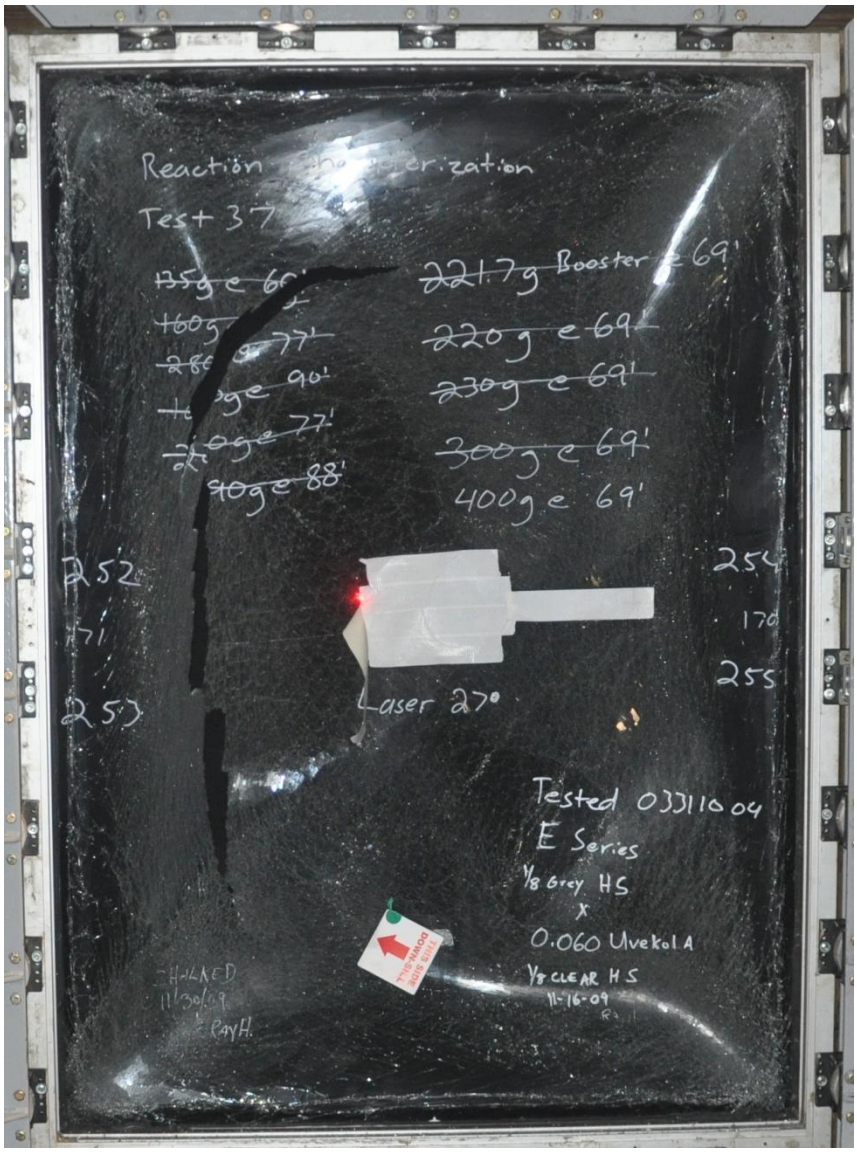

Figure 8.40 Post Test to Failure Window Glazing with Torn Interlayer

8.1 Pressure Results

Figure 8.41 is the pressure data from the initial attempt to cause window failure. The average peak pressure was 50.3 kPa with an impulse of 268.2 kPa·ms.

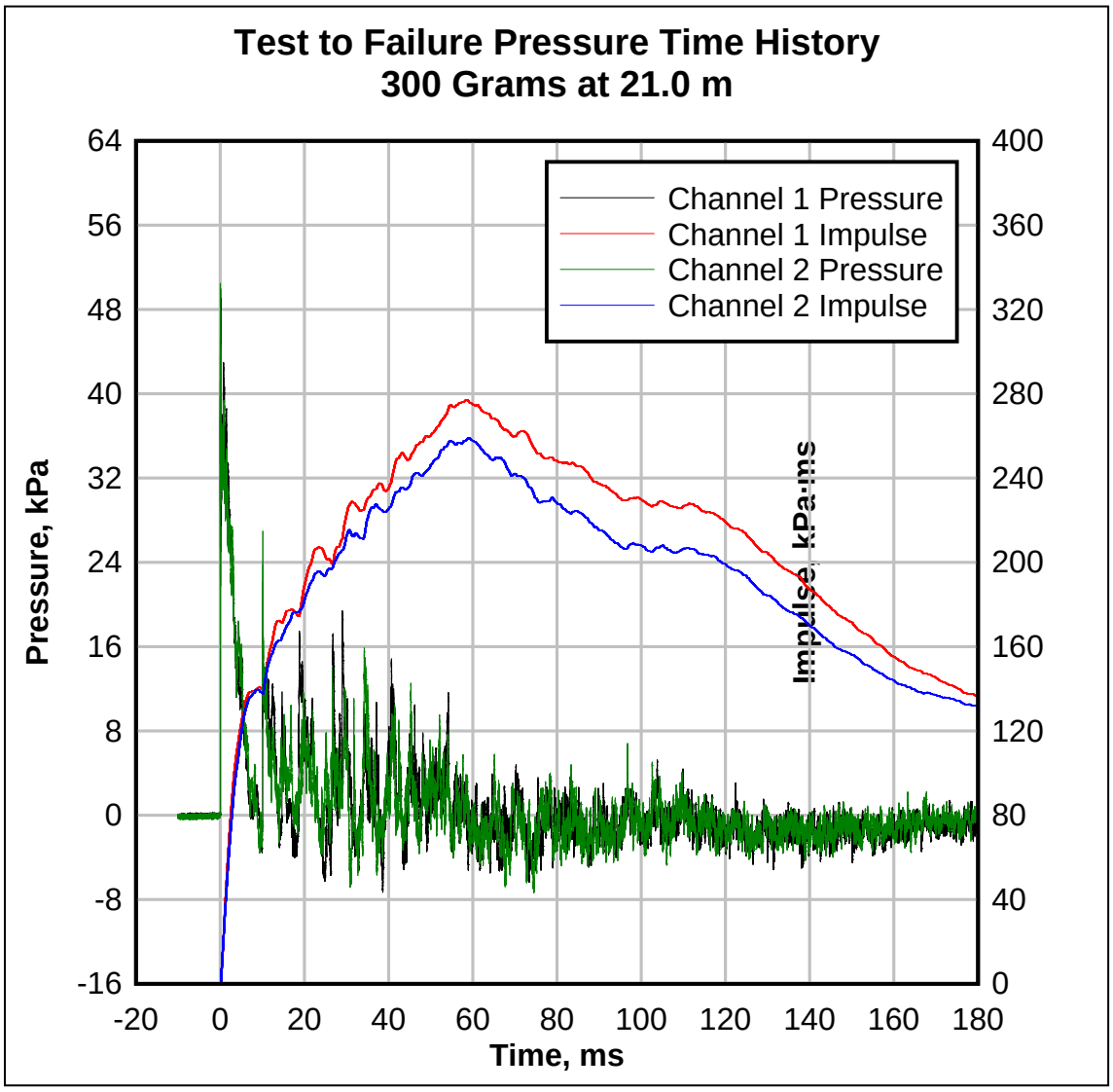

Figure 8.41 Test to Failure Pressure Time History, 300g Charge

The asymmetry in blast loading is becoming more obvious in the impulses measured in the two channels. The measured difference was just under 7%. The shock tube generates an approximately uniform planar blast wave. The triangular equivalent used for modeling purposes is shown in Figure 8.42.

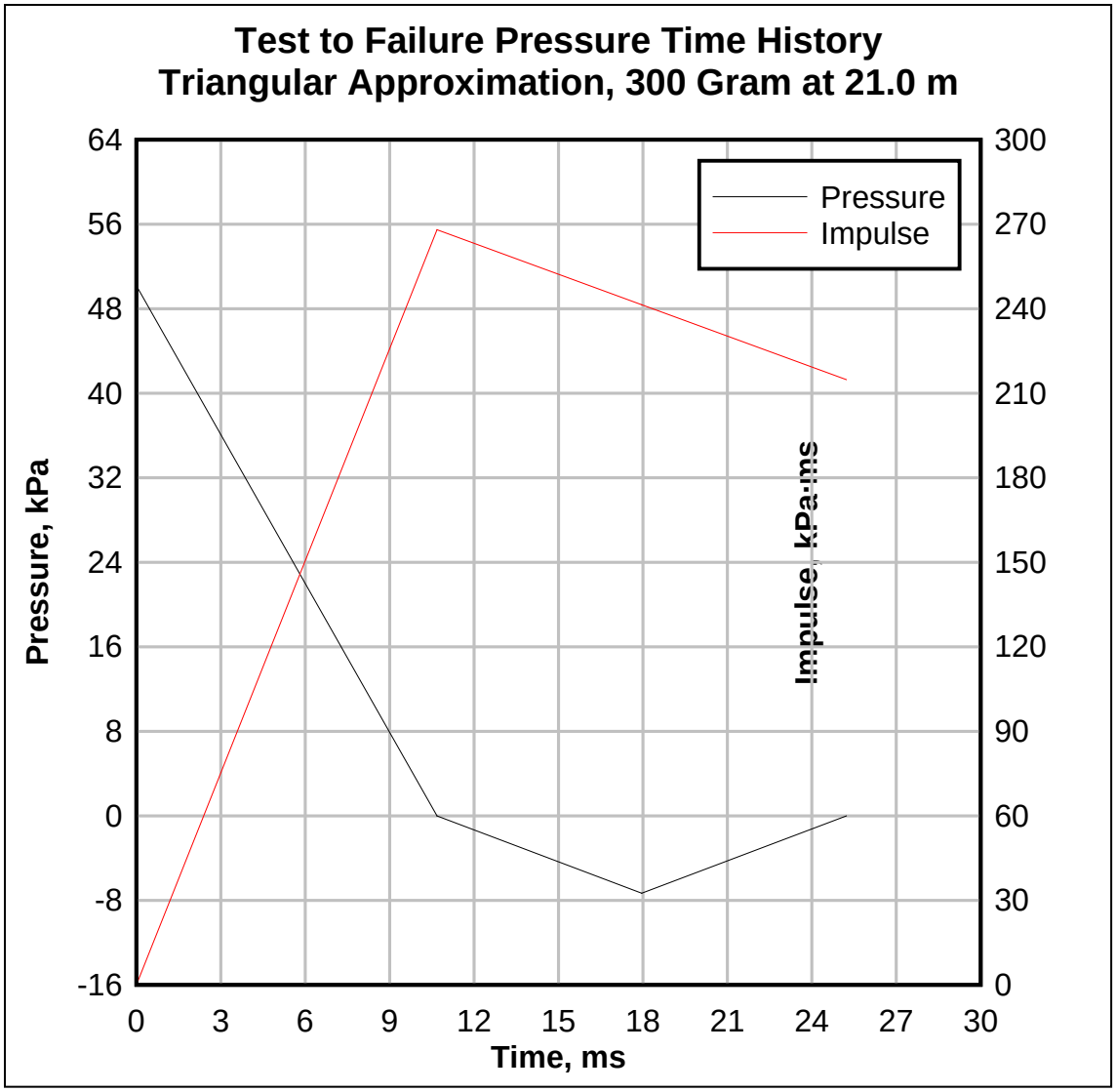

Figure 8.42 Test to Failure Triangular Approximation of Pressure Time History, 300g Charge

The final waveform generated during the course of testing can be seen in Figure 8.43. The shock tube was loaded with 400 grams of desensitized RDX at a distance of 21.0 m which shattered the glass window.

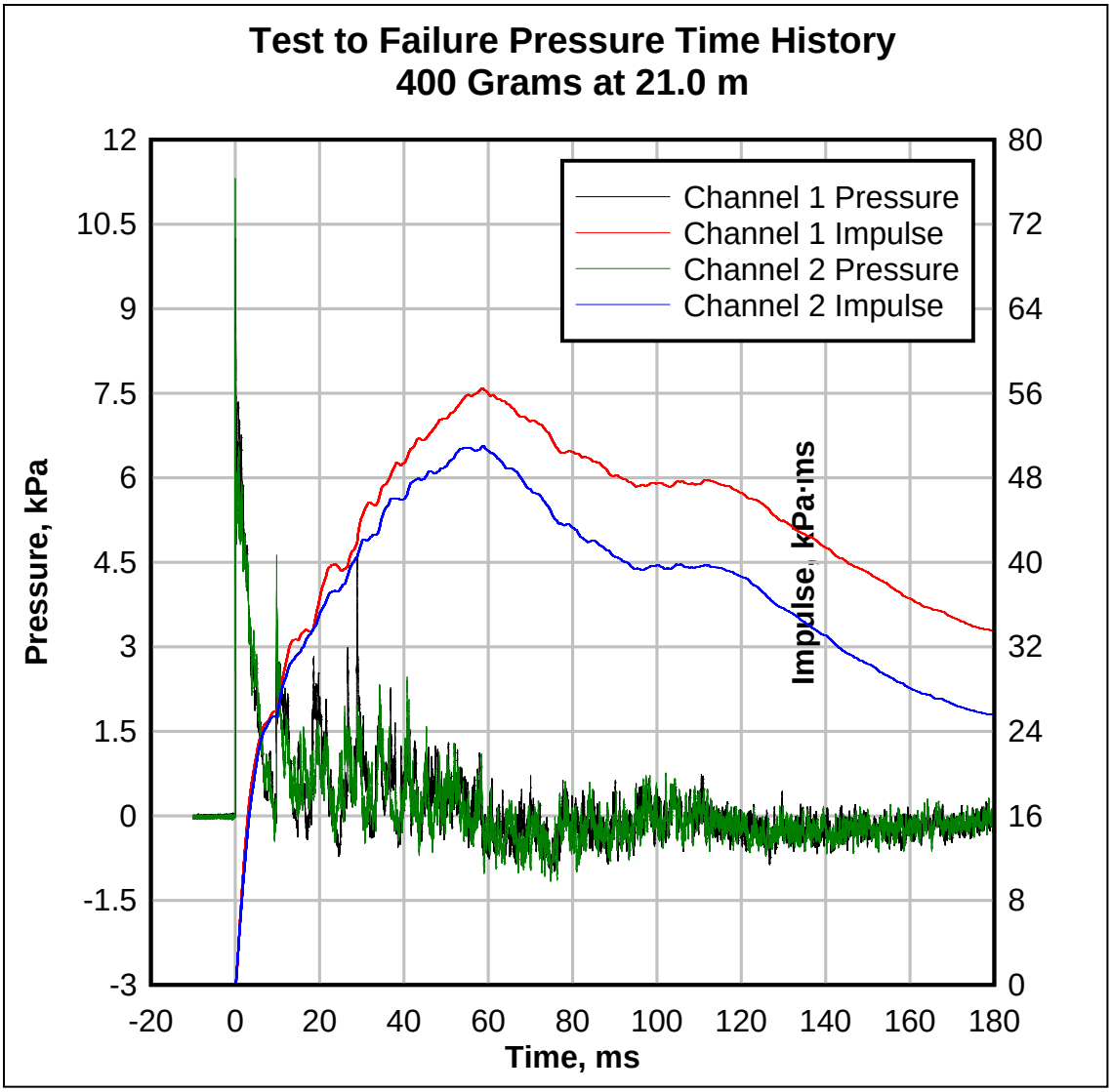

Figure 8.43 Test to Failure Pressure Time History, 400g Charge

The difference in blast loading from side to side is most obvious with this large charge. The measured difference was nearly 11%. The explanation for this could be any number of things. The likely scenarios include clearing effects due to the placement of the pressure sensors or distortion of the shock tube causing spatial irregularities. The triangular equivalent used for modeling purposes is shown in Figure 8.44.

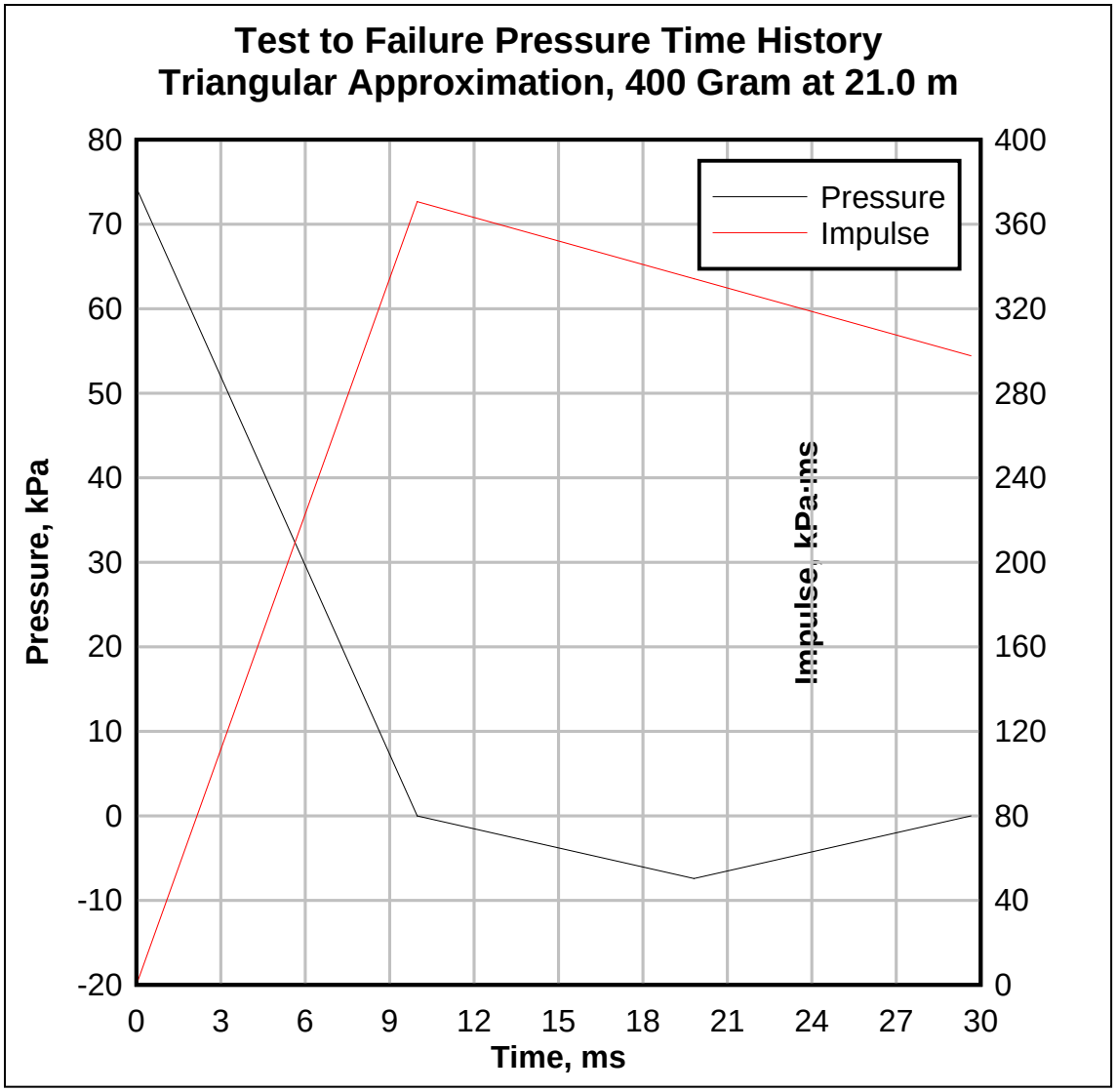

Figure 8.44 Test to Failure Triangular Approximation of Pressure Time History, 400g Charge

8.2 Deflection Results

Figure 8.45 shows the deflection measured at the midspan of the window for the first attempt. The window deflected to an ultimate value of 1.84 inches before springing back to nearly 0.5 inches in the opposite direction.

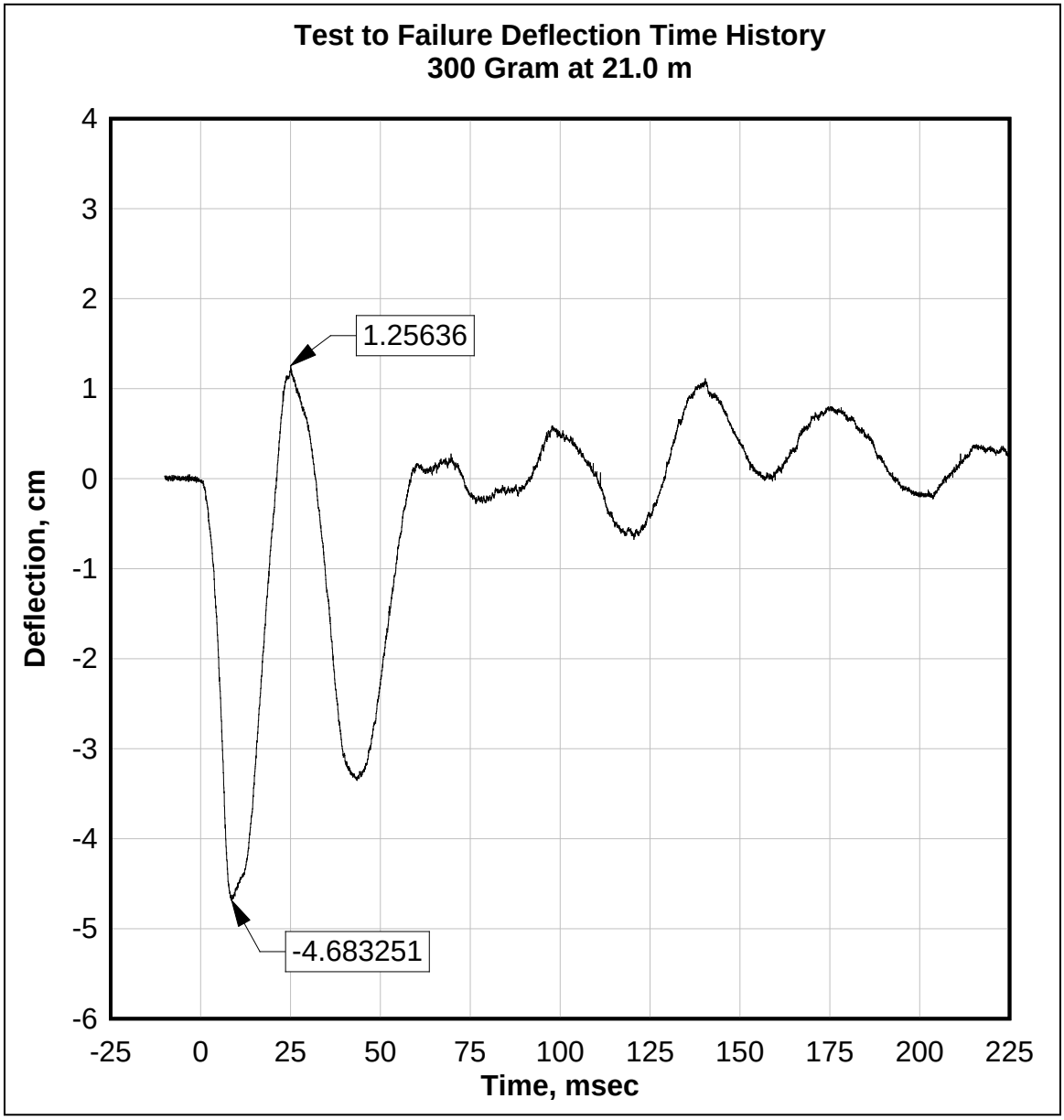

Figure 8.45 Test to Failure Deflection Time History, 300g Charge

Figure 8.46 shows the deflection time history for the window as it failed. From examining the graph, the glass fractures approximately 8.4 milliseconds after the blast wave arrives and the window travels approximately 2.1 inches. Upon fracturing, the interlayer then dominates the response. It deflects outward to just over 10 inches before rebounding. It is likely that the membrane tears after flexing inward over 10 inches as the deflection time trace becomes erratic at that point. The tape was noted to have been pulled free from the glass at some point as seen in Figure 8.40 meaning the laser was impinging upon fractured glass. This is the likeliest reason for the erratic measurements from this point forward.

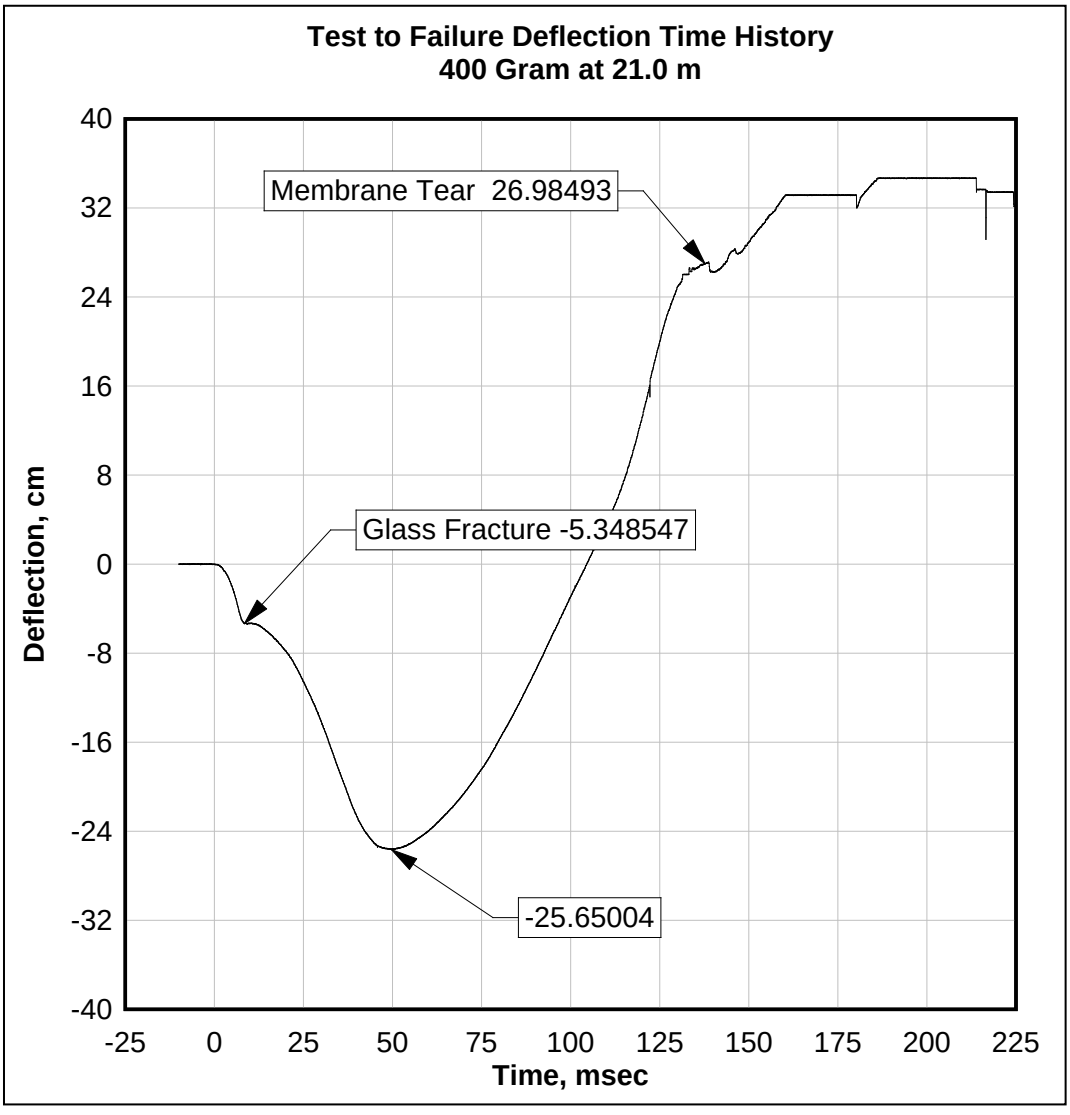

Figure 8.46 Test to Failure Deflection Time History, 400g Charge

8.3 Reaction Results

The reaction forces, normal to the window plane, encountered during the two tests to induce failure are listed in Table 8.19.

Table 8.19 Test to Failure Summary Reaction Forces

Blast Event	Force (kN)			
Test Record	Position D	Position E	Position Q	Position R
36, 300g, Z Axis	2.03	3.19	4.04	1.88
37, 400g, Z Axis	2.41	3.21	3.90	2.17

The sum of the reaction forces during these two tests were not substantially different from one another, 11.13 kN and 11.69 kN. The peak reaction force for the second trial was just 5% higher just prior to window fracture. The reaction force time histories are seen in Figures 8.47 and 8.48, grouped by their positions opposite one another.

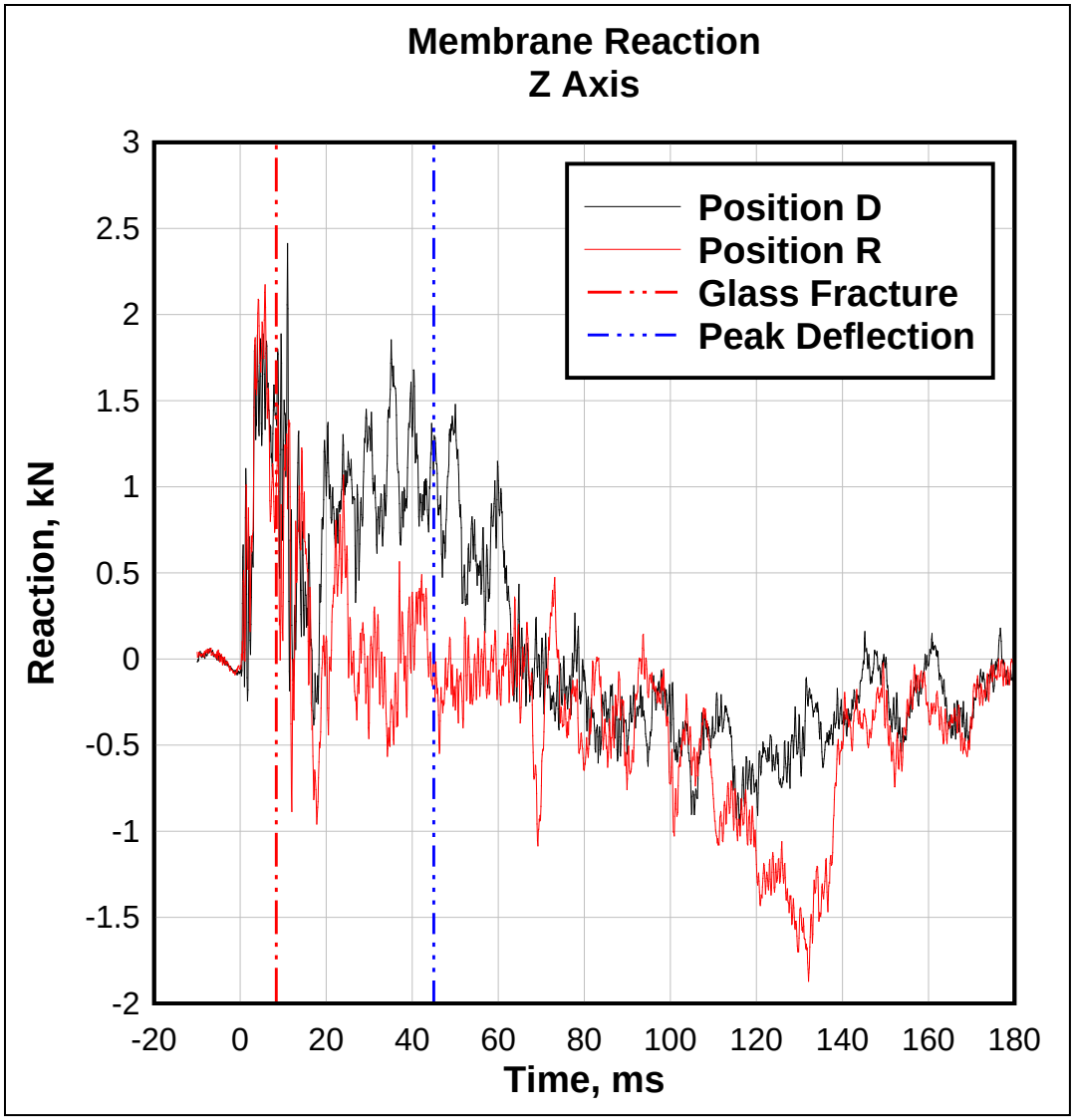

Figure 8.47 Test to Failure Membrane Reaction, Z Axis, 400g Charge

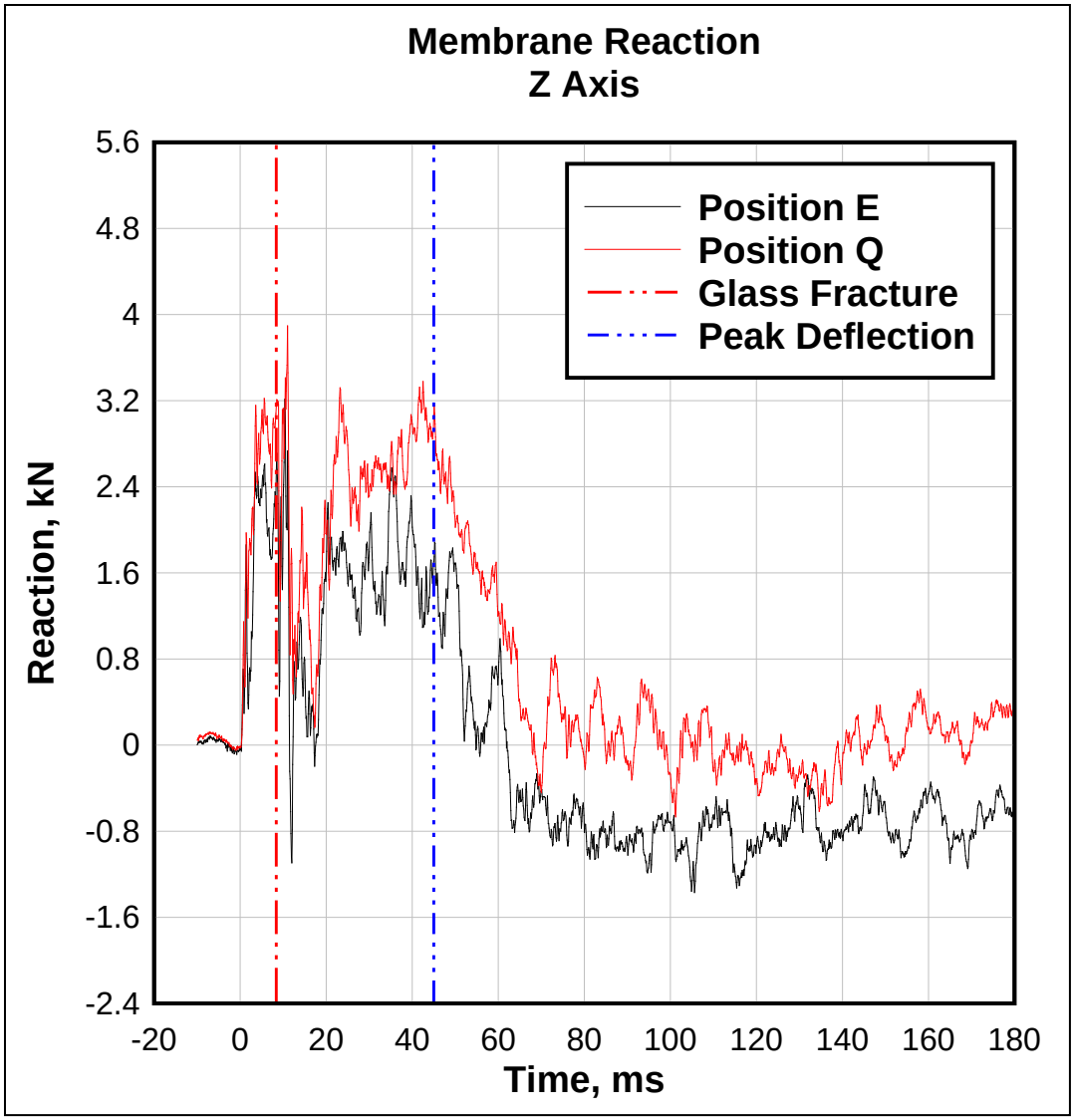

Figure 8.48 Test to Failure Membrane Reaction, Z Axis, 400g Charge

The general trend noted from the data is the rapid rise in reaction forces up to the point of glass failure. At this point the reaction forces drop to nearly zero and begin to rise again as the membrane begins transferring the loading to the sensors. This builds to the peak reaction force encountered during the membrane phase which coincides with the peak membrane deflection. As the window begins to oscillate, the forces change sign as the window membrane is pulled out towards the origin of the blast. The noted irregularity in the data is that position R apparently does not

participate in the reaction loading due to the membrane action initially. The reason is unknown and is contrary to expectations. It could be related to the irregularity in reaction loading seen at the various attachment points during the perimeter testing, such as the load path preferentially flowing through the points to either side of R.

The tensile response of the membrane between points D and R is seen in Figures 8.49 and 8.50. The shaded area in the first graph is the tension acting on the portion of the membrane between the two positions opposite one another. The second graph is the tension acting on the membrane.

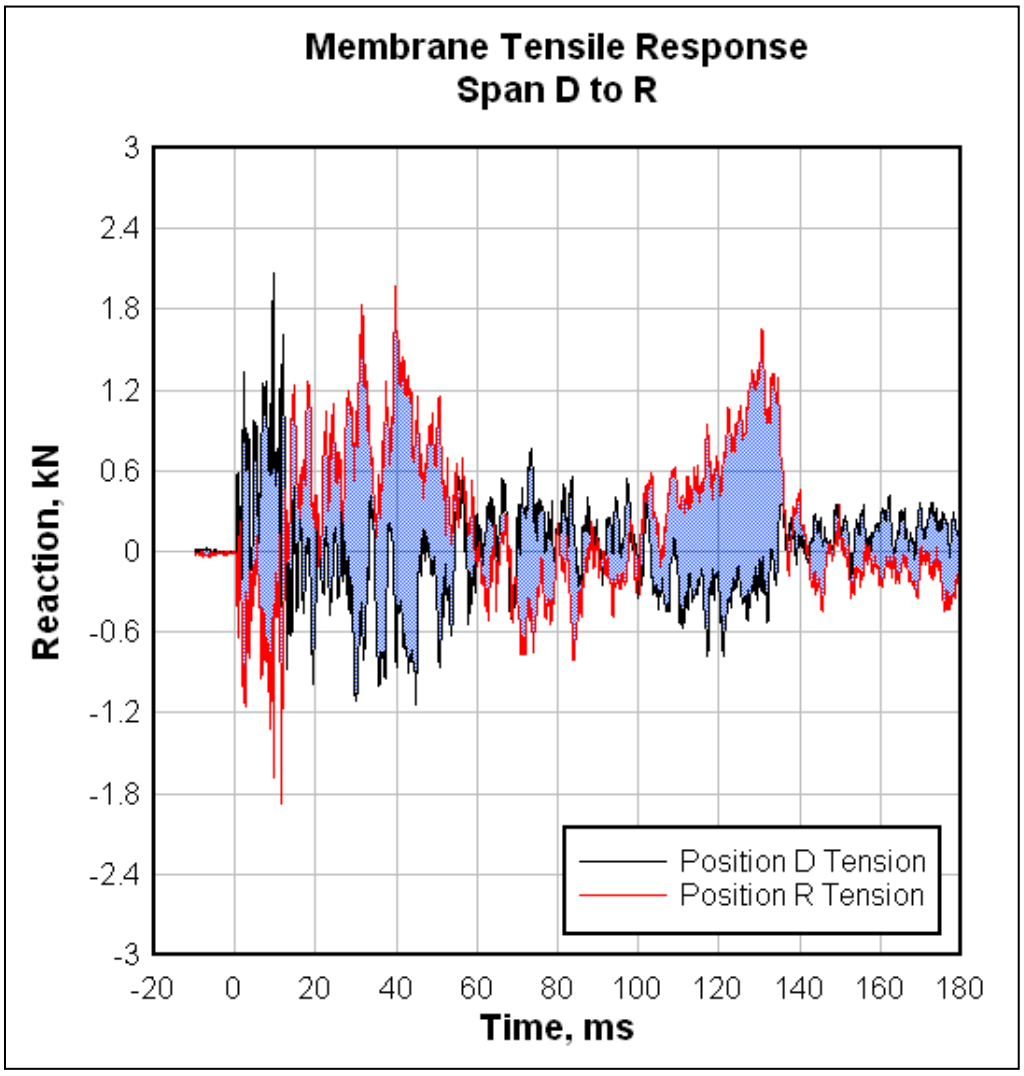

Figure 8.49 Membrane Tensile Response across Span D to R

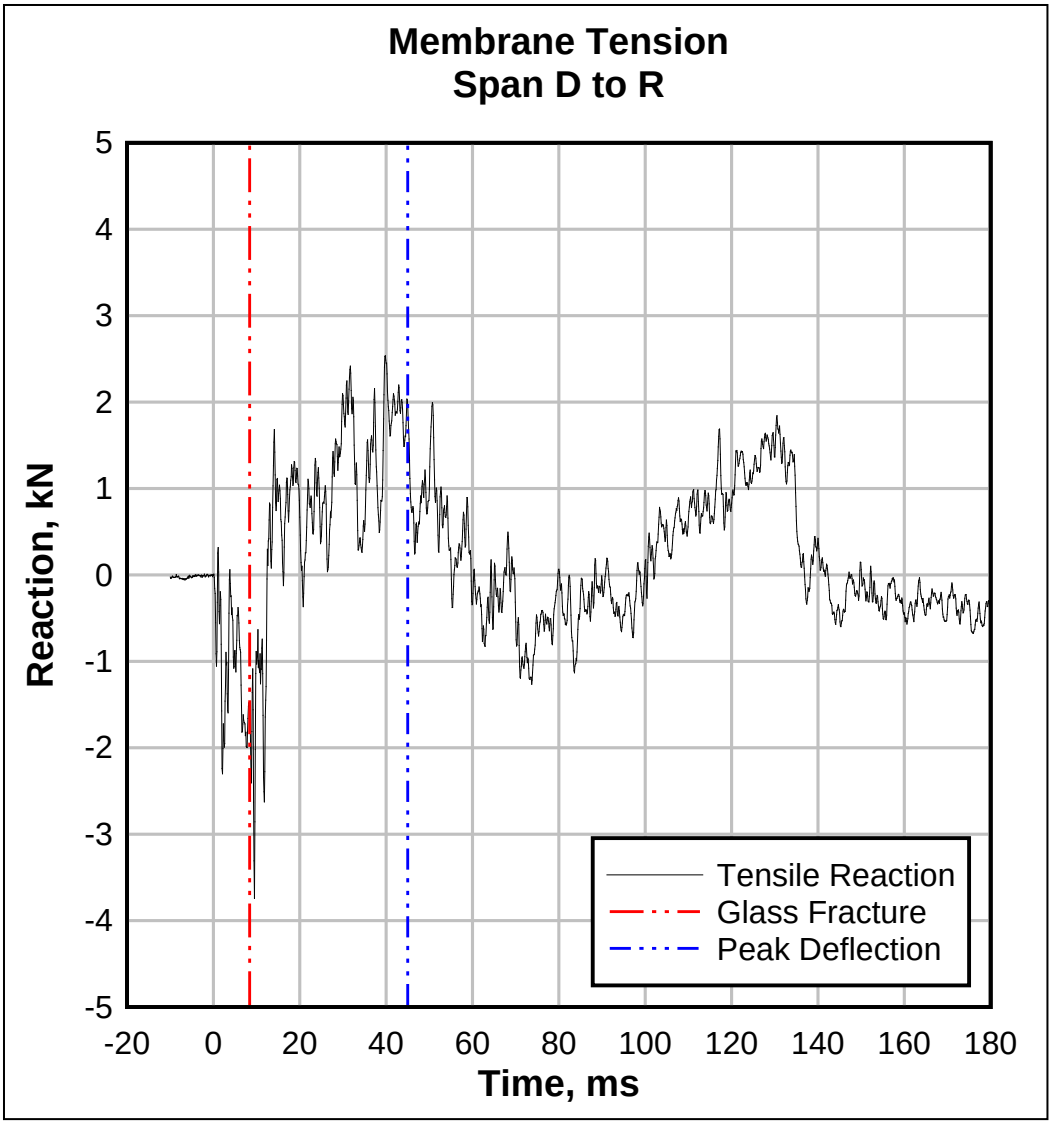

Figure 8.50 Tension within Membrane across Span D to R

The early peak prior to glass fracture is likely the result of the moment applied by the loading as the supports flex. This quickly drops to zero as the fractured glass can no longer transmit that moment. The tensile response is then seen as it builds to the point of peak membrane deflection. As the window rebounds, this becomes momentarily negative. The membrane has already plastically deformed and presses against the sides as it passes through the point that would be zero

deflection. The tension builds as the window pulls outward in the negative phase of the blast.

Figures 8.51 and 8.52 are the same set of graphs for the span running from points E to Q.

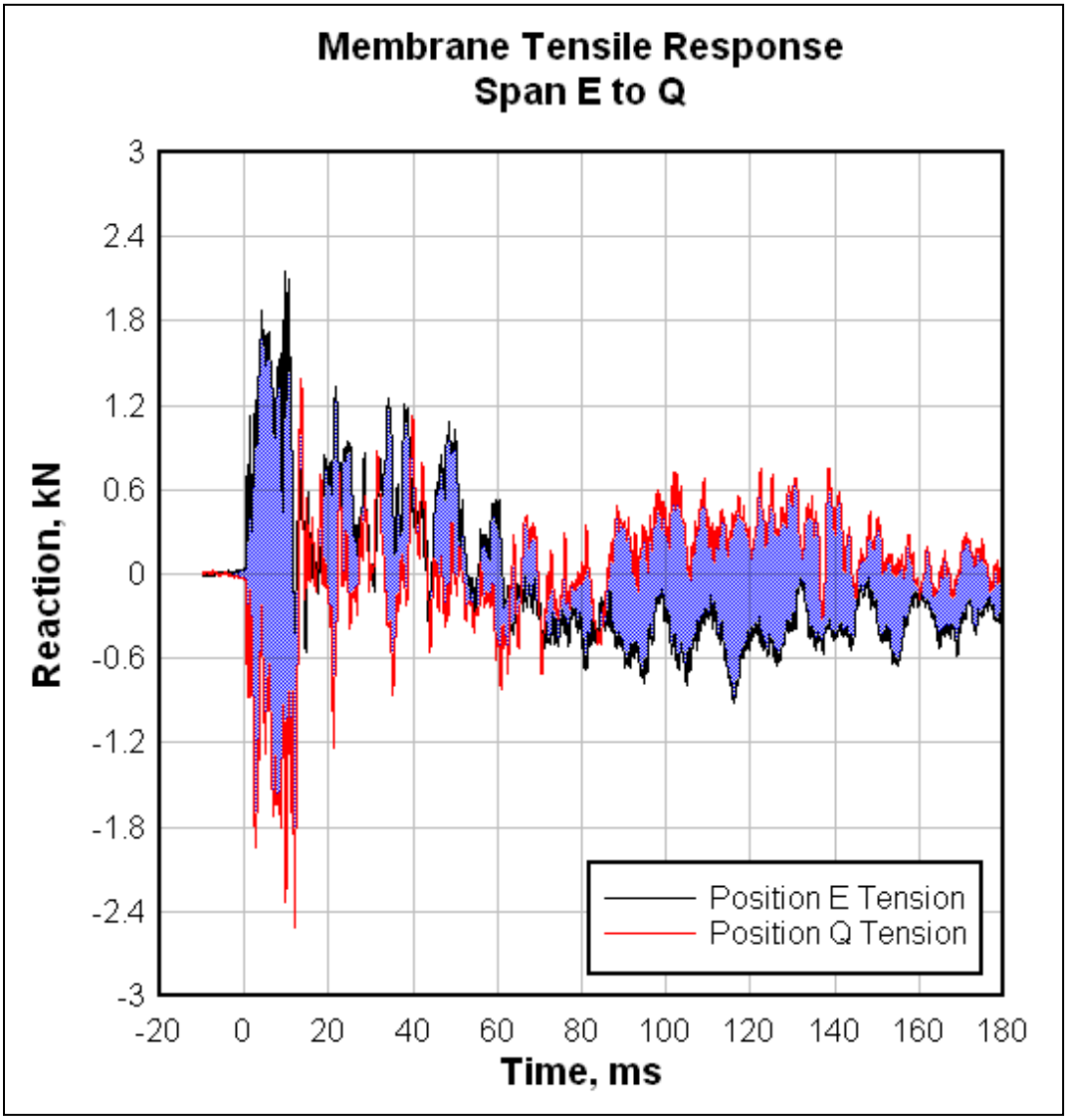

Figure 8.51 Membrane Tensile Response across Span E to Q

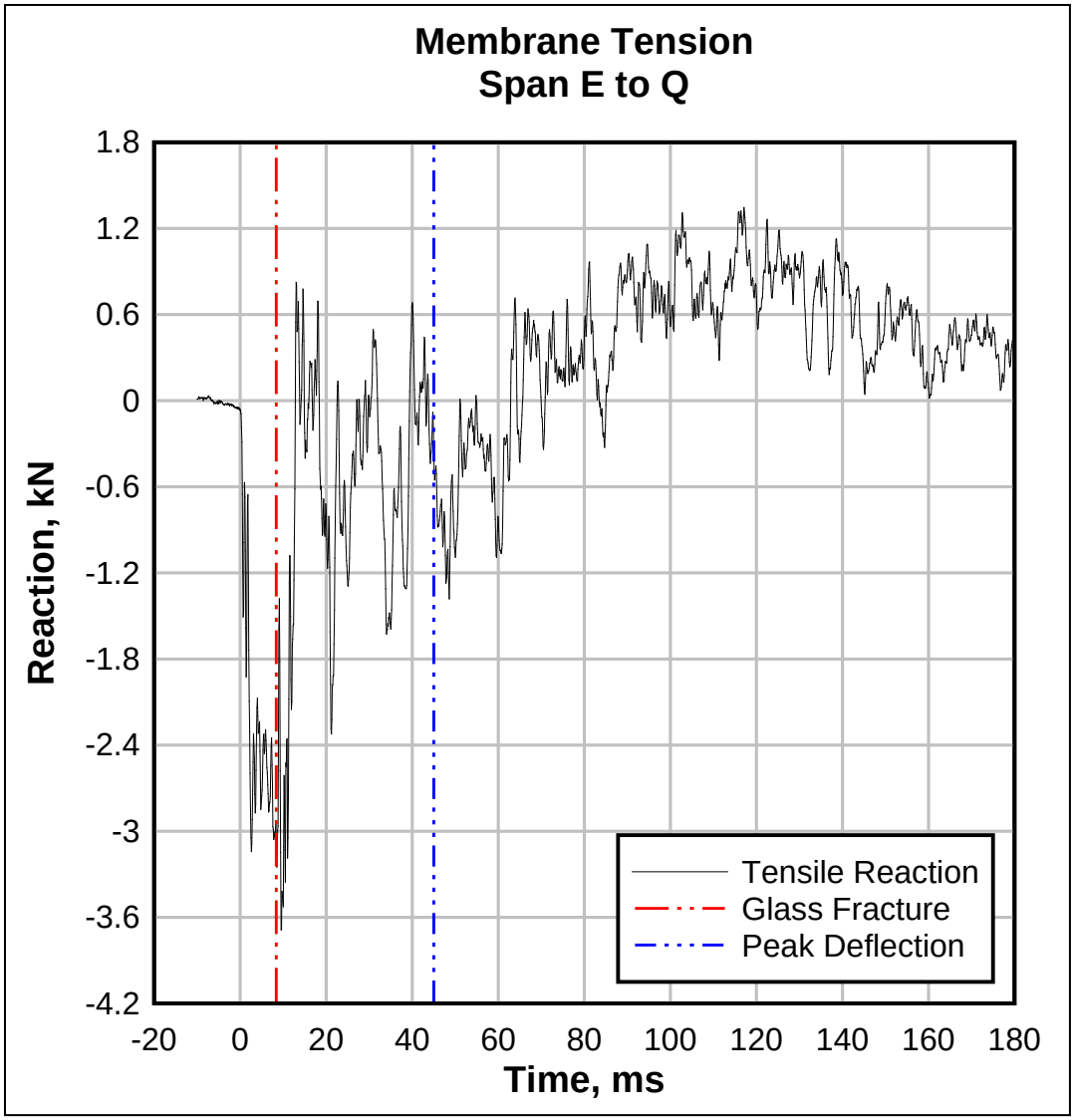

Figure 8.52 Tension within Membrane across Span E to Q

The behavior of the span between E and Q behaves differently than the previous span. The early and latter portion of the response behave as before. The time between the moments of glass fracture and peak membrane deflection are erratic. This highlights the difficulty in measuring the tensile response.

8.4 Modeling Results

8.4.1 SDOF Modeling Results

The output from the SDOF model is summarized in Table 8.20 for the initial attempt at fracturing the glass.

Table 8.20 Test to Failure SDOF Modeling Results, 300g Charge

SDOF Model Output				***Experimental***
Max Deflection		9.57	cm	4.67
At Time		6.62	ms	9.27
Final Resistance Function Region		1		---
Peak Reaction Force		76.46	kN	60.27*
At Time		6.11	ms	10-12
Long Edge	Peak Reaction Force	24.61	kN	---
	Peak Loading	146.8	N / cm	---
Short Edge	Peak Reaction Force	13.62	kN	---
	Peak Loading	81.2	N / cm	---

The SDOF model fails to properly reproduce this scenario. It predicts that the glass fractures at this loading after deflecting 3.94 cm. This results in an ultimate deflection of 9.57 cm, the majority coming from the membrane action of the interlayer. The peak reaction force is expected to be 76.46 kN which is considerably different than the predicted value based upon scaling up the force measurements, 60.27 kN. There is a 27% difference between the two predictions.

As a “what if” scenario, the Static Resistance Function was modified to prevent the glass breakage. This is accomplished by extended the last segment of the Static Resistance Function, seen in Figure 6.30, of the glass indefinitely. The resulting output is summarized in Table 8.21.

Table 8.21 Test to Failure SDOF Scenario Modeling Results, 300g Charge

SDOF Model Output				*Experimental*
Max Deflection		4.16	cm	4.67
At Time		6.62	ms	9.27
Final Resistance Function Region		1		---
Peak Reaction Force		79.10	kN	60.27*
At Time		6.11	ms	10-12
Long Edge	Peak Reaction Force	25.49	kN	---
	Peak Loading	152.0	N / cm	---
Short Edge	Peak Reaction Force	14.06	kN	---
	Peak Loading	83.9	N / cm	---

In this “what if” scenario, the deflection is much closer to the experimentally measured value, only differing by 12.2%. As with the previous modeling attempts, the value of the deflection is less than that of the experiment. The predicted peak reaction force increases slightly over the previous model. This is due to the extra capacity granted when modifying the resistance function.

The results of modeling the final blast event that led to failure of the window glass are in Table 8.22

Table 8.22 Test to Failure SDOF Modeling Results, 400g Charge

SDOF Model Output				*Experimental*
Max Deflection		13.79	cm	25.65
At Time		6.62	ms	9.27
Final Resistance Function Region		1		---
Peak Reaction Force		84.78	kN	63.29*
At Time		6.11	ms	10-12
Long Edge	Peak Reaction Force	27.17	kN	---
	Peak Loading	162.1	N / cm	---
Short Edge	Peak Reaction Force	15.22	kN	---
	Peak Loading	90.8	N / cm	---

The deflection during the tensile membrane formation is dramatically understated. There are clearly difficulties associated with the Static Resistance Function that was available for the modeling. Nevertheless, the value of the SDOF method has certainly proven itself to be an effective tool for modeling this window's behavior. It was able to accurately predict displacement, reaction forces, and loading around the perimeter, and was straightforward to implement.

8.4.2 Equivalent Design Results

The practice detailed in ASTM E1300 was completed for the blast resistant glazing system under test. The procedure most relevant to the construction of the BRGS was number "6.6 *For Single-Glazed Laminated Glass (LG) Constructed with PVB Interlayer Simply Supported Continuously Along Four Sides Where In-Service Laminated Glass (LG) Temperatures Do Not Exceed 50°C (122°F),"* (2009). The non-factored load was found to be 2.3 kPa for the 122 cm by 168 cm window tested via figure A1.28, the Non-Factored Load Chart for 6.0 mm Laminated Glass with Four Sides Simply Supported. Heat strengthened glass has a Glass Type Factor of 2.0 for short duration loads as shown in Table 1 of the specification. This yields a load resistance, or LR, of 4.6 kPa.

With the load resistance calculated, it is straightforward to back calculate an appropriate bomb weight and standoff. The static equivalence chart from ASTM F 2248-03, Figure 2.6, was used with the equivalent design load set equal to the load resistance determined above. Several bomb weight and standoff distance combinations can then be read off the chart. Three weights were chosen which were as follows in Table 8.23.

Table 8.23 Equivalent Threats

Equivalent Threats via ASTM F 2248-03		
	Bomb Weight (kg)	Standoff Distance (m)
Threat Ⅰ	27.2	15.2
Threat Ⅱ	45.4	22.9
Threat Ⅲ	454	91.4

The Blast Effects Computer was utilized to determine the pressure and impulse based on the threats calculated previously. The tool, published by the Department of Defense Explosives Safety Board, calculates the parameters of the blast, such as reflected pressure and impulse, positive phase duration, and time of arrival (2001). The values for the threats determined previously are summarized in Table 8.24.

Table 8.24 Equivalent Threat Blast Parameters

Equivalent Threat Blast Parameters		
	Reflected Pressure (kPa)	Impulse (kPa·ms)
Threat Ⅰ	98.4	372
Threat Ⅱ	63.5	341
Threat Ⅲ	24.7	379

The results suggest that the procedure detailed in ASTM F 2248-03 are based largely on the impulse generated from a particular blast. The pressure encountered by the glazing covers a broad range over these three threat levels. Perhaps the hazard rating associated with a given BRGS is largely governed by the impulse and its effects on the tensile membrane. It seems that high pressures would cause higher velocity glass fragments with a higher chance of piercing the interlayer. Early failure of the interlayer and the subsequent spread of fragments in the witness area would certainly contribute to poor performance within the ASTM F 1642 framework. The impulses are much more consistent with an average of 364

kPa·ms. This compares with the experimental results of 74.5 kPa and 371 kPa·ms that caused failure.

The standard calls out the performance of the glazing system to have a hazard rating of Minimal Hazard or better for this level of blast loading. Unfortunately, no formal witness area was used during the testing, but prior experience suggests that this window would have rated Very Low Hazard for this level of loading. The membrane did not tear until after it rebounded which strongly suggests few if any fragments outside of the 1 meter zone closest to the window. The reason for the Very Low Hazard is due to the tearing of the interlayer. The Uvekol A interlayer exhibited a long tear that would have been approximately 25% to 30% of the glazing sight perimeter. While speculative, it is suggested that the window would have achieved a Minimal Hazard rating had the interlayer been either Uvekol S or PVB. For this scenario, the equivalent design method was likely a good alternate means for developing a blast resistant glazing system.

8.4.3 Finite Element Analysis Results

Figure 8.53 shows the deflection experienced by the window during the first attempt to initiate window failure.

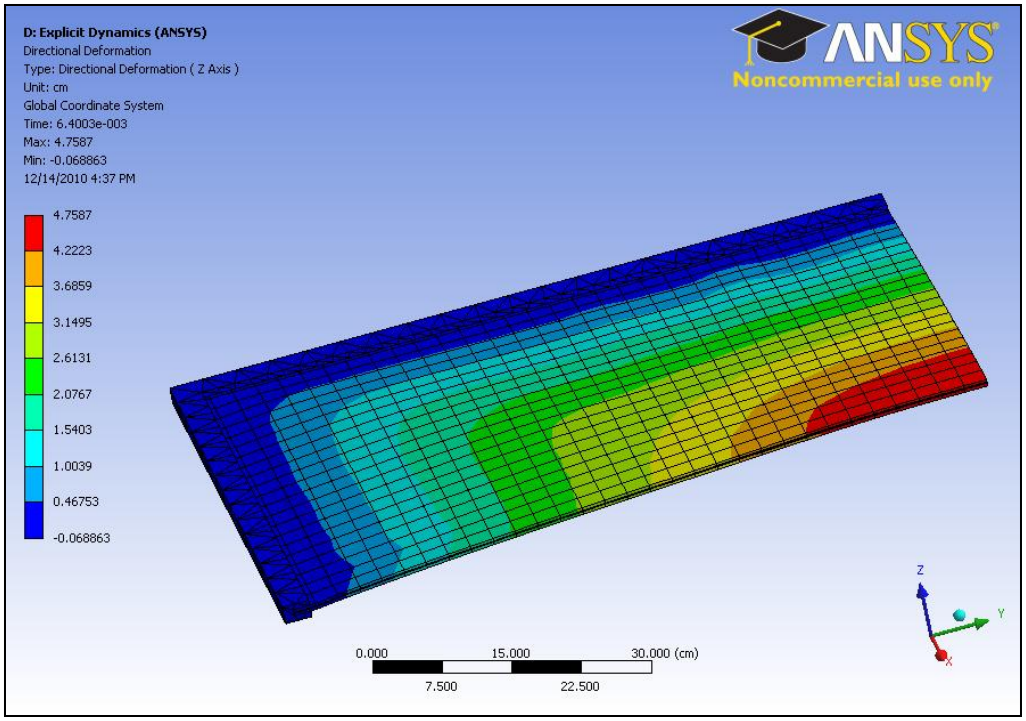

Figure 8.53 Test to Failure Deflection via FEA, 300g Charge

The maximum deflection predicted by the finite element model, 4.76 cm, agreed with reality. The percent error was less than 2%. The ripples developing in the glass are visible.

Figure 8.54 shows the safety margin for this blast loading event. The factor of safety was a scant 1.026 which implies the window was very near to failure at this load level.

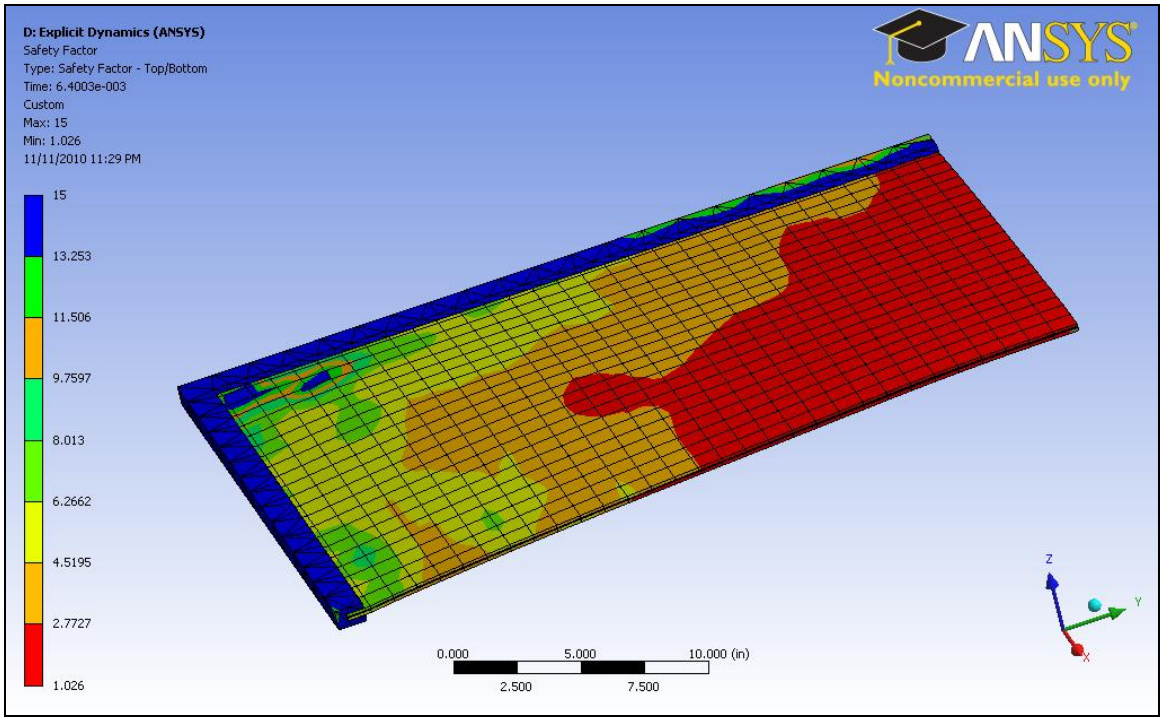

Figure 8.54 Test to Failure Safety Factor using Griffith's Criterion via FEA, 300g Charge

Figure 8.55 shows the expected deflection in the window system just prior to fracture. It predicts 4.95 cm of deflection before fracture occurs. When compared to the experimental results, this differs by 8.2%. Fracturing of the glass occurs between 5.2 and 5.6 milliseconds after the arrival of the blast wave. In reality, it occurs at 8.4 milliseconds, so this is a discrepancy in the modeling effort .

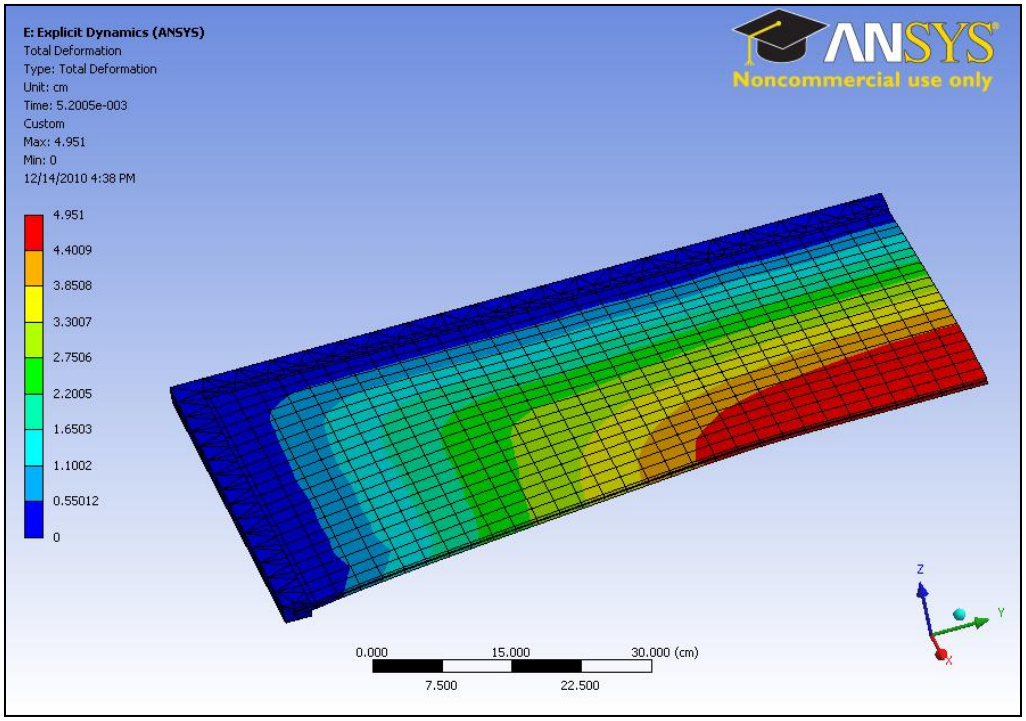

Figure 8.55 Test to Failure Deflection via FEA, 400g Charge

The distribution of stresses in the window glass can be seen in Figure 8.56. The stresses are concentrated slightly down from the center of the part, perhaps indicative of the vibrational mode dominating the window response. The peak principal stress was found to be 167 MPa prior to window fracture. There is no way of determining where the fracture initiated in the window from the experimental data.

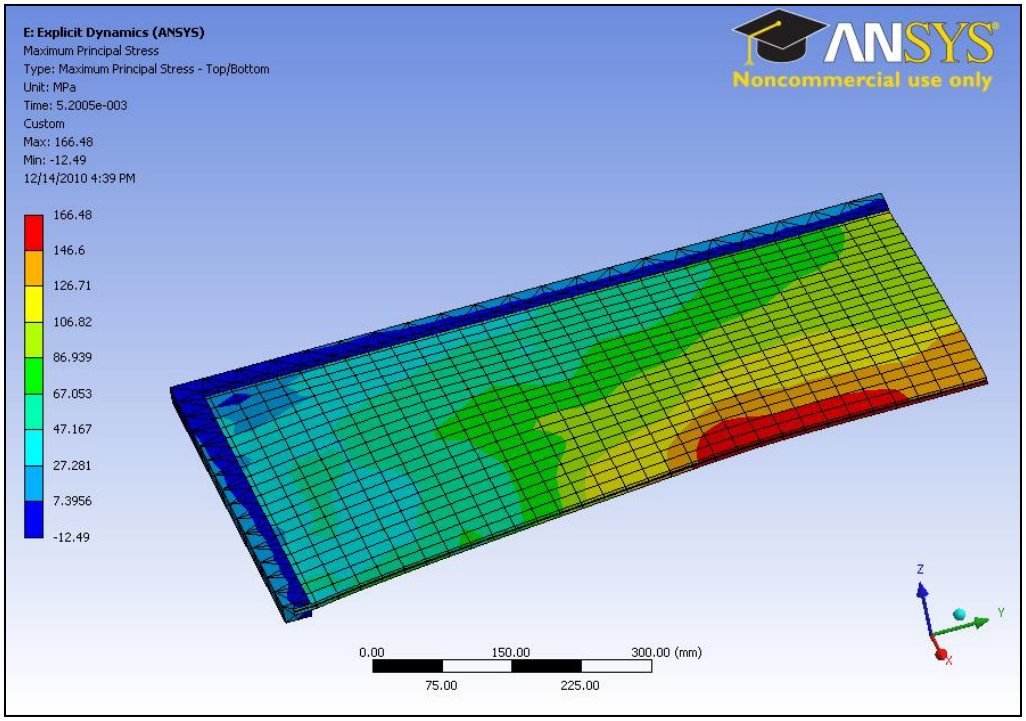

Figure 8.56 Test to Failure Maximum Principal Stress via FEA, 400g Charge

Chapter 9 Conclusions

The results of the perimeter testing show that the SDOF model for displacement, reaction forces, and loading around the perimeter to be very accurate for the ease with which it can be implemented. The key to the SDOF method is in the Static Resistance Function. The ability to generate the Static Resistance Function for a window system of interest would be a great boon to those developing such a system. It would be interesting to apply stochastic methods to the development of Static Resistance Functions so as to better predict the onset of glass fracture.

The results of the equivalent design exercise were encouraging. When one takes into consideration the use of Uvekol A instead of either Uvekol S or PVB, the system performed as expected. Retesting with the alternate interlayer material would serve to confirm this expectation. There is still a concern as to the disparity between peak pressures at either end of the equivalent static load as per ASTM F 2248. The higher pressures could lead to higher fragment velocities with greater likelihood of piercing the interlayer prematurely. Additional testing at these extreme conditions could shed more insight into this mechanism.

The predictions produced by HazL were disappointing. The window survived over 30 tests that HazL predicted would individually cause glass fracture in excess of 90% of the time. At first thought, this seems to be the result of some conservative assumptions at work. The unfortunate implication is that the window is capable of transmitting a substantially higher load to the supporting members than predicted by HazL. If the supporting members are undersized for this load, it could lead to severe damage to the building's façade as compared to the case where the glass fails first. This is counter to the design principle that the glass should be the first element to fail and could result in progressive collapse of the structure.

The key to modeling blast resistant glazing systems in ANSYS Explicit Dynamics is proper modeling of the connections to the glass. The window glass behaves in a manner somewhere between the simply supported and fixed edge conditions. Accurate material test data is the key to modeling. The model as detailed in this

work is descriptive at best due to the abstractions necessary. Any predictive model would require significantly more characterization of the aluminum frame and silicone glazing supports. The distinct lack of test data for the Uvekol material was also a problem of note for the modeling effort. Despite these problems the FEA model provided additional insight into the stress distribution in the window glass.

There is no obvious way to predict what the total reaction force a window experiences based upon measurements taken at any four points. The perimeter testing verified the accuracy of the SDOF model while the repeatability testing established that reactions to a given load are consistent from test to test. The values from those measurement points could not be used to predict what the total reaction force was as predicted by the SDOF model. It seems the reactions at the edge are functions of the support condition, the magnitude of the load, and the composition of the BRGS.

The tensile membrane can be measured directly through the application of triaxial force sensors. Like the distribution of forces around the perimeter of the window, the membrane response varies from span to span. In hindsight, this is not so unexpected considering the variations seen around the window perimeter.

The various modeling efforts have their limitations which must be understood before relying upon them. The only acceptable solution for design and verification of blast resistant glazing systems is to test physical samples of the window. The test should be conducted in a manner consistent with the application in the field and should be tested to the point of failure.

References

Allen, T. J., Locke, J., and Scranage, J. K., 1998, “Breaking of flat glass – part 4 size and distribution of fragments from vehicle windscreens,” *Forensic Science International,* February, Vol. 93, No. 1, pp. 209 – 218.

Aşik, Mehmet Zülfü, 2003, “Laminated glass plates: revealing of nonlinear behavior,” *Computers and Structures,* July, Vol. 81, pp. 2659 – 2671.

ASTM, 2003, “Standard practice for specifying an equivalent 3-s duration design loading for blast resistant glazing fabricated with laminated glass,” *F 2248-03,* West Conshohocken, PA.

ASTM, 2004a, “Standard specification for heat-treated flat glass-kind heat strengthened, kind fully tempered coated and uncoated glass,” *C 1048-04,* West Conshohocken, PA.

ASTM, 2004b, “Standard test method for glazing and glazing systems subject to airblast loading,” F *1642-04,* West Conshohocken, PA.

ASTM, 2009, “Standard practice for determining the load resistance of glass in buildings,” *E 1300-09a,* West Conshohocken, PA.

Barry, J. C., and Ford, S., 2001, “An electron microscopic study of nickel sulfide inclusions in toughened glass,” *Journal of Materials Science,* February, Vol. 36, No. 15, pp. 3721 – 3730.

Bielecki, S., Reben, M., Wasylak, J., 2008, “Nickel sulphide inclusions in tempered glass,” *Advanced Materials Research,* April, Vol. 39-40, pp. 563 – 566.

Biggs, John M., 1964, *Introduction to Structural Dynamics,* McGraw Hill, 341 pp.

Bordeaux, F., and Kasper, A., 1997, “Reliable and shorter heat soak test to avoid spontaneous fracture of heat strengthened and tempered glasses,” *Glass Processing Days 1997 Proceedings of the 5th International Glass Conference,* Vol. 1, September 13-15, 1997, Tampere, Finland.

Brodsley, Laurel, Frank, Sir Charles, and Steeds, John M., 1986, “Prince rupert’s drops,” *Notes and Records of the Royal Society of London,* October, Vol. 41, No. 1, pp. 1 – 26.

Ettouney, Mohammed, Smilowitz, Robert, and Rittenhouse, Tod, 1996, “Blast resistant design of commercial buildings,” *Practice Periodical on Structural Design and Construction,* February, Vol. 1, No. 1, pp. 31 – 39.

Griffith, A. A., 1921, “The phenomena of rupture and flow in solids,” *Philosophical Transactions of the Royal Society of London,* Vol. A, No. 221, pp. 163 – 198.

GSA, 2003, “US general services administration standard test method for glazing and window systems subject to dynamic overpressure loadings,” United States GSA, GSA-TS01-2003, January 1, 2003, 6 pp.

Haldimann, Matthias, Luible, Andreas, and Overend, Mauro, 2008, *Structural Use of Glass,* International Association for Bridge and Structural Engineering, 188 pp.

Hautekeer, Jean-Paul, Monga, Federico, Giesecke, Axel, O’Brien, Bill, and Dow Corning Corporation, 2001, “The use of silicone sealants in protective glazing applications,” *Glass Processing Days 2001 Proceedings of the 7th International Glass Conference,* Vol. 1, June 18 – 21, 2001, Tampere, Finland.

HazL, 1998, https://pdc.usace.army.mil/software/hazl/, *Protective Design Center*, Omaha District Corps of Engineers, Omaha, NE.

Hinman, Eve, and Arnold, Christopher, 2010, *Handbook for Blast-Resistant Design of Buildings,* John Wiley and Sons, 512 pp.

Jacob, Leon, 1997, “Factors that Influence spontaneous failure in thermally treated glass – nickel sulphide,” *Glass Processing Days 1997 Proceedings of the 5th International Glass Conference,* Vol. 1, September 13-15, 1997, Tampere, Finland.

Karman, T. von, 1910, “Festigkeitsprobleme im maschinbau,” *Encyl. der Mathematische Wissenschaften,* Vol. IV-4 C, Leipzig, Germany, pp. 348 – 352.

Kiger, Sam A. and Woodson, Stanley C., 2009, *Explosion Effects and Structural Design for Blast,* two day training course manual, Columbia, Missouri.

Lacy, J. M., Novascone, S. R., Richins, W. D., Larson, T. K., 2007, “A method for selecting software for dynamic event analysis i: problem selection,” *Proceedings of the 19th International Conference on Structural Mechanics in Reactor Technology,* Vol. 1, August 12 – 17, 2007, Toronto, Canada.

Lacy, J. M., Novascone, S. R., Richins, W. D., Larson, T. K., 2007, “A method for selecting software for dynamic event analysis ii: the taylor anvil and dynamic brazilian tests,” *Proceedings of the 16th International Conference on Nuclear Engineering,* Vol. 1, May 11 – 15, 2008, Orlando, Florida.

Larcher, Martin, Gebbeken, Norbert, Teich, Martien, and Solomos, George, 2009, “Simulation of laminated glass loaded by air blast waves,” *Dymat 2009 9th International Conference on the Mechanical and Physical Behavior of Materials under Dynamic Loading, September,* Vol. 2, pp. 1553 – 1559.

Ledbetter, Stephen R., Walker, Andrew R., and Keiller, Alan P., 2006, “Structural use of glass,” *Journal of Architectural Engineering,* September, Vol. 12, No. 3., pp. 137 – 149.

Leitch, Katherine K., 2005, “Structural Glass Technology: Systems and Applications,” Master’s Thesis, Massachusetts Institute of Technology, Cambridge, MA, 73 pp.

Li, Q. M., and Meng, H., 2002, “Pressure-impulse diagram for blast loads based on dimensional analysis and single-degree-of-freedom model,” *Journal of Engineering Mechanics,* January, Vol. 128, No. 1, pp. 87 – 92.

Lusk, Braden and Wedding, William, 2010, “Method for developing explosion damage potential contours in urban areas,” *Proceedings of the Thirty-Sixth Annual Conference on Explosives and Blasting Technique*, Vol. 1, February 7-10, 2010, Orlando, FL, ISEE.

Meyers, Gerald E., Baldwin, Donald, and Mlakar, Paul, 1994, “State of the Art of Blast Resistant Windows,” Department of Energy, Defense Technical Information Center, ADA507460, 25 pp.

Minor, Joseph E., and Norville, H. Scott, 2006, “Design of window glass for lateral pressures,” *Journal of Architectural Engineering,* September, Vol. 12, No. 3, pp. 116 – 121.

Ngo, T., Mendis P., Gupta A., and Ramsay, J., 2007, “Blast loading and blast effects on structures – an overview,” *Electronic Journal of Structural Engineering*, Special Issue, Vol. 7, pp. 79 – 91.

Nichols, R. T. and Sowers, R. M, 2009, “Laminated materials, glass,” *Kirk-Othmer Encyclopedia of Chemical Technology*. 1 – 17.

NIST, 2003, *NIST / SEMATECH e-Handbook of Statistical Methods*, http://www.itl.nist.gov/div898/handbook/.

Norville, H. Scott, Bove, Paul, Sheriden, Darrel L., and Lawrence, Stacey, 1993, “Strength of new heat treated window glass lites and laminated glass units,” *Journal of Structural Engineering,* March, Vol. 119, No. 3, pp. 891 - 901.

Norville, H. Scott, Harvill, Natalie, Conrath, Edward J., Shariat, Sheryll, and Mallonee, Sue, 1999, “Glass-related injuries in the Oklahoma city bombing,” *Journal of Performance of Constructed Facilities,* May, Vol. 13, No. 2, pp. 50 – 56.

Norville, H. Scott, and Conrath, Edward J., 2001, “Considerations for blast-resistant glazing design,” *Journal of Architectural Engineering,* September, Vol. 7, No. 3. pp. 80 – 86.

Norville, H. Scott, and Conrath, Edward J., 2006, “Blast-resistant glazing design,” *Journal of Architectural Engineering,* September, Vol. 12, No. 3. pp. 129 – 136.

Oklahoma Department of Civil Emergency Management, 1995, “After Action Report Alfred P. Murrah Federal Building Bombing”, Department of Central Services Central Printing Division, Oklahoma.

Salim, Hani, 2010, “Static resistance explanation,” email correspondence with author, October 21, 2010.

Smith, David, 2001,”Glazing for injury alleviation under blast loading – united kingdom practice,” *Glass Processing Days 2001 Proceedings of the 7th International Glass Conference,* Vol. 1, June 18 – 21, 2001, Tampere, Finland.

Smith, Peter D., and Rose, Timothy A., 2006, “Blast wave propagation in city streets – an overview,” *Progress in Structural Engineering and Materials,* Vol. 8, pp. 16 – 28.

Swofford, Jason L., 1996, “Damage Resulting from the Oklahoma City Bomb,” Master’s Thesis, Texas Tech University, Lubbock, TX, 129 pp.

TM 5 – 1300, *The Design of Structures to Resist the Effects of Accidental Explosions,* Technical Manual, US Department of the Army, Navy, and Air Force, Washington DC, 1990.

Unified Facility Criteria 4-010-01, *Department of Defense Minimum Antiterrorism Standoff Distances for Buildings,* Technical Manual, US Department of Defense, Washington DC, 2007.

Vallabhan, C. V. G., Das, Y. C., Maghhi, M, Asik, M. Z., Bailey, J. B., 1993, “Analysis of laminated glass units,” *Journal of Structural Engineering,* May, Vol. 119, No. 5, pp. 1572 – 1585.

Vallabhan, C. V. G., Asik, M. Zulfu, and Kandil, K., 1997, “Analysis of structural glazing systems,” *Computers and Structures,* Vol. 65, No. 2, pp. 231 – 239.

Vargas, Carol, 2006, “Lamination 101: class in session,” *Door and Window Manufacturer Magazine,* pp. 58 – 62.

Ward, Jerry, M., 2001, “*DDESB Blast Effects Computer Version 5.0*,” DOD Design Spreadsheet, Department of Defense Explosives Safety Board, August 16, 2001.

Weggel, David C., and Zapata, Brian J., 2008, “Laminated glass curtain walls and laminated glass lites subjected to low-level blast loading,” *Journal of Structural Engineering,* March, Vol. 134, No. 3, pp. 466 – 477.

Wikimedia Commons, 2006, “File: prince ruperts drops.jpg,” http://en.wikipedia.org/wiki/File:Prince_Ruperts_drops.jpg.

Zijlstra, A., and Burggraaf, A. J., 1968, “General survey of strength and fracture behavior of strengthened glass,” *Journal of Non-Crystalline Solids,* December, Vol. 1, No. 1, pp. 46 – 68.

VITA

William Chad Wedding was born in Morganfield, Kentucky, USA on December 10, 1976. He graduated from Union County High School in 1995 at the top of his class. He then enrolled in the University of Kentucky as a National Merit Finalist. In May of 2000, he graduated cum laude from UK with a Bachelor of Science Degree in Mechanical Engineering. He was a founding member and officer of the UK chapter of the Society of Automotive Engineers.

Chad began his professional career in August of 2000 with Lexmark International in Lexington, Kentucky. During his nine year stint, he rose to the rank of senior mechanical engineer.